Investigation of the endocannabinoid system using *in vivo* and *in vitro* models

Dissertation

zur

Erlangung des Doktorgrades (Dr. rer. nat.)

der

Mathematisch-Naturwissenschaftlichen Fakultät

der

Rheinischen Friedrich-Wilhelms-Universität Bonn

vorgelegt von

Svenja Ternes

aus

Wuppertal

Bonn, April 2013

Angefertigt mit Genehmigung der Mathematisch-Naturwissenschaftlichen Fakultät der Rheinischen Friedrich-Wilhelms-Universität Bonn

1. Gutachter: Prof. Dr. A. Zimmer
2. Gutachter: Prof. Dr. A. Haas

Tag der Promotion: 03.07.2013

Erscheinungsjahr: 2013

Abbreviations

AA	Arachidonic acid
ABHD	Aβ-hydrolase domain-containing protein
2-AG	2-arachidonoyl glycerol
AEA	Arachidonoyl ethanolamine (Anandamide)
AMPA	α-amino-3-hydroxy-5-methyl-4-isoxazolepropionic acid
APC	Allophycocyanin
ATP	Adenosine triphosphate
BAC	Bacterial artificial chromosome
BBB	Blood brain barrier
BCP	1-bromo-3-chloropropane
BLA	Basolateral amygdala
bp	Base pair
BSA	Bovine serum albumine
CB	Cannabinoid
CD	Cluster of differentiation
cm	Centimeter
CNS	Central nervous system
dB	Decibel
DAG	Diacylglycerol
DAGL	Diacylglycerol lipase
DIG	Digoxigenin
DMEM	Dulbecco's Modified Eagl Medium
DMSO	Dimethylsulfoxid
DNA	Desoxyribonucleic acid
DTT	Dithiothreitol
ECS	Endocannabinoid system
EDTA	Ethylene glycol tetraacetic acid

ELISA	Enzyme-linked immunosorbent assay
ES cells	Embryonic stem cells
ESdM	Embryonic stem cell derived microglia
EtOH	Ethanol
FAAH	Fatty acid amid hydrolase
FACS	Fluorescence activated cell sorter
FCS	Fetal calf serum
FITC	Fluorescein isothiocyanate
fl	Floxed (flanked by loxP sites)
G418	Geneticin
GABA	γ-aminobutyric acid
g	Gravitational force
g	Gram
GM-CSF	Granulocyte macrophage-colony stimulating factor
GPR	G-protein coupled receptor
h	Hour
HBSS	Hank's buffered salt solution
HGF	Hepatocyte growth factor
ICAM-1	Intercellular adhesion molecule-1
IFN	Interferon
IL	Interleukin
iNOS	Inducible nitric oxide synthase
NO	Nitric oxide
kb	Kilobase
kDa	Kilodalton
kg	Kilogram
kHz	Kilohertz
ko	Knockout
LIF	Leukemia inhibitory factor
loxP	"locus of X-ing over" in Phage P1
LPS	Lipopolysaccharide

M	Molar
m	Meter
mM	Millimolar
mA	Miliampere
MAGL	Monoacyl glycerol lipase
min	Minutes
MMR	Macrophage mannose receptor
mPFC	Medial prefrontal cortex
mRNA	Messenger RNA
ms	Milliseconds
n	Number (sample size)
NADA	N-arachidonoyl dopamine
NAPE	N-arachidonoyl-phoshatidylethanolamine
NAPE-PLD	NAPE-phospholipase D
n.d.	Not detected
neo	Gene mediating neomycin resistance
nm	Nanomolar
Noladin ether	2-arachidonoyl glycerol ether
n.s.	Not significant
ng	Nanogram
OD	Optical density
PBS	Phosphate buffered saline
PCR	Polymerase chain reaction
PE	Phosphatidylethanolamine
Pe	Phycoerythrin
Pgk-1	Phosphoglycerate kinase-1 promotor
PI	Phosphatidylinositol
PLC	Phospholipase C
PIP2	Phosphatidylinositol-2-phosphat
RNA	Ribonucleic acid
RT	Room temperature

RT-PCR	Reverse transcriptase-PCR
s	Second
SDS	Sodium dodecyl sulfate
SEM	Standard error of the mean
SSC	Saline sodium citrate
TE	Tris EDTA
TGF	Transforming growth factor
TNF	Tumor necrosis factor
Tris	Tris (hydroxymethyl) aminomethane
TRPV1	Transient receptor potential vanilloid type-1
U	Unit
UV	Ultraviolet
WHO	World Health Organisation
wt	Wild type
THC	Δ9-tetrahydrocannabinol
µl	Microliter
µM	Micromolar

Summary

The endocannabinoid system (ECS) is a retrograde signaling system that plays an important, pro-homeostatic role in the central nervous system (CNS) by adjusting synaptic communication. The system comprises a set of presynaptic cannabinoid receptors and several different ligands (endocannabinoids), which are produced on the post-synaptic site of a synaptic connection. Upon release into the synaptic cleft, the endocannabinoids 2-AG (2-arachidonoyl glycerol) and anandamide (arachidonoyl ethanolamine, AEA) can bind and activate presynaptic cannabinoid receptors and thus initiate ECS-mediated signaling.

Due to the fact that both endocannabinoids are capable of activating cannabinoid receptors, it is difficult to attribute a certain signaling effect to a certain endocannabinoid. To address this problem, this study aimed at generating conditional knockout mice for the 2-AG synthesizing enzymes DAGLα and DAGLβ. These mouse models will facilitate a detailed characterization of 2-AG-mediated signaling. Conditional targeting vectors were generated for both isoforms. The generation of conditional knockout mice was successful for the Daglα targeting construct. A set of preliminary behavioral experiments performed with homozygous Daglα knockout animals (Daglα$^{ko/ko}$) and a group of wild type animals initiated the behavioral phenotyping of this new mouse line. First results point out an important role of 2-AG-mediated signaling in anxiety and fear memory processing.

ECS-mediated signaling is important to maintain homeostasis in healthy tissues. Besides this function, it also plays an important role under pathological conditions, as for example during an inflammatory resonse of the CNS. Microglial cells act as key players in neuroinflammation and have been shown to communicate via the ECS. In order to facilitate a better understanding of ECS-mediated signaling in microglial cells, a second part of this study focused on this versatile cell type. Different pro-and anti-inflammatory activation states of primary microglia were induced and characterized. Comprehensive gene expression profiling revealed that genes encoding cannabinoid receptors, as well as endocanabinoid synthesizing- and degrading enzymes are differentially regulated in microglia upon stimulation with pro-or anti-inflammatory substances. These data indicate an important function of the ECS in microglia and provide first insights into the regulation of ECS components in different microglial phenotypes.

Contents

1 Introduction

1.1 The Endocannabinoid System

“Cannabis is a generic term used to denote the several psychoactive preparations of the plant *Cannabis sativa*.” (WHO, 2013). The history of cannabis use for medical or recreational purposes can be traced back for more than 4000 years (Murray et al. 2007). Nevertheless, the major psychoactive component Δ9-tetrahydrocannabinol (THC) was first isolated in 1964 by Raphael Mechoulam and co-workers (Gaoni & Mechoulam 1964). From this point on, it took more than another two decades until the molecular target of this substance was identified. The first cannabinoid receptor (CB_1) was characterized in the late 1980’s (Devane et al. 1988; Matsuda et al. 1990) and initiated the research era of the so-called endocannabinoid system (ECS).

This signaling system comprises a set of endogenous lipid mediators, termed endocannabinoids, and cannabinoid receptors. The ECS is involved in a multitude of physiological processes. Its arrangement and signaling mechanism is well characterized in the CNS, where it acts as a retrograde signaling system. Endocannabinoids are synthesized on demand at the postsynaptic site of a synaptic connection. After release into the synaptic cleft, these lipid messengers bind and activate presynaptic cannabinoid receptors, thereby initiating ECS-mediated signaling. The following sections will give a short overview of the main ECS constituents, the signaling mechanism and its role in diverse biological processes.

1.2 Receptors and ligands

Shortly after CB_1, a second receptor for cannabinoids was characterized and named cannabinoid receptor 2 (CB_2) (Munro et al. 1993). Both receptors are G-protein coupled, but display distinct expression patterns. CB_1 is most abundant in neuronal tissue (Matsuda et al. 1990) and is detected only at low levels in peripheral organs such as heart, testis and in the immune system (Bouaboula et al. 1993; Galiègue et al. 1995). In contrast, the CB_2 receptor is mainly present in immune cells (Munro et al. 1993; Pacher & Mechoulam 2011). Receptors like the transient receptor potential vanilloid type-1 (TRPV-1) receptor and the orphan G-protein coupled receptor GPR55 are discussed to be non-CB_1/CB_2 cannabinoid receptors (Zygmunt et al. 1999; Huang et al. 2002; Ryberg et al. 2007). More recently, the orphan G-protein coupled receptor GPR18 was proposed as a possible novel

cannabinoid receptor, as it was shown to be activated by THC and other cannabinoids (McHugh et al. 2012).

Anandamide (arachidonoyl ethanolamine, AEA) and 2-arachidonoyl glycerol (2-AG) were the first endocannabinoids that were characterized and are still considered as the "main endocannabinoids" (Devane et al. 1992; Mechoulam et al. 1995; Sugiura et al. 1995). Both are derived from lipid precursor molecules, similar to the more recently identified endocannabinoids 2-arachidonoyl glycerol ether (noladin ether), 2-arachidonoyl dopamine (NADA) and virodhamine (Hanus et al. 2001; Bisogno et al. 2000; Porter et al. 2002).

1.2.1 Synthesis and degradation of anandamide and 2-AG

Due to their lipophilic nature, anandamide and 2-AG cannot be stored in intracellular vesicles, but have to be produced on demand in an activity-dependent process. Anandamide is generated from the plasma membrane constituent phosphatidylethanolamine (PE) in a two-step process (see Figure 1 a). First, N-arachidonoyl-phoshatidylethanolamine (NAPE) is formed by N-acylation that is mediated by a membrane bound N-acyltransferase. Subsequently, NAPE is hydrolyzed by a Ca^{2+}-sensitive phosphodiesterase of the phospholipase D type (NAPE-PLD) to N-arachidonoyl ethanolamine (Hansen et al. 2000; Okamoto et al. 2004). The pathway described here is the most direct pathway leading to the generation of anadamide. However, overall four different pathways have been described for its synthesis (for review see: Di Marzo 2008).

2-AG is formed from a diacylglycerol (DAG) molecule that contains arachidonic acid at its *sn*-2 position (see Figure 1 b). This precursor is provided by phospholipase C (PLC)-mediated hydrolysis of the membrane phospholipid phosphatidylinositol (PI). In a second step, the enzyme diacylglycerol lipase (DAGL) hydrolyzes DAG into the monoacyl glycerol 2-AG and fatty acid (Prescotts & Majerus 1983; Sugiura et al. 1995). Overexpression studies of the DAGL enzymes, pharmacological blockage or knockout approaches indicate that this is the main pathway leading to the generation of 2-AG (Bisogno et al. 2003; Jung et al. 2005; Tanimura et al. 2010). However, other pathways involving the activity of phospholipase-A1 and lyso-PLC have been described (Sugiura et al. 1995).

The degradation of anandamide and 2-AG is mediated by the enzymes fatty acid amide hydrolase (FAAH) and monoacyl glycerol lipase (MAGL), respectively (Figure 1). FAAH was initially isolated from rat liver membranes and was shown to hydrolyze anandamide into arachidonic acid (AA) and ethanolamine (Cravatt et al. 1996). The enzyme is highly expressed in the central nervous system (CNS), where it is mainly localized at intracellular membranes of Ca^{2+} storing organelles such as mitochondria or

the smooth endoplasmatic reticulum (Gulyas et al. 2004). The serine hydrolase MAGL cleaves 2-AG into arachidonic acid (AA) and glycerol. It was the first enzyme identified to be involved in 2-AG hydrolysis (Dinh et al. 2002). MAGL is abundantly expressed in CB_1-positive nerve terminals and its activity accounts for approximately 80-85 % of total 2-AG degradation in the CNS (Dinh et al. 2002; Dinh et al. 2004; Saario et al. 2005). However, more recently the Aβ-hydrolases ABHD6 and ABHD12 have been reported to play a role in the termination of 2-AG signaling. ABHD6 is an integral membrane protein with the active site facing to the cell interior (Blankman et al. 2007). Located on the post-synaptic site of neuronal circuits, ABHD6 monitors the intracellular levels of 2-AG and is responsible for approximately 4 % of 2-AG degradation in the CNS (Blankman et al. 2007; Marrs et al. 2010). Less is known about ABHD12, which catalyzes up to 9 % of 2-AG inactivation. Like ABHD6, this enzyme is an integral component of the plasma membrane, but its active site is directed towards the extracellular space. In the CNS, this hydrolase was shown to be mainly present on microglia (Fiskerstrand et al. 2010).

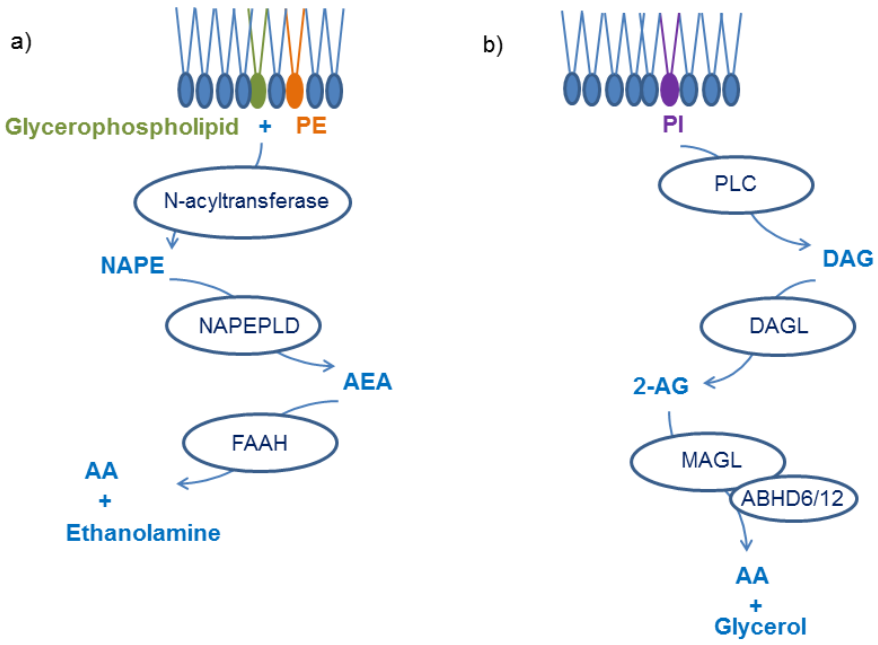

Figure 1: Synthesis and degradation of anandamide and 2-AG. a) For the synthesis of anandamide, PE is acylated by N-acyltransferase to produce NAPE, which is subsequently converted to AEA by NAPE-PLD. Degradation of anandamide is mediated by FAAH and results in the generation of AA and ethanolamine. b) The production of 2-AG originates from PI, which is cleaved by PLC to generate DAG. DAG is then further hydrolyzed by DAGL to 2-AG. The enzymes involved in 2-AG degradation are MAGL and ABHD6 and 12. These enzymes convert 2-AG into its constituents AA and glycerol. PE: phosphatidylethanolamine, NAPE: N-arachidonoyl-phosphatidylethanolamine, NAPE-PLD: N-arachidonoyl-phosphatidylethanolamine specific phospholipase D, AEA: anandamide, FAAH: fatty acid amid hydrolase, AA: arachidonic acid, PI: phosphatidylinositol, PLC: phospholipase C, DAG: diacylglycerol, DAGL: diacylglycerol lipase, 2-AG: 2-arachidonoyl glycerol, MAGL: monoacyl glycerol lipase, ABHD6 /12: Aβ-hydrolase 6 and 12

1.2.2 The diacylglycerol lipases (DAGL) α and β

DAGL enzymes are responsible for the generation of 2-AG. Two isoforms, termed DAGLα and DAGLβ, have been described. Initially, their enzymatic activity was revealed in human platelets, where stimulation with thrombin led to a DAGL-mediated hydrolysis of DAG (Bell et al. 1980). The first comprehensive characterization of the two isoforms DAGLα and DAGLβ was facilitated by a bio-informatic approach in 2003 (Bisogno et al. 2003). Both enzymes are closely related and display *sn-1* specificity regarding to their substrate DAG. Nevertheless, differences were found concerning their expression pattern in the developing organism. While DAGLα is constantly expressed during neuronal development and also in the adult CNS, DAGLβ is less abundant in the adult brain (Bisogno et al. 2003). In contrast, analysis of DAGLα and DAGLβ knockout mice revealed that DAGLβ is the main enzyme producing 2-AG in the liver (Gao et al. 2010). During brain development, both enzymes are localized on the axonal tracts and - together with CB_1 - on growth cones of growing neurons, implicating an important function of the ECS in axon guidance and path finding (Bisogno et al. 2003; Berghuis et al. 2007). Later, in the adult brain, DAGLα expression is restricted to the postsynaptic dendritic compartment. As a multi-pass transmembrane protein, it is inserted into the plasma membrane in close proximity to the post-synaptic density (Bisogno et al. 2003). Several reports indicate an important function of DAGLα and β not only during brain development, but also during adult neurogenesis in the subventricular zone (SVZ) and the hippocampus (Goncalves et al. 2008; Gao et al. 2010). Thus, the DAGL enzymes are key players of the ECS and their contribution to ECS-mediated functions has to be further investigated.

1.2.3 ECS signaling

The ECS is a complex signaling system that has been shown to be involved in a multitude of physiological processes. Besides its prevalence in the CNS, the ECS exerts important peripheral functions related to immunity, bone metabolism, cardiovascular-, gastrointestinal- and reproductive functioning (Downer 2011; Idris & Ralston 2010; Montecucco & Di Marzo 2012; Izzo & Sharkey 2010; Battista et al. 2012). However, its subcellular arrangement and operating mode is best characterized in the neuronal environment. Here, the ECS acts as pro-homeostatic, retrograde signaling system in GABAergic- as well as in glutamatergic circuits (for review see: Ohno-Shosaku et al. 2012).

The localization of the individual components of the ECS is representatively depicted for an excitatory glutamatergic nerve terminal in Figure 2. Basal synaptic communication, which is characterized by presynaptic glutamate release upon Ca^{2+} influx

and activation of postsynaptic ionotropic glutamate receptors, does not evoke ECS activity. In contrast, when excessive signaling leads to a massive release of glutamate, postsynaptic type I metabotropic glutamate receptors (mGluR1/mGluR5) become activated and trigger the production of DAG by PLCβ. Subsequent DAGL activity catalyzes the conversion of DAG into the endocannabinoid 2-AG, which is then released into the synaptic cleft and activates presynaptic CB_1 receptors. Subsequently, CB_1-associated Gi/o-proteins mediate the inhibition of voltage gated Ca^{2+} channels and reduce neurotransmitter release from the presynaptic site. For the termination of CB_1 activation, 2-AG is rapidly removed from the synaptic cleft and degraded by the presynaptically located MAGL (for review see: Katona & Freund 2008).

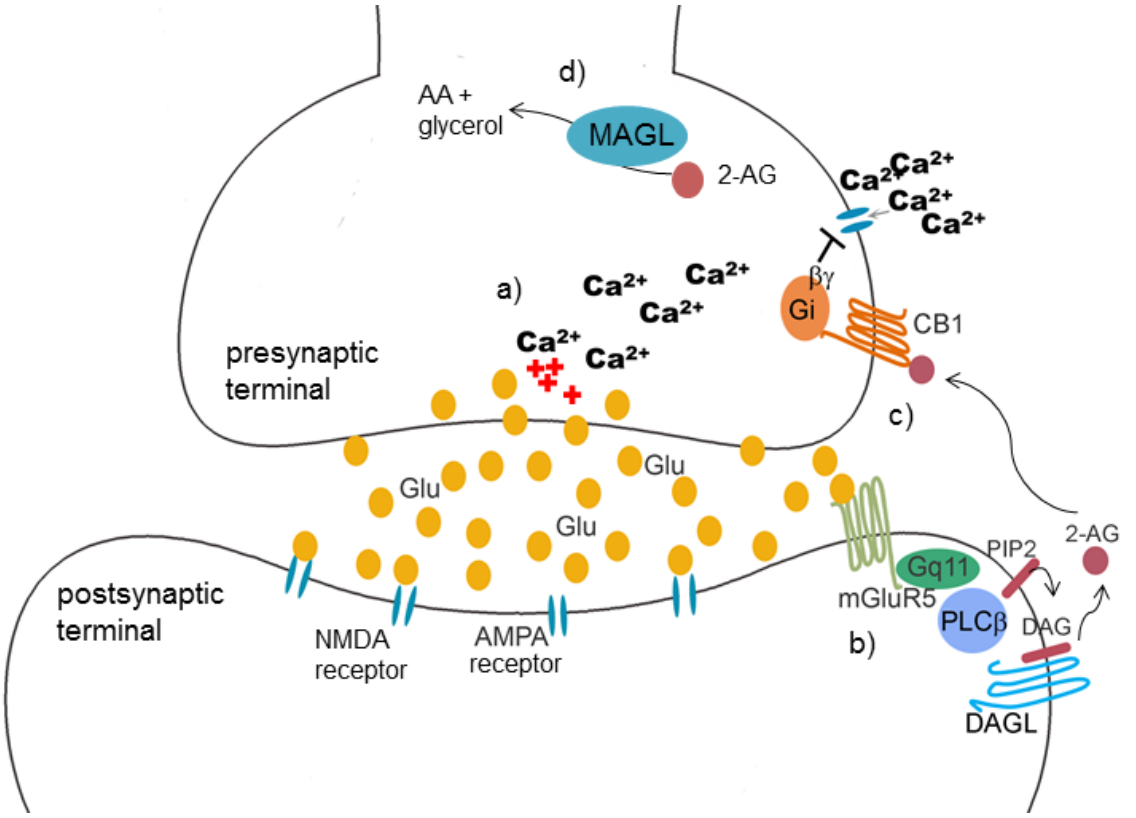

Figure 2: Retrograde signaling of the endocannabinoid system exemplarily illustrated for a glutamatergic nerve terminal. a) High frequency stimulation of the presynaptic neuron leads to a Ca^{2+} influx into the presynaptic bouton and subsequently to a massive release of glutamate (Glu) into the synaptic cleft. b) The large amount of glutamate activates postsynaptic AMPA/NMDA receptors, but also metabotropic glutamate receptors (mGluR5), located at the edge of the postsynaptic density. The activated Gq11 protein in turn activates PLCβ, which generates DAG from PIP2. DAG is further cleaved by DAGL to 2-AG. 2-AG is released into the synaptic cleft, where it binds and activates presynaptic CB_1 receptors. c) The βγ subunit of the associated Gi protein inhibits voltage gated Ca^{2+} channels, which leads to a reduction of neurotransmitter release from the presynaptic side. d) Rapid uptake of 2-AG and degradation by presynaptic MAGL terminates CB_1 signaling. Glu: glutamate, AMPA: α-amino-3-hydroxy-5-methyl-4-isoxazolepropionic acid receptor (ionotropic glutamate receptor), NMDA: *N*-methyl-D-aspartate receptor (ionotropic glutamate receptor), mGluR5: metabotropic glutamate receptor 5, PLCβ: phospholipase-Cβ, DAGL: diacylglycerol lipase, PIP2: phosphatidylinositol-2-phosphat, DAG: diacylglycerol, 2-AG: 2-arachidonoyl glycerol, CB_1: cannabinoid receptor 1, MAGL: monoacyl glycerol lipase, red crosses symbolize enhanced vesicle release

As 2-AG and anandamide are hydrophobic messenger molecules. They can easily cross lipid bilayers by diffusion. However, the existence of membrane transporter molecules that mediate the re-uptake these endocannabinoids was proposed by several researchers and is still a matter of debate (for review see: Fowler 2012).

The illustrated mechanism of retrograde signaling ascribes an important role to the ECS in stabilizing the internal environment and supporting the maintenance of healthy conditions (De Petrocellis & Di Marzo 2009). However, ECS signaling is also important under pathological conditions, as for example in neuroinflammatory processes (Centonze et al. 2007). Microglia, the resident immune cells of the CNS, play an important role in coordinating inflammatory reactions (for review see: Graeber et al. 2011). These cells have been shown to communicate via the ECS, thus implicating an important function of this signaling system in the regulation of an inflammatory response (for review see: Stella 2009; Pandey et al. 2009). The following sections will introduce microglia as key players in the immune response of the CNS. In addition, a short overview will be given about how microglia utilize the ECS as an immunomodulatory system.

1.3 Microglia: multifaceted cells

Microglial cells are, similar to macrophages in the periphery, highly versatile and adaptive cells. Their exact origin was a matter of debate for a long time. By now, there is accumulating evidence that microglia precursors originate from the embryonic yolk sac. These precursors are detectable as early as day 7.5 - 8.5 of embryonic development and their generation requires the activity of Pu.1 and Irf8 transcription factors. How these precursors populate the brain is still under investigation, but a functional blood circulation and the activity of matrix metalloproteinases seem to be indispensable (Ginhoux et al. 2010; Greter & Merad 2013; Kierdorf et al. 2013).

Under healthy conditions, microglia display a quiescent, so-called “resting state”, which is characterized by a highly-ramified morphology. But the term “resting state” is misleading, as these cells are constantly active, scanning their environment by extending and retracting fine protrusions (Nimmerjahn et al. 2005). Thereby, microglia are able to detect biochemical alterations or invading pathogens. In addition, microglia form transient contacts with synapses and support remodeling of synaptic contacts (Hanisch & Kettenmann 2007; Wake et al. 2009).

Microglia can be activated in response to environmental changes and adapt their phenotype accordingly. The concept of different activation states is well established for macrophages. A pro-inflammatory (often referred to as M1/ classical activation state) and an anti-inflammatory subtype (M2a/ alternative activation state) are clearly distinguishable

by a specific pattern of antigen presentation and cytokine release (Martinez et al. 2009). Another activation state (designated M2c or acquired deactivation state) inducible by interleukin-10 (IL-10) or transforming growth factor β (TGFβ) displays anti-inflammatory properties, which are supposed to be distinct from M2a (Gordon 2003; Mantovani et al. 2004; Colton & Wilcock 2010).

The different activation states of microglia are currently in the focus of numerous research projects. Challenging microglia with pro-inflammatory substances, such as lipopolysaccharide (LPS) or interferon γ (IFNγ) leads to a rapid activation, which is accompanied by the production of pro-inflammatory cytokines as for example interleukin-6 (IL-6), tumor necrosis factor α (TNFα) or interleukin-1β (IL-1β). In addition, activated microglia can release large amounts of nitric oxide (NO) or reactive oxygen species (Lee et al. 1993; Colton et al. 1996; Hanisch 2002). This pro-inflammatory "M1-like" activation state (see Figure 3 a) is important during the induction of an inflammatory response to promote tissue defense and killing of pathogens by releasing cytotoxic molecules. In addition, microglia can act as antigen presenting cells. Therefore, they display major histocompatibility complex II (MHC II) peptide complexes and co-stimulatory molecules such as CD80 (B7-1), CD86 (B7-2) or even intercellular adhesion molecule-1 (ICAM-1) to invading T-cells, thus promoting the local adaptive immune response (Shrikant & Benveniste 1996; Yang et al. 2010).

In order to prevent self-damage from an exacerbated immune response, the final phase of infection fades to wound healing processes, including tissue repair and phagocytosis of cellular debris. During this phase, the pattern of cytokine release changes. Microglia, as well as astrocytes and even neurons produce anti-inflammatory cytokines- mainly interleukin-4 (IL-4), interleukin-13 (IL-13), IL-10 or TGFβ (Colton & Wilcock 2010). A shift in the cytokine environment leads to an alteration of microglial activity. Stimulation of microglia with IL-4 or IL-13 evokes a so-called "M2a-like" phenotype (see Figure 3 b), which is characterized by reduced mRNA levels of the NO-synthesizing enzyme iNOS and a diminished release of pro-inflammatory cytokines (Ledeboer, et al. 2000; Colton et al. 2006). In contrast, surface expression of pattern recognition receptors as for example the macrophage mannose receptor (MMR) is increased (Colton 2009). Moreover, enhanced production was detected for molecules like chitinase-3-like-3 (Ym1) and found-in-inflammatory-zone-1 (FIZZ1), which are both involved in the generation of extracellular matrix (Raes et al. 2002; Colton et al. 2006). Arginase 1 (Arg1), an enzyme involved in arginine metabolism, is also induced upon IL-4 stimulation. It competes with iNOS for arginine, thus reducing NO production in an indirect way (Colton & Wilcock 2010). Moreover, IL-4 treated microglia have been shown to generate insulin-like growth factor-1 (IGF-1), thus conveying a survival signal and

facilitating regenerative processes in oligodendrocyte-lineage cells or neurons, respectively (Neumann et al. 2009). The detection and subsequent phagocytosis of apoptotic cells by microglia enhances the production and release of TGFβ and IL-10. Acting in an auto- and paracrine way, these molecules attenuate the immune response, promote neuronal survival and support the re-establishment of the blood brain barrier integrity (Colton 2009). The activity state induced by the encounter of apoptotic cells and accompanied with increased TGFβ and IL-10 production is here referred to as “M2c-like” phenotype (see Figure 3 c). This phenotype is supposed to be distinct from the one induced by IL-4 and IL-13, although both phenotypes promote tissue repair and wound-healing processes (Colton & Wilcock 2010).

Taken together, there is increasing evidence that microglia play an important role in different phases of a CNS immune response. They act as sensitive surveillants of the CNS and can adjust their activity in response to environmental stimuli. However, an immune response is complex, involving a variety of different cell types and a sophisticated system of intercellular communication, one of which is the ECS.

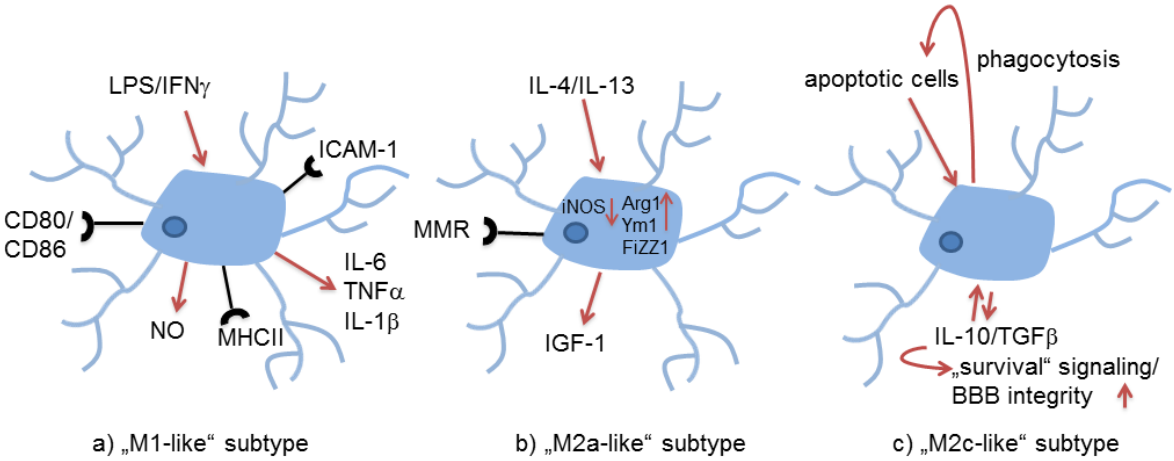

Figure 3: Different activation states in microglia. a) Challenging microglia with pro-inflammatory stimuli results in a reactive “M1-like” phenotype. b) Stimulation of microglia with IL-4 and/or Il-13 evokes an anti-inflammatory response and shifts microglia towards an “M2a-like” phenotype. c) A phenotype distinct from M2a, but also with anti-inflammatory properties is induced by apoptotic cells and/or stimulation with IL-10 and TGFβ and is referred to as "M2c-like" activation state. LPS: lipopolysaccharide, IFNγ: interferon γ, ICAM-1 intercellular adhesion molecule-1, CD80/CD86. costimulatory molecules, NO: nitric oxide, MHC II: major histocompatibility complex II, IL-6: interleukin-6, TNFα: tumor necrosis factor α, IL-1β: interleukin-1β, MMR: macrophage mannose receptor, IGF-1: insulin-like growth factor-1, IL-4: interleukin-4, IL-13: interleukin-13, iNOS: inducible nitric oxide synthase, Arg1: arginase 1, Ym1: chitinase-3-like-3, FIZZ1: found-in-inflammatory-zone 1, IL-10: interleukin-10, TGFβ : transforming growth factor β, BBB: blood brain barrier

1.3.1 ECS signaling in microglia

The effect of cannabis consumption on immune function has been addressed in numerous *in vivo* and *in vitro* studies (for review see Klein et al. 1998). By now, an immunomodulatory function of the ECS is well accepted. The pivotal point, which creates the connection of the ECS with the immune system, is the CB_2 receptor. Careful expression analysis revealed its prevailing appearance in immune cells of the myeloid, and lymphoid lineage (Munro et al. 1993; Galiègue et al. 1995).

Microglia in the CNS are capable of expressing CB_1 and CB_2 receptors. However, while CB_2 levels are variable with respect to changes in phenotype and activation state, the CB_1 receptor expression appears to be rather constant (Carlisle, et al. 2002). Compared to resting microglia, the expression level of the CB_2 receptor is elevated, when these cells become activated. Various pro-inflammatory stimuli, such as LPS or IFNγ in combination with GM-CSF (granulocyte macrophage-colony stimulating factor) have been shown to modulate CB_2 expression (Carlisle et al. 2002; Maresz et al. 2005; Stella 2011). However, the extend of CB_2 production by microglia in response to a neuroinflammatory process is dependent on the molecular environment generated by pathogens, toxins or cytokines (Stella 2009). More recent findings indicate that the putative cannabinoid receptor GPR18 is expressed in microglia. Activation of this receptor by N-arachidonoyl glycine (NAGly), a metabolite of anandamide, influences migration of microglia derived from the cell line BV-2 (McHugh et al. 2012).

In addition to cannabinoid receptors, microglia are able to produce 2-AG as well as anandamide (Carrier et al. 2004). Another study addressing the production of endocannabinoids in microglial cells revealed that exogenous ATP triggers the production of 2-AG by activation of purinergic $P2X_7$ receptors (Witting, et al. 2004). Degradation of endocannabinoids in this cell type occurs through the activation of FAAH and MAGL (Witting, et al. 2004; Muccioli et al. 2007). More recently, the Aβ-hydrolase ABHD12 has been shown to be abundantly expressed in microglia. Up to now, 2-AG is the only known substrate for this hydrolase and it is tempting to speculate that ABHD12 activity accounts for the degradation of the main proportion of microglia-derived 2-AG (Fiskerstrand et al. 2010).

Taken together, microglia express all important components of the ECS and signaling appears disengaged from the classical pre-and postsynaptic arrangement of the ECS in neurons. How endocannabinoid signaling is orchestrated between different cell types under pathological conditions is still under investigation. Neuronal damage is accompanied by extensive release of glutamate and ATP. Both molecules can stimulate endocannabinoid production and release in adjacent neurons and surrounding microglia (Stella 2009; Pandey et al. 2009). 2-AG stimulates proliferation of microglia and induces

site-specific migration, an effect, which was shown to be sensitive to CB_1- and CB_2 antagonists (Walter et al. 2003; Carrier et al. 2004; Eljaschewitsch et al. 2006). Acting on LPS-stimulated microglia, anandamide effectively reduced the production and the release of pro-inflammatory mediators such as NO, IL-6, IL-1α and IL-1β (Puffenbarger et al. 2000; Eljaschewitsch et al. 2006). In contrast, anandamide was shown to enhance the production of the anti-inflammatory cytokine IL-10 in a CB_2-mediated manner (Correa et al. 2010). Across the plethora of studies that were performed in this field, the major findings suggest that the ECS functions as a communication and regulation system among different cell types. However, neuroinflammation can be triggered by a multitude of events. Thus, careful investigation is required to dissect the signaling events which involve the ECS and influence the respective activation state of microglia during different phases of the inflammatory response of the CNS.

1.4 Aim of the thesis

One aim of this study was to create conditional knockout mouse lines for the two diacylglycerol lipases DAGLα and DAGLβ. These mouse lines will allow a detailed and specific analysis of 2-AG-mediated effects *in vivo* as well as in primary cell cultures *in vitro.* The conditional knockout approach enables a cell type-specific deletion of 2-AG synthesis. Therefore, diverse questions concerning the role of 2-AG signaling in different tissues can be addressed. In addition, inducible Cre-expressing mouse lines enable the investigation of developmental effects in DAGL knockout mice.

A second aim of the present thesis focused on the different activation states of primary microglial cells. Therefore, primary microglial cell cultures were established and several states of activation were induced by a set of different substances. Distinct phenotypes were characterized by the expression patterns of different marker molecules. In the first instance, these microglial cells can serve as a tool for the detailed functional analysis of microglia phenotypes *in vitro*. Within the scope of this work another question was of central importance: Which elements of the ECS are responsive to different pro- or anti-inflammatory conditions? Comprehensive gene expression profiling was performed with microglia shifted into different activation states. This approach identified responsive candidate genes and provided important insights into the regulation of the ECS in microglia in response to a pro- or anti-inflammatory environment.

2 Material

2.1 Equipment

Technical instrument	Identifier, Company
Analytical balance	BP 121 S, Sartorius
Cell culture incubator	Binder GmbH
Centrifuges	Biofuge fresco, Heraeus Instruments
	Biofuge pico, Heraeus Instruments
	Biofuge stratos, Heraeus Instruments
	Megafuge 1.0R, Heraeus Instruments
Digital gel documentation	ChemiDoc MP imaging systems, Bio-Rad Laboratories
Electroporation system	Gene pulser Xcell, Micropulser, Bio-Rad Laboratories
Electrophoresis chamber	Sub-Cell GT System, Bio-Rad Laboratories
Film processing machine	CP1000, AGFA
Flow cytometer	FACS Canto II, BD Bioscience
Hot plate test device	TSE Systems
Hybridization oven	HB-1000 Hybridizer, UVP
Laminar flow hood	Herasafe, Kendro
Liquid handling platform	Janus®, Perkin Elmer
Magnetic stirrer	MR 3001 K, Heidolph, Fisher
Microplate analyzer	MRX TC II, Dynex Technologies
Microscope	Eclipse TS 1000, Nikon
	Zeiss Stemi 2000 Binocular Stereo Microscope, Zeiss
Open field test device	Open field ActiMot, TSE Systems
PCR cycler	iCycler, Bio-Rad Laboratories

Technical instrument	Identifier, Company
pH meter	inoLab, WTW
Real-time PCR cycler	7900HT Fast Real-time PCR System, Applied Biosystems
Spectrophotometer	NanoDrop 1000, Thermo scientific
Startle response box	TSE startle response test system, TSE Systems
Sterilizing oven	Varioklav 25T, H+P Labortechnik
Tissue homogenizer	Precellys 24, Bertin Technologies
UV crosslinker	UV Stratalinker 2400, Stratagene
Vortexer	Vortex-Genie 2, Scientific Industries

2.2 Chemicals and reagents

2.2.1 Kits

Kits	Company
BAC Subcloning Kit	Genebridges™
Quick & Easy Conditional Knock out Kit (loxP/Cre)	Genebridges™
QiaPrep MiniPrep Buffers P1-P3	Qiagen
GeneElute™ HP Plasmid MidiPrep Kit	Sigma
High Pure PCR Product Purification Kit	Roche
PCR DIG Labeling Mix	Roche
GoTaq PCR Master Mix	Promega

2.2.2 Selection cassettes used for cloning

Selection casette	Company
loxP-PGK-gb2-neo-loxP	Genebridges™
FRT-PGK-gb2-neo-FRT-loxP	Genebridges™

2.2.3 Molecular weight standards

Marker	Company
DNA Molecular weight marker II	Roche
100 bp DNA ladder	Invitrogen
1 kb DNA ladder	Invitrogen

2.2.4 Enzymes and antibodies

All restriction endonucleases were purchased from New England Biolabs (NEB).

Enzyme	Company
Proteinase K	NEB
Superscript II Reverse Transcriptase	Invitrogen
Taq Polymerase	NEB
Phusion High Fidelity DNA Polymerase	NEB

2.3 BACs, Plasmids, Bacteria

2.3.1 BACs:

RP23-13J22: A pBACe3.6 vector containing a fragment of the Daglα gene. The BAC vector is kept in DH10B *E. coli* and was purchased from imaGenes.
RP23-453H13: A pBACe3.6 vector containing a fragment of the Daglβ gene. The BAC vector is kept in DH10B *E. coli* and was purchased from imaGenes.

2.3.2 Plasmids:

All plasmids used were part of the cloning kits provided by Genebridges™. For detailed information see the Genebridges™ manual of the Quick & Easy Conditional Knockout Kit.

Minimal vector: A linear vector with a CoIE1 origin of replication and an ampicillin resistance gene.
pRedET: A plasmid encoding the genes of a protein pair of 5' - 3' exonucleases under an arabinose-inducible promotor. Upon expression, these proteins mediate the recombination between regions of homology.
706-Cre: A plasmid containing a gene encoding the Cre recombinase and a gene that mediates tetracycline resistance.

2.3.3 Bacteria:

DH10B: An *E.coli* strain harboring the unmodified BAC clones. The initial subcloning steps were performed in this strain.
TOP10: An *E.coli* strain used for the transformation of subsequent recombinant plasmids.

2.4 Antibiotics

Substance	Company	Working concentration
Ampicillin	Applichem	50 µg/ml
Chloramphenicol	Sigma Aldrich	15 µg/ml
Kanamycin	Applichem	50 µg/ml
Tetracycline	Applichem	10 µg/ml

2.5 Cells

The embryonic stem (ES) cell lines used in this work are murine cell lines.

MPI2 cells: An ES cell line derived from 129/Sv mice. The cell line was generated at the Max Planck Institute Göttingen in the laboratories of Prof. P. Gruss (Voss et al. 1998).
Bruce4: An ES cell line derived from C57BL/6 mice (Kontgen et al. 1993). The cell line was kindly provided by Ralf Kühn, Max-Planck Institute for Biochemistry, Martinsried, Germany.
Primary mouse embryonic fibroblasts (MEF): These cells were used as feeder cells for the cultivation of ES cells.
Primary microglial cells: These cells were prepared from newborn mice at postnatal days 1-5. A detailed description of the preparation is given in section 3.3.5.

2.6 Solutions

All solutions were prepared with sterile deionized H_2O. If not stated otherwise, all chemicals and reagents used were purchased from Applichem, Invitrogen, Merck, Roth or Sigma-Aldrich.

2.6.1 Cultivation of bacteria

LB medium

H_2O		
Tryptone	1	% (w/v)
Yeast extract	0.5	% (w/v)
NaCl	1	% (w/v)
autoclaved at 121°C, 20 min		
for LB agar add agarose	1.5	%

2.6.2 DNA Isolation

Lysis buffer

Tris/HCl pH 8	100	mM
EDTA	5	mM
NaCl	200	mM
SDS	0.2	% (w/v)

TE buffer

Tris	10	mM
EDTA, pH 8	1	mM
adjusted to pH 7.4		

2.6.3 Southern blot

Depurination

HCl	250	mM

Denaturation

NaOH	500	mM
NaCl	1.5	M

Neutralization

Tris/HCl, pH 7	500	mM
NaCl	1.5	M

SSC (20x)

NaCl	3	M
Na-citrate dihydrate	300	mM
adjusted to pH 7		

Maleic acid buffer

Maleic acid	100	mM
NaCl	150	mM
adjusted to pH 7.5		

Blocking solution (10x)

Maleic acid buffer		
Blocking reagent	10	% (w/v)
autoclaved at 121°C, 20 min		

Hybridization buffer

SSC (20x)	25	% (v/v)
SDS	0.2	% (w/v)
Blocking solution (10x)	10	% (v/v)
N-lauroylsarcosine	1	% (w/v)

Washing buffer

Maleic acid buffer		
Tween 20	0.3	% (v/v)

Detection buffer

Tris/HCl, pH 9.5	100	mM
NaCl	50	mM
$MgCl_2$	25	mM

2.6.4 Agarose gel electrophoresis

6x loading dye

Glycerol	30	% (v/v)
Orange G	0.4	% (w/v)

TAE buffer (1x)

Tris-acetate	40	mM
EDTA, pH 8	1	mM

2.6.5 Cell culture media

For the selection of neomycin resistant cells, geneticin (G418) at a final concentration of 170 ng/ml was added to the respective ES cell medium.

MPI ES cell medium

DMEM, high glucose		
FCS (ES cell approved)	20	% (v/v)
Sodium pyruvate	1	% (v/v)
Penicillin streptomycin mix	0.5	% (v/v)
Nonessential amino acids (100x)	1	% (v/v)
β-mercaptoethanol	70	nM
LIF	500	U/ml

Bruce4 ES cell medium

DMEM, high glucose		
FCS (ES cell approved)	12.5	% (v/v)
Sodium pyruvate	1	% (v/v)
Penicillin streptomycin mix	1	% (v/v)
Nonessential amino acids (100x)	1	% (v/v)
β-mercaptoethanol	0.1	mM
LIF	1000	U/ml

Mouse embryonic fibroblast medium

DMEM, high glucose		
FCS	10	% (v/v)
Sodium pyruvate	0.5	% (v/v)

Mitomycin solution

Mouse embryonic fibroblast medium		
Mitomycin C	10	µg/ml

Freezing medium

DMEM, high glucose	40	% (v/v)
FCS, ES cell approved	40	% (v/v)
DMSO	20	% (v/v)

Microglia medium

DMEM, high glucose		
FCS, heat inactivated	9	% (v/v)
Non-essential amino acids	0.9	% (v/v)
Penicillin-streptomycin mix	0.9	% (v/v)
β-mercaptoethanol	0.05	mM

2.6.6 Stimulants for cell culture

Stimulant	Species	Company	Concentration
Interleukin-4 (IL-4)	mouse	eBioscience	100 U/ml
Interleukin-10 (IL-10)	mouse	eBioscience	100 U/ml
Interferon γ (IFNγ)	mouse	R & D Systems	20 ng/ml
Lipopolysaccharide (LPS)	*E. coli*	Invivogen	100 ng/ml
Transforming growth factor β1 (TGFβ)	human	R & D Systems	20 ng/ml

2.7 Antibodies for flow cytometry

Antigen	Species	Conjugation	Company
CD11b	rat	APC	ebioscience
CD11b	rat	Biotin	BD Pharmingen
CD11b	rat	eFluor 450	eBioscience
CD11b	rat	FITC	Biozol
CD11b	rat	Pe	eBioscience
CD40	rat	Biotin	eBioscience
CD80	hamster	Pe	Biozol
CD86	rat	Pe	BD Pharmingen
Fc-Block (CD16/CD32)	rat	unconjugated	Biozol
ICAM-1 (CD54)	rat	FITC	eBioscience
ICAM-1 (CD54)	rat	Pe	eBioscience
MMR	rat	Alexa 488	Biozol
MMR	rat	Biotin	Biozol
Streptavidin	streptomyces	PerCP-Cy5.5	BD Pharmingen

2.8 ELISA assays

Assay	Solutions Provided	Solutions Prepared	Standard concentration
Mouse HGF Duo Set R & D Systems	Substrate Solution	Reagent diluent (1 % BSA in PBS) Wash Buffer (0.05 % TWEEN 20 in PBS) Stop Solution (2 N H_2SO_4) PBS	320 ng/ml
Mouse IL-6 Ready-SET-Go! eBioscience	Coating Solution 5 x Assay diluent Substrate Solution	Wash Buffer (0.05 % TWEEN 20 in PBS) Stop Solution (1 M H_3PO_4)	1 µg/ml
Mouse TNFα Ready-SET-Go! eBioscience	Coating Solution 5 x Assay diluent Substrate Solution	Wash Buffer (0.05 % TWEEN 20 in PBS) Stop Solution (1 M H_3PO_4)	1 µg/ml

2.9 Taqman assays

Target mRNA	Assay ID
Daglα	Mm00813830_m1
Daglβ	Mm00523381_m1
Arg1	Mm00475988_m1
FIZZ1 (Retnla)	Mm00445109_m1
GAPDH	Mm99999915_g1
iNOS (NOS2a)	Mm00440485_m1
Ym1 (Chitinase-3-like-3)	Mm00657889_m1
18 sRNA	Hs99999901_s1

3 Methods

This chapter is divided into two parts. The first part explains molecular biological experiments that were conducted to generate the conditional knockout targeting vectors. Additionally, this part contains methods dealing with the cultivation and manipulation of ES cells. All experiments listed in this section were performed in the laboratories of the Institute of Molecular Psychiatry at the University Medical Center Bonn. The second methods section focuses on the isolation and cultivation of primary mouse microglial cells and includes the experimental setup used for the characterization of this cell type.

All manufacturers' protocols mentioned are archived at the Institute of Molecular Psychiatry and are available upon request.

3.1 Molecular biology methods

Methods concerning the cultivation, transformation and long-term storage of *E. coli* were performed according to the protocols of Sambrook, Fritsch and Maniatis (Sambrook, Fritsch and Maniatis, 1989). Agarose gel electrophoresis and detection of DNA in agarose gels by ethidium bromide staining were conducted as described in Molecular Cloning by Sambrook and Russel (Sambrook and Russel, 2001).

3.2 DNA preparation

3.2.1 DNA preparation from *E. coli*

Plasmid DNA was amplified in *E. coli*. In order to isolate plasmid DNA, commercially available Mini and Midi kits for plasmid purification were used. For Mini preparation the plasmid DNA isolation protocol provided in the Quick & Easy Conditional Knockout Kit manual (Genebridges™) was used. For Midi preparation, the GeneElute™ HP Plasmid MidiPrep Kit (Sigma) was utilized according to the manufacturer's instructions.

3.2.2 DNA preparation from ES cells and tissue samples

Cultured ES cells or tissue samples from mouse tail biopsies were incubated overnight in lysis buffer and proteinase K (1 mg/ml) at 56°C on an agitating shaker (550 rpm). Subsequently, the insoluble material was pelleted by spinning down the samples

(16000 *g*, 10 min). After transferring the supernatant into a fresh tube, the DNA was precipitated by adding the same volume of isopropanol. The DNA pellet was then washed twice with 70 % ethanol, air-dried for approximately 30 min and dissolved in TE buffer.

3.2.3 Measurement of DNA concentration

The concentration of DNA preparations was determined using a spectrophotometer. DNA absorbs ultraviolet light at a wavelength of 260 nm (A_{260}). The absorbance of 1 unit at A_{260} is equivalent to a DNA concentration of 50 µg/ml. The purity of a DNA preparation is assessed by the ratio of absorbance at 260 and 280 nm. A pure DNA preparation exhibits an A_{260}/A_{280} ratio of approximately ≈ 1.8.

3.2.4 Purification of DNA fragments

DNA fragments in solution were purified by a phenol-chloroform extraction. Therefore, phenol was added to the sample (1:1). After careful mixing and centrifugation (16000 *g*, 10 min), the supernatant was transferred into a fresh tube and the same volume of phenol/chloroform/isoamylalcohol (25:24:1) was added. This step was followed by careful mixing and centrifugation. The supernatant was supplemented with the same amount of chloroform. Another centrifugation and phase separation step was performed. In order to precipitate the DNA, the sample was mixed with 3 M sodium acetate (1:10) and ethanol (2.5:1). The precipitated DNA was washed twice with 70 % ethanol, air-dried and dissolved in TE buffer.

3.2.5 Digestion of DNA

The sequence-specific cleavage of DNA was performed with restriction endonucleases in their recommended buffer systems. DNA digestion for analytical purposes was performed with 1 µg DNA for 1 h. For preparative digestions the amount of DNA was increased up to 60 µg. In this case the samples were incubated overnight.

3.2.6 Amplification of DNA fragments by polymerase chain reaction

For sequence specific amplification of DNA fragments, polymerase-chain reaction (PCR) was applied. Each PCR reaction was specifically adapted to the temperature requirements of the oligonucleotides and the length of the desired PCR product. Established PCR conditions and a list of oligonucleotides used are provided in the appendix.

3.2.7 PCR conditions for Southern blot probes

The Southern blot probes were labeled by digoxigenin-coupled nucleotides.

Southern blot probe for the identification of positive ES cell clones for DAGLα:

PCR setup (50 µl)

Sterile water	34.5	µl
10 x PCR-buffer	5	µl
Forward primer (probe_a_fwd1, 100 µM)	2	µl
Reverse primer (probe_a_rev1, 100 µM)	2	µl
DIG labeled dNTPs	5	µl
Taq polymerase	1	µl
Daglα BAC DNA (1µg/µl)	0.5	µl

Southern blot probe for the identification of positive ES cell clones for DAGLβ:

PCR setup (50 µl)

Sterile water	34	µl
10 x PCR-buffer	5	µl
Forward primer (probe_b_fwd1, 100 µM)	2	µl
Reverse primer (probe_b_rev1, 100 µM)	2	µl
DIG labeled dNTPs	5	µl
Taq polymerase	1	µl
Daglβ BAC DNA (400 ng/µl)	1	µl

Cycling parameters

1 x	Initial denaturation	94°C	2 min
25 x	Denaturation	94°C	15 s
	Annealing	50.4°C	15 s
	Elongation	72°C	45 s
1 x	Final elongation	72°C	5 min
	Cooling	4°C	∞

Southern blot probe for the identification of DAGLα knockout mice

PCR setup (50 µl)

Sterile water	34.5	µl
10 x PCR-buffer	5	µl
Forward primer (BamHI_fwd1, 100 µM)	2	µl
Reverse primer (BamHI_rev1, 100 µM)	2	µl
DIG labeled dNTPs	5	µl
Taq polymerase	1	µl
Daglα BAC DNA (1µg/µl)	0.5	µl

Cycling parameters

1 x	Initial denaturation	94°C	2 min
25 x	Denaturation	94°C	30 s
	Annealing	56°C	30 s
	Elongation	72°C	45 s
1 x	Final elongation	72°C	5 min
	Cooling	4°C	∞

3.2.8 Southern blot

Identification of homologous recombined ES cell clones and genotyping of mouse tail tissue was performed by Southern blot. With the help of this technique, DNA fragments are specifically detected using digoxigenin-labeled DNA probes. As a first step, genomic DNA was digested with restriction endonucleases overnight. After separation by agarose gel electrophoresis, the DNA was depurinated by treatment with a 250 mM HCl solution for 10 min. This step was followed by denaturation and neutralization for 30 min respectively.

Subsequently the gel was blotted on a nylon membrane at 5 mbar for 1.5 h. In order to immobilize the DNA on the membrane, UV cross-linking was performed. Before adding the probe, the membrane was treated with salmon sperm DNA to block unspecific binding. Hybridization of the membrane with the specific digoxigenin-labeled probe was conducted in a hybridization oven at 68°C overnight.

The next morning, several washing steps followed. At first, the membrane was incubated with 2 x SSC/1 % SDS two times for 10 min at RT on an agitating shaker. Subsequently, the membrane was re-transferred into the hybridization oven and washed (3 x for 10 min) in 0.2 x SSC/0.1 % SDS at 68°C. After equilibration in maleic acid buffer, the blot was incubated in blocking solution for 1 h. At the end of the incubation time, the anti-digoxigenin antibody (1:20000) was added to the blocking solution for about 40 min. Afterwards, the membrane was washed three times with washing buffer (3 x 10 min). After equilibration in detection buffer, the membrane was treated with CDP-Star (Roche, 1:100

in detection buffer) for 5 min. The results were obtained by applying a hyperfilm (Amersham, Pharmacia) on the membrane for about 1 h.

3.2.9 Cloning of target vectors by Red/ET recombination

All oligonucleotides designed to generate the targeting vectors were purchased from Metabion or Invitrogen and are listed in the appendix.

For both targeting vectors, BAC plasmids harboring the genomic sequence of the target genes were used as starting material. As BAC plasmids contain large fragments of DNA, this type of plasmid is very inconvenient to handle. Therefore, the sequence supposed to be modified was subcloned from the BAC plasmid into a vector of smaller size. This was performed using the BAC subcloning kit (Genebridges™). The Genebridges company developed a special cloning technique, called Red/ET technology. This method is based on homologous recombination and enables site-specific cloning that is largely independent of restriction sites. Basically, the recombination is facilitated by a phage-derived protein pair that consists of a DNA annealing protein and a 5'→3' exonuclease. A vector encoding these proteins together with a PCR product obtained from a minimal vector is introduced into *E. coli*. The linearized PCR product is equipped with homology regions flanking the sequence of interest. By addition of 10 % L-arabinose the expression of the recombination proteins is induced and homologous recombination will occur. Subsequent cloning steps were performed with the Red/ET technology as well, using the Quick and Easy Conditional Knock Out Kit (Genebridges™). This kit provides the basic tools for homologous recombination and can be used to insert a set of different selection cassettes into the targeting vector. For convenient cloning these cassettes come with a set of loxP and Frt sites. In order to obtain correctly recombined target constructs, both cloning kits were applied according to the manufacturer's protocol.

3.2.10 RNA preparation

RNA was isolated from frozen brain tissue samples or primary microglial cells for subsequent quantitative gene expression analysis. Brain tissue was transferred into MagnaLyser® tubes and homogenized in TRIzol® (100 mg tissue/1 ml TRIzol®) by vigorous shaking in the Precellys tissue homogenizer. The tissue breakup was interrupted by short incubation steps on ice and repeated several times to ensure complete homogenization. After centrifugation (14000 *g*, 10 min 4°C) the homogenate was transferred into a fresh tube.

Primary microglial cells (6 x 10^5 cells per sample) were collected in TRIzol® and homogenized by pipetting. Subsequently 1-bromo-3-chloropropane (BCP) (1:5) was added and the samples were mixed well by sustained vortexing for 30 s. After 3 min incubation at room temperature and centrifugation (14000 *g*, 10 min, 4°C), the RNA containing upper phase was transferred into a fresh tube. The RNA was then precipitated with isopropanol (1:1) and washed two times with ethanol (75 %). The air-dried RNA pellet of tissue- or cell-isolation was eluted in 100 or 20 µl RNAse-free water, respectively, and stored at -80°C.

3.2.11 Measurement of RNA concentration

The concentration of the isolated RNA was measured using a spectrophotometer. RNA has an absorption maximum at a wavelength of 260 nm (A_{260}).The absorbance of 1 unit at 260 nm is equivalent to a RNA concentration of 40 µg/ml. The purity of the RNA preparation is estimated by the ratio of absorbance at 260 and 280 nm. Pure RNA has an A_{260}/A_{280} ratio of 2.0. Contaminants with different absorption maxima may influence this ratio.

3.2.12 Reverse transcriptase polymerase chain reaction (RT-PCR)

Isolated RNA was transcribed into cDNA by reverse transcription. As a first step the absolute amount of RNA per sample (200-1000 ng) was adjusted to a volume of 10 µl. Subsequently, 1 µl (0.5 µg/µl) of Oligo(dt) primers (Invitrogen) was added to each reaction. The cDNA synthesis was performed with the following master mix and an intermittent cycling program.

Master mix per reaction:

Sterile water	1 µl
5 x first strand buffer	4 µl
DTT (0.1 M)	2 µl
dNTP (10 mM)	1 µl

Cycling parameters:

10 µl RNA (200-1000 ng/ml, dissolved in RNAse-free water) + 1 µl Oligo(dt) primer	
70°C	10 min
4°C	3 min
add 8 µl master mix per sample	
42°C	2 min
4°C	3 min
add 1 µl reverse transcriptase per sample	
42°C	60 min
70°C	15 min
4°C	10 min

The obtained cDNA was adjusted to a concentration of 10 ng/µl and stored at -20°C.

3.2.13 Real-time reverse transcription-PCR (real-time RT-PCR)/ TaqMan gene expression analysis

Real-time RT-PCR is used to quantify the expression level of a certain gene of interest. The TaqMan gene expression analysis is one option for real-time RT-PCR. This method makes use of the so-called FRET method. A short gene-specific oligonucleotide probe, fluorescently labeled at the 5' end (FAM/VIC) and quenched by a non-fluorescent tag (TAMRA/MGB) at the 3' end, is added to the cDNA sample together with an unlabeled pair of primers. During the annealing phase of a PCR reaction, the probe hybridizes with the target sequence. Due to the 5'→3' exonuclease activity of the polymerase, the labeled probe is cleaved during the PCR reaction and the fluorescent signal is no longer quenched. The fluorescent signal increases with each PCR cycle proportionally to the amount of available cDNA template. For relative quantification, the gene expression level of the gene of interest is compared to the gene expression level of a well-characterized and constitutively expressed housekeeping gene.

PCR setup for Taqman gene expression analysis

cDNA (10 ng/µl)	4	µl
Taqman assay	0.5	µl
Taqman assay master mix	5	µl
Sterile water	0.5	µl

Cycling parameters

1x	95°C	10 s
40 x	95°C	15 s
	60°C	60 s

3.3 Cell culture experiments

3.3.1 Cultivation of ES cells

ES cells were grown on a layer of mitotically inactivated mouse embryonic fibroblasts (MEF) at 37°C and 5 % CO_2. At a confluence of approximately 70 %, which corresponds to a growth interval of 48 hours, the ES cells were split in a ratio of 1:5 to 1:10. For this purpose, the ES cells were washed once with HBSS (Hank's buffered salt solution) and incubated with 0.25 % trypsin/EDTA for 3 min at 37°C. After detachment of the ES cells, trypsin was inactivated by adding the same amount of medium. Subsequently, the ES cells were pelleted by short centrifugation (950 *g*, 2 min), re-suspended in fresh medium and distributed on cell culture dishes with fresh feeder cells.

3.3.2 Cultivation of mouse embryonic fibroblasts (MEF)

Mouse embryonic fibroblasts were prepared by Anne Zimmer and Caroline Hamsch (Institute of Molecular Psychiatry). Cells were obtained from embryos at E13.5. In order to receive neomycin-resistant fibroblasts, the embryos were taken from mice carrying a gene for neomycin resistance. Pregnant mice were sacrificed and the embryos were dissected from the uterus. Inner organs and limbs were removed from the embryos and the remaining tissue was chopped up into small pieces. Tissue of up to 12 embryos was incubated in 50 ml 0.25 % trypsin/EDTA for 20 min at 37°C and 5 % CO_2. Every third minute the tube was gently inverted. The digested tissue was then pelleted by centrifugation (950 *g*, 2 min). The pellet was re-suspended in fibroblast medium and plated on a cell culture dish. After 3 to 4 days cells were split in a ratio of 1:4 in order to expand the culture. Another 3 days later, cells were prepared for long-term storage at -80°C.

3.3.3 Deep-freezing and re-cultivation of ES cells

For long-term storage, ES cells were trypsinized and pelleted by centrifugation (950 *g*, 2 min). The pellet was re-suspended in complete medium and freezing medium (1:1) and transferred into cryopreservation vials. The deep-freezing was performed stepwise (4°C/20 min, -20°C/1 h, -80°C/2-3 days). After 2-3 days at -80°C, the cells were transferred into a tank of liquid nitrogen. For re-cultivation, cells were defrosted quickly at 37°C, re-suspended in complete medium and pelleted by centrifugation (950 *g*, 2 min). After re-suspension in fresh medium, cells were dispensed on cell culture dishes containing a monolayer of feeder cells.

3.3.4 Electroporation and selection of ES cell clones

In order to prepare ES cells for electroporation, the cells were expanded on feeder cells in 15 cm cell culture dishes and cultivated until they reached a confluence of 70 %. Two hours before starting the electroporation protocol, the medium was changed. Cells were then harvested by trypsinization and washed twice with HBSS. Subsequently, the cell number was determined using a hemocytometer. 2 x 10^7 cells were used per electroporation. After counting, the cells were spun down (950 *g*, 2 min) and re-suspended in the appropriate volume of HBSS to reach a cell concentration of 2 x 10^7 cells in 0.8 ml. Finally, 20 µl of linearized plasmid DNA (1 µg/µl) were added, the suspension was transferred into an electroporation cuvette and the cells were elcetroporated (500µF, 250 V). Afterwards the mixture was incubated on ice for 10 min and dispensed on 15 cm cell culture dishes supplied with feeder cells.

Selection for neomycin resistance was started 24 h after electroporation by adding geneticin- (G418) containing selection medium to the cells. The selection period took 7-9 days. During this time, the medium was changed daily. Remaining ES cell colonies were transferred into 96-well plates (1 colony per well). Each colony was trypsinized for 3 min at 37°C and 5 % CO_2 to obtain a single cell suspension. Afterwards, the ES cells of one colony were dispensed into one well of a 24-well plate, which had been prepared with feeder cells in advance. The medium was changed every 24 h for the next 3 days. Clones were harvested by trypsinization and re-suspended in 1 ml freezing medium. About 700 µl of the cell suspension were transferred into a new well of a 24-well plate, mixed with complete medium (1:1) and prepared for deep-freezing. The rest of the cell suspension (300 µl) was dispensed into the original well and cultivated further for subsequent DNA preparation.

3.3.5 Isolation of primary microglial cells

Primary mouse microglial cells were isolated from newborn C57BL/6J (Charles River) mice at postnatal days 1-5. The mice were decapitated and the brains were dissected. Subsequently, the two hemispheres were separated and delivered from the meninges. The cortical regions were purified and transferred into HBSS. Cortices of up to 70 mice were pooled and the tissue was homogenized by pipetting up and down. This step was followed by an incubation step on ice for 5 min to sediment insoluble fragments. Afterwards, the supernatant was transferred into a fresh tube. Alternatively the homogenizing step was repeated until no insoluble fragments remained. The homogenate was spun down (1200 *g*, 5 min), re-suspended in microglia medium and plated into poly-L-lysine coated cell culture flasks (2.5 hemispheres = 1 ml homogenate/ flask). After 24 h,

the medium was changed for the first time. During the cultivation period (37°C, 8 % CO_2), the medium was renewed every third day. The time needed to reach complete confluence varied between different preparation batches (14-30 days).

3.3.6 Harvesting and re-plating of primary microglia

Up to now, a variety of protocols for the isolation and cultivation of primary microglia is available from the literature, one of the earliest was published by Giulian and Baker in 1986. The majority of protocols uses cortices from newborn mice or rats. The minced tissue is then further cultivated for different time periods, until a confluent mixed glial culture is formed. In order to collect microglia from this culture, mainly two different approaches are used. In the “shaking method” described by Giulian and Baker, microglial cells are detached from the confluent cell layer by incubation on an agitating shaker. This method yields a population of microglia with a purity of up to 98 %, but the obtained cell number is comparably low with 10 % of the starting material (Giulian & Baker 1986). Saura and colleagues developed a harvesting method, in which the confluent layer is detached by mild trypsinization (Saura et al. 2003), whereas microglial cells stay attached to the bottom of the cell culture flask. This population of microglia is then detached by a second incubation with trypsin at a higher concentration. As stated by Saura and colleagues, this method is supposed to yield up to five times more microglia compared to the shaking method. In this work, the “shaking-” as well as the “trypsinization method” were tested.

3.3.6.1 Detachment of microglia by mild trypsinization (“trypsinization method”)

In order to enrich microglia from the mixed glial culture described in section 3.3.5, microglial cells were harvested by mild trypsinization. Therefore, the mixed cell culture was washed once with HBSS before adding a mixture of DMEM, high glucose and 0.25 % trypsin/EDTA (1:2). After an incubation time of 15-20 min at 37°C and 8 % CO_2, the confluent monolayer started to detach in large patches. The detached patches were removed by aspiration and the remaining cells were washed again with HBSS. Next, the resident cells were incubated with 0.25 % trypsin/EDTA for 5 min at 37°C and 8 % CO_2. The digestion by trypsin was blocked by adding the same amount of complete microglia medium. To make sure that the remaining cells can be collected completely, the flasks were scratched with a cell scraper. The harvested cells were pooled and counted in a hemocytometer. After centrifugation (1200 *g*, 5 min), the cell pellet was re-suspended in fresh microglia medium and dispensed into 24-well plates at a density of 1.5-2 x 10^5 cells/ml.

3.3.6.2 Detachment of microglia by mechanical shaking ("shaking method")

The procedure described here represents a modified version of the protocol developed by Giulian and Baker (Giulian & Baker 1986). As stated in the preceding section, microglia were collected from mixed glial cultures, when the cell layer in the culture flask had reached complete confluence. Microglia were then detached from the confluent layer by shaking on an agitating shaker (550 rpm) for 2 h at RT. Subsequently, the cell culture medium was collected from each flask. Detached cells in the medium were spun down (1200 *g*, 5 min) and re-plated into 24-well plates at a density of 1.5-2 x 10^5 cells/ml.

3.3.7 Stimulation experiments

Stimulation of microglial cells with different substances was started one day after re-plating the cells into 24-well plates, as described in the preceding section. For stimulation, all substances used were diluted in microglia medium to obtain the appropriate concentrations and subsequently added to the medium. Microglial cells were incubated with interleukin-4 (IL-4), interleukin-10 (IL-10) or TGFβ for 48 h, respectively. LPS and IFNγ were applied overnight. Unstimulated cells served as controls. For each condition, cells of at least 3 wells of a 24-well plate were treated. After the stimulation time had elapsed, cells were prepared for flow cytometry staining or TaqMan gene expression analysis. Supernatants were collected separately, shock-frozen in liquid nitrogen and stored at -20°C.

3.3.8 Staining for flow cytometry

All antibodies used were diluted 1:200 in FACS buffer (2 % FCS in PBS, sterile filtered). During the staining procedure, samples were permanently kept on ice and shielded from direct light. First, microglial cells had to be collected from 24-well plates by incubating them with a PBS solution containing 2 mM EDTA and 0.1 % FCS. Detachment of the cells was accelerated by pipetting up and down. The harvested cells were spun down (5500 *g*, 5 min, 4°C) and washed once with FACS buffer. In order to block unspecific binding of the antibodies to Fc-receptors, an Fc-block (CD16/CD32) (1:300) was applied for 15 min, followed by washing and centrifugation as described before. Next, the cells were incubated (15 min) with a mixture of directly labeled antibodies. Depending on their fluorescent tag, up to 5 antibodies were combined.

After incubation with the primary antibodies, the washing and centrifugation steps were repeated once more. If biotin-coupled antibodies were included in the mixture of primary antibodies, a second labeling-step (15 min) with PerCP-Cy5.5 coupled streptavidin was necessary. Hereafter, another washing step with FACS buffer and subsequent

centrifugation was performed. Finally, the cells were re-suspended in 200 µl FACS buffer and filtered through a mesh of gauze, to exclude aggregated cells. Flow cytomtry was performed using a FACS Canto II (BD Biosciences), equipped with FACSDiva software (BD Biosciences). Data analysis was performed using FlowJo software, Version 9.5.2 (Tree Star Inc.).

3.4 ELISA assay performance

Supernatants of stimulated microglial cells were collected and shock-frozen before the cells were prepared for flow cytometry staining or TaqMan gene expression analysis. In order to check for different patterns of cytokine release, the samples were tested in several ELISA assays. The assays were performed according to the manufacturer's protocols. The procedure described here, represents the standard protocol provided by ebioscience. Differing instructions provided by the protocol of R & D Systems are specified in brackets.

In general, MaxiSorp® flat-bottom 96-well plates, purchased from Nunc, were coated with the appropriate capture antibody. Therefore, the antibody was diluted 1:250 in coating buffer and the 96-well plate was filled with 100 µl antibody solution per well. The coating step was performed overnight at 4°C (RT). The next day, the 96-well plate was washed 5 times (3 times) with 200 µl (400 µl) washing buffer per well. This was followed by a blocking step with 200 µl (300 µl) assay diluent per well for 1 h at RT. The blocking step was followed by washing, as described before. Afterwards, 100 µl of standard and samples were pipetted into the wells and incubated for 2 h at RT. Dilutions of the samples were prepared, if necessary, in cell culture medium. Samples and standard concentrations were tested as duplicates. After washing, the appropriate detection antibody was diluted 1:250 in assay diluent. 100 µl of the diluted antibody was added to each well. An incubation of 1 h (2 h) at RT and subsequent washing was followed by 30 min (20 min) incubation with an antibody coupled to streptavidin-HRP, which was diluted 1:250 in assay diluent. Subsequently, the plate was washed 7 times (3 times), filled with 100 µl substrate solution per well and incubated for 15 min (20 min) at RT. The reaction was stopped by the addition of 50 µl 1 M H_3PO_4 (2 N H_2SO_4) per well. The samples were analyzed at 450 nm in a microplate reader.

3.5 Array-based gene expression profiling

Stimulated microglial cells were analyzed for differential gene expression by array-based gene expression profiling. The following steps were conducted by the group of Prof. Dr. Joachim Schultze (Laboratory for Genomics and Immunoregulation, LIMES Institute, Bonn). Sorting of stimulated microglia by FACS (Aria III cell sorter, BD Biosciences) was followed by RNA extraction and subsequent cRNA preparation. For genome wide expression analysis of the mouse genome, MouseWG-6 v2 Expression BeadChips (Illumina Inc.) were utilized. Microarray analysis was conducted using an Illumina iScan Array Scanner (Illumina Inc.). The obtained data were analyzed using Partek Genomic Suite V6.6 Microarray Analysis Software (Partek Inc.). After normalization, transcripts with variable expression and genes that displayed differential expression between different conditions were calculated using two-way ANOVA including batch correction. Differentially expressed (DE) genes were defined by a fold change (FC) greater 2 and an unadjusted p-value < 0.05.

3.6 Animal experiments

For the generation of the new mouse lines, the infrastructure of the animal facility at the University Medical Center of Bonn was engaged. The animal facility represents a standardized S1 (Sicherheitsstufe 1, §§4-7 GenTSV) environment. Blastocyst injections for the generation of chimeric mice were performed in collaboration with the microinjection service of the animal facility. Work routines concerning animal care and breeding were approved by legal authorities (Landesamt für Natur, Umwelt und Verbraucherschutz NRW). All procedures described, were conducted in compliance with national regulations (Tierschutzgesetz v 18.5.2006 BGBI. I S. 1206, 1313) (letzte Änderung Art. 20 G 9.12.2010 (BGBI. I S. 1934, 1940 f.) and institutional guidelines. Breeding pairs consisted of one or two female and one male animal. Litters were weaned and ear-tagged at day 21 after birth. In general, animals were group-housed with up to six animals per cage and had free access to food pellets and drinking-water.

3.6.1 Tissue preparation

Mice were sacrificed and the desired tissue was dissected rapidly. Tissue integrity was preserved by immediately shock-freezing the samples in ice-cooled isopentane. Until further processing, tissue samples were kept at -80°C.

3.6.2 Lipid measurement by mass spectrometry (LC-MS/MS)

Hippocampal tissue of a wild type animal and a Dagl$\alpha^{ko/ko}$ animal was prepared as described in the preceding section. The following steps were conducted by Dr. Ermelinda Lomazzo and Dr. Laura Bindila (Prof. Beat Lutz, Institute of Physiological Chemistry, University Medical Center, Mainz). Endocannabinoids were extracted from homogenized frozen brain tissue samples. Endogenous 2-AG levels were measured employing a 5500 QTrap® triple-quadrupole linear ion trap mass spectrometer (AB SCIEX). For quantification, triplicate calibration curves were run. Quantification of 2-AG was performed using Analyst 1.6.1 software. The obtained data were normalized to the tissue weight.

3.6.3 Generation of chimeric mice

Chimeric animals were generated by blastocyst injection. Therefore, correctly recombined ES cell clones were cultivated and dispersed prior to injection, in order to obtain a single cell suspension. ES cell clones on a C57BL/6 background were injected into blastocysts on Balb/C background. ES cell clones on 129Sv background were injected into blastocysts on a C57BL/6 background. After injection of ES cells, the blastocysts were re-transferred into pseudo pregnant foster animals (Balb/C or C57BL/6, respectively). Chimeric animals were recognized by coat-color. Injection of C57BL/6 ES cells that had been injected into Balb/C-derived blasotcysts led to the generation of chimeric animals with black-white brindled fur. ES cells on 129Sv background that had been injected into C57BL/6 balstocysts led to the generation of chimeras with black-agouti mixed fur color. Chimeras were mated with wild type mice on a C57BL/6 background. Germ-line transmission of the genetic manipulation was also observed by coat color differentiation (black for C57BL/6 ES cells, agouti for 129/Sv ES cells).

3.6.4 Animal breeding

The targeting constructs contained a neomycin resistance gene, flanked by FRT sites to facilitate positive selection of the ES cell clones. In order to excise this gene in the animals, mice carrying the FRT-flanked neomycin gene (DAGL$\alpha^{wt/fl}$) were mated with mice expressing the FLP recombinase under the human β-actin promotor (Rodríguez et al. 2000). This mouse line was kindly provided by Dr. Tobias Goller (Institute of Molecular Immunology, LIMES Institute, Bonn). In offspring that had inherited the gene encoding FLP recombinase, FLP-mediated recombination occurred and led to a ubiquitous deletion of the neomycin resistance gene. The conditional knockout approach of the targeting constructs enabled a cell type-specific deletion of the targeted gene. Thus, as a next

breeding step, mice devoid of the neomycin gene were crossed with different mouse lines, which express the Cre recombinase under a cell type-specific promotor. To achieve a complete loss of the targeted gene, Pgk1-Cre mice were chosen (Lallemand et al. 1998). For neuron-specific deletion, Syn1-Cre mice, purchased from The Jackson Laboratory (Zhu et al. 2001), were utilized. A third breeding colony with LysM-Cre mice was set up, to facilitate a loss of function of the targeted gene in myeloid cells such as granulocytes and macrophages (Clausen et al. 1999). This Cre line was kindly provided by Dr. Luisa Klotz (Institute of Molecular Medicine and Experimental Immunology, University Medical Center, Bonn).

3.6.5 Nomenclature of mouse lines

Genetic modifications are indicated as superior letters adjacent to the respective gene name. For discrimination of hetero- or homozygosity, both alleles are illustrated, separated by a forward slash. Unmodified homozygous wild type animals were indicated by the description wt. The abbreviation ko indicates a knockout of the respective gene. The abbreviation fl stands for “floxed”, which means “flanked by loxP sites”

Identifier	**heterozygous**	**homozygous**
knockout	$gene^{wt/ko}$	$gene^{ko/ko}$
floxed (flanked by loxP sites)	$gene^{wt/fl}$	$gene^{fl/fl}$

3.6.6 Behavioral experiments

All behavioral experiments were conducted in the animal facility of the University Medical Center of Bonn. 8-10 week old C57BL/6 wild type animals, $CB_1^{ko/ko}$ and $Dagl\alpha^{ko/ko}$ animals on C57BL/6 background were bred in-house. Both male and female animals were tested.

3.6.6.1 Open field test

The open field test is a behavioral paradigm commonly used to assess locomotor activity and exploratory behavior of rodents. The set up shown in Figure 4 consists of an infrared beam-operated open field arena (45 x 45 x 23 cm), which is placed in a sound-attenuated environment. The infrared-beam enables the tracking of the animal’s movement. At the beginning of a test session, the animal was placed in a corner of the arena. Subsequently, the movements of each animal were recorded for 30 min. The test was performed under dim-light conditions. Generally, 4 parameters are evaluated at the same time. These

parameters include the time spent moving (s), the distance travelled (m) by the animal during the test-session, the number of rearings (n) and the time spent (s) in the center of the arena. The analysis of the distance travelled and time spent moving reveals potential deficits in locomotor activity, whereas the time spent in the center of the arena is commonly interpreted as an indicator for anxious behavior. Thus, anxious animals would spend more time at the walls or in the corners than exploring the open area.

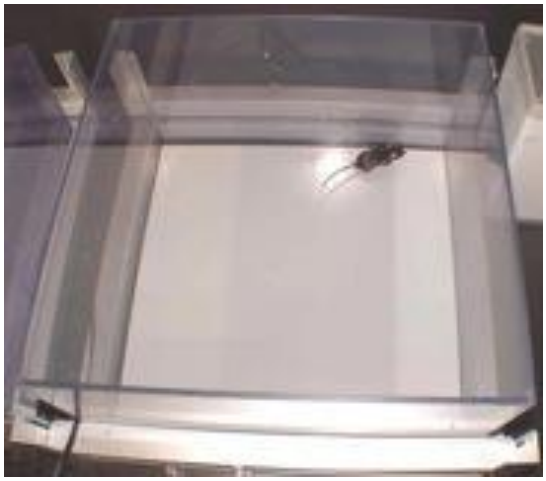

Figure 4: Top view on an infrared beam-operated open field arena. The animal's locomotor activity was tracked for 30 min in a sound-attenuated environment under dim-light conditions

The behavior of Daglα$^{ko/ko}$ animals was tested in the open field. C57/BL6 wild type animals served as controls.

3.6.6.2 Hot plate test

The hot plate test is used to analyze the acute pain reaction of rodents to a noxious heat stimulus. As shown in Figure 5, an animal was placed into an acrylic glass cylinder on a heated surface (52°C). The latency (s) from time point zero (placing the animal on the surface) to the first pain reaction (shaking of the hind-paw) was measured. If the animal did not show a pain reaction, the animal was removed from the heated plate after 30 s. In order to reveal potential differences in pain sensitivity, Daglα$^{ko/ko}$ mice were tested in this paradigm. C57BL/6 wild type mice served as controls.

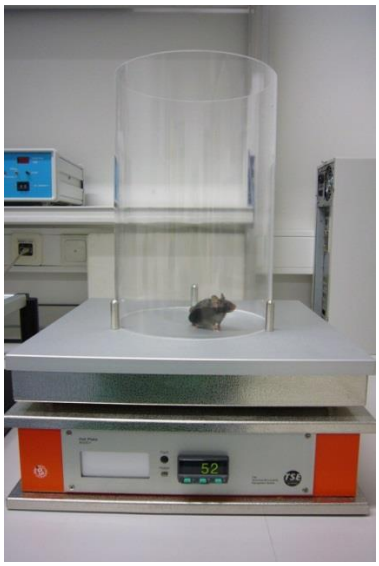

Figure 5: Hot plate test device. The animal was placed on a heated surface (52°C). Next, the latency to the first pain reaction (shaking of the hind-paw) was measured

3.6.6.3 Fear conditioning paradigm

Fear extinction is a process, which leads to a decline of conditioned fear responses. In order to study this phenomenon, a behavioral paradigm based on the principle of Pavlovian fear conditioning was used. In this paradigm, a neutral auditory stimulus (tone, conditioned stimulus) is paired with an aversive stimulus (electric foot-shock, unconditioned stimulus). Animals exposed to these stimuli will learn to associate the tone with the unpleasant experience of the shock and will later express fear, even when the tone is presented alone. In rodents, freezing behavior indicates fear. Freezing is defined as a “cessation of all bodily movements except those required for respiration” (Myers & Davis 2007). A decline in fear response and thus in freezing behavior is achieved, when the tone is presented several times without application of another foot-shock. This effect is referred to as fear extinction. The paradigm conducted in this work consisted of a fear conditioning trial and several extinction trials, as schematically illustrated in Figure 6. Fear conditioning was performed on day 0. The subsequent extinction trials (E1-E3) were performed at 3 consecutive days starting 24 h after the conditioning trial. No extinction trial was performed on day 4 and 5. Extinction trial E6 was conducted on day 6 after fear conditioning. Another extinction trial, termed recall was performed on day 7. Therefore, the animal was placed into the cage where it had received the foot-shock. During the recall it received 180 s of tone presentation after a habituation of 300 s.

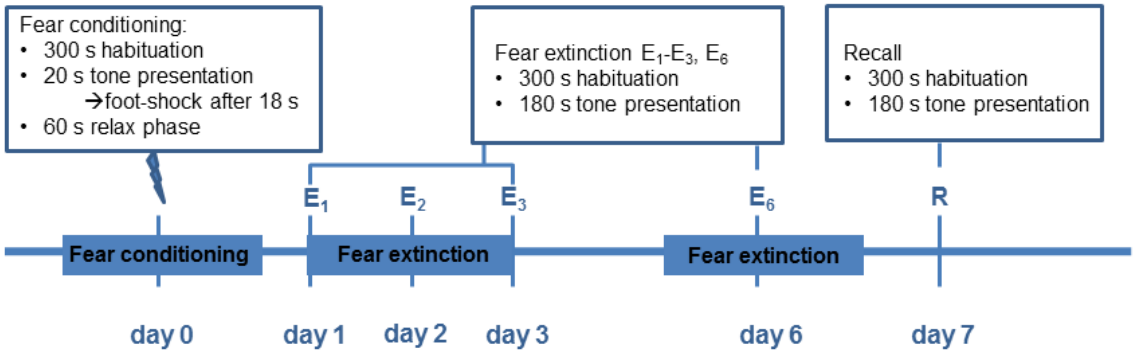

Figure 6: Experimental set up of the fear extinction paradigm. Fear conditioning was performed on day 0. Fear extinction training started 24 h later and was performed at the first 3 consecutive days, as well as on day 6 after fear conditioning. On day 7, a recall was performed

The fear conditioning at day 0 was performed as follows. The test animal was placed in a small cage with a metal grid and transferred into a sound-isolated box (Figure 7) to avoid disturbances from the environment. After a habituation period of 300 s, a tone of 9 kHz, (conditioned stimulus) was presented for 20 s with an intensity of 80 dB. Between the 18th and 20th second, a brief electric foot-shock of 0.7 mA was applied (unconditioned stimulus). The shock was followed by a relaxing phase of 60 s. Subsequently, the animal was returned to the home cage for 24 h.

For the extinction trials E1-E6, the animal was placed into a glass beaker and re-transferred into the sound-isolated box. The habituation period (300 s) was now followed by 180 s of tone presentation (9 kHz, 80 dB). During extinction, no foot-shock was applied. Movements of mice were measured by vibration-sensitive transducer platforms.

For the recall trial performed at day 7, the animal was placed into the metal cage that had been used for fear conditioning at day 0. The animal was re-transferred into the sound-proof box and an extinction trial, consisting of 300 s habituation and 180 s of tone presentation, was performed.

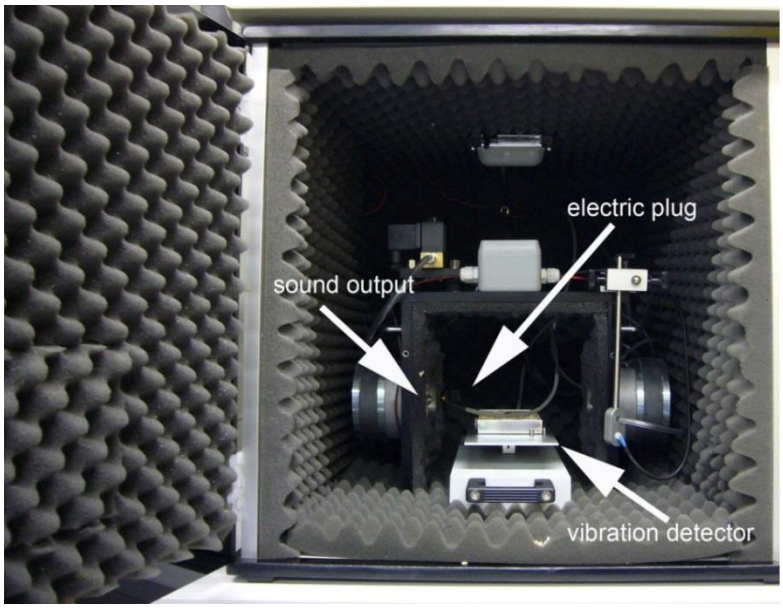

Figure 7: Startle response box used for the fear conditioning paradigm. The set up consisted of a sound-protected box equipped with an electric device for the application of the foot-shock, loud speakers for tone presentation and a vibration-sensitive platform, which detected the animal's movements

Vibrations caused by the movements of the test animal were recorded during all extinction trials and the recall trial. Periods of immobility that exceeded 2 s were considered as freezing behavior. The percentage of time that the animal spent freezing during a test session was calculated for each trial and served as an indicator for the decline in fear response from one session to the next (between-session extinction). In addition, the course of freezing behavior during a single extinction trial was analyzed. Therefore, the 180 s of tone presentation was divided into 60 s intervals. (0-60 s, 61-120 s, 121-180 s). The percentage of time spent freezing was calculated for each interval separately. The decline in freezing response over the whole period of tone presentation within one session served to analyze within-session extinction. Both, $CB_1^{ko/ko}$ animals as well as $Dagl\alpha^{ko/ko}$ animals were analyzed in this paradigm. C57BL/6 wild type animals served as control animals, respectively.

3.7 Statistical analysis

Behavioral data were analyzed using Student's t-test or two-way repeated measures ANOVA. In the case of a significant main effect, detected by two-way repeated measures ANOVA, a Bonferroni's *post-hoc* test for pair-wise comparison was performed. A p value of $p < 0.05$ (*) was considered as statistically significant. Lower p values (** $p < 0.01$, *** $p < 0.001$) were considered to be highly significant. GraphPad Prism software (Version 5.0d, GraphPad Software Inc.) was used for the analysis of behavioral data.

Data obtained from experiments with microglial cells were analyzed using GraphPad Prism, as well. For determination of statistical significance, one-way ANOVA was used. Significant ANOVA was followed by Bonferroni's *post-hoc* test for group-wise comparison. A p value of $p < 0.05$ (*) was considered as statistically significant. Lower p values (** $p < 0.01$, *** $p < 0.001$) were considered to be highly significant.

4 Results

The results section of this thesis is divided into two parts. Initially, the generation of conditional knockout mice for Daglα and Daglβ is described. The respective targeting constructs were generated using the Cre-loxP recombination system of Genebridges™, which enables a cell type specific deletion of the targeted gene region. In a second section, results of the primary microglial cell culture establishment as well as the characterization of different microglia activation states are presented.

4.1 Generation of conditional knockout mice for Daglα and Daglβ

Comprehensive analysis of Bisogno and colleagues revealed that the genes encoding the two isoforms of the diacylglycerol lipases DAGLα and DAGLβ share extensive regions of homology, but differ concerning length and sequence of their catalytic domain. In addition to four transmembrane domains, sequence analysis predicted a serine-lipase motif and a lipase-3 motif, which catalyze the conversion of diacylglycerol (DAG) to 2-AG. The corresponding genes are found in a variety of species and are highly conserved between man and mouse (Bisogno et al. 2003).

The murine Daglα gene (gene ID: ENSMUSG00000035735) is located on chromosome 19 on the reverse strand and comprises 20 exon, out of which the first exon is untranslated. The gene encoding Daglβ (gene ID: ENSMUST00000045593) is found on the forward strand of chromosome 5 and contains 15 exons. Concerning the Daglβ gene, the translation starts within the first exon. An illustration of the respective gene structure is depicted in Figure 8.

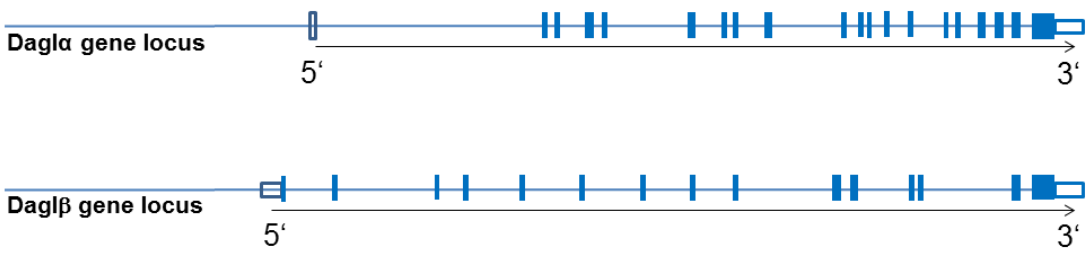

Figure 8: Gene structure of the murine form of Daglα and Daglβ. Daglα (top) consists of 20 exons and is located on chromosome 19 on the reverse strand. Daglβ (bottom) comprises 15 exons and is found on the forward strand of chromosome 5. Filled blue boxes represent translated exons. Empty boxes depict untranslated exons

For the generation of the Daglα and Daglβ conditional knockout targeting vectors, the same cloning strategy was chosen. The respective first exon and a sequence compassing about 1 kb at the 5' end of the first exon was selected to be flanked by loxP sites. This approach enables a Cre recombinase-mediated loss of the targeted region. A detailed description for the generation of both targeting vectors is given in the following sections.

4.1.1 Generation of the Daglα targeting vector

For the generation of the Daglα targeting vector, the Red/ET technology (Genebridges™) was employed. Each step of the construction process is depicted in Figure 9. The BAC clone RP23-13J22 harbored a fragment of the Daglα gene and served as donor plasmid for the creation of the Daglα subclone. First, the minimal vector composed of a ColE1 origin and a gene for ampicillin resistance was flanked by short homology sequences (50 bp) by PCR. These short regions were homolog to sequences of the Daglα gene locus confining the subcloning region (Figure 9 a). At both ends of the targeting construct, restriction sites for Sal I were introduced. The Daglα subclone consisted of a long homology arm (5.6 kb) upstream of exon 1 and a short homology arm (2.8 kb) at the 3' end of the first exon (Figure 9 b). Next, a loxP-flanked neo cassette mediating neomycin resistance was introduced upstream of exon 1, as depicted in Figure 9 c. Subsequently, the neo cassette was removed by Cre-mediated recombination in *E. coli*. After Cre-mediated recombination, one loxP site remained in the sequence (Figure 9 d). The insertion of another neo cassette completed the targeting construct. This selection cassette was flanked by FRT sites and an additional loxP site at its 3' end (Figure 9 e).

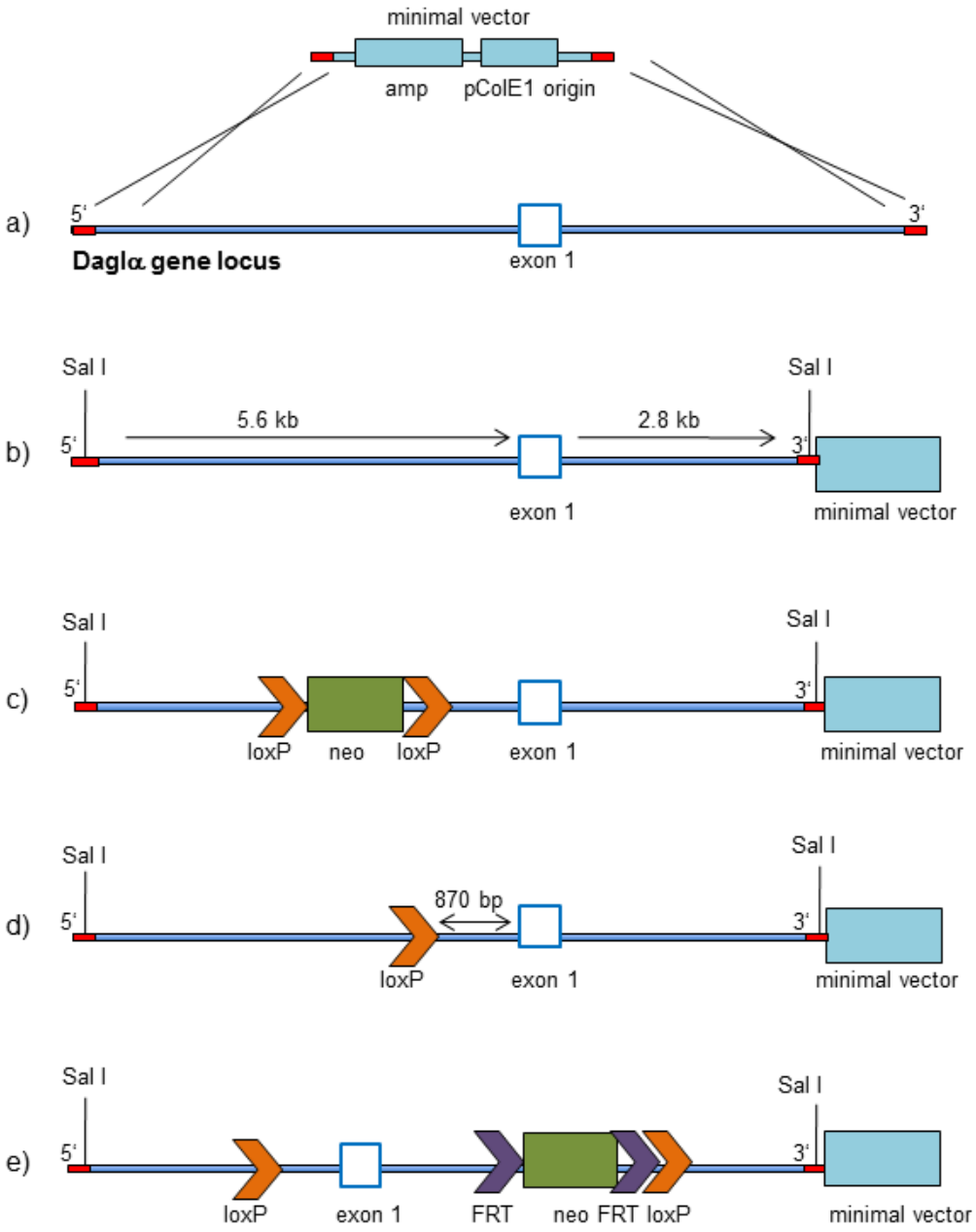

Figure 9: Cloning strategy of the conditional knockout vector for the murine Daglα gene locus. a) An 8.4 kb fragment flanking the first exon of the Daglα gene was introduced into a minimal vector by homologous recombination. b) The subcloned gene region included a 5.6 kb fragment at the 5' end of exon 1 and a fragment of 2.8 kb at its 3' end. Restriction sites of Sal I confined the subcloning region. c) A neo cassette (green) flanked by loxP sites (orange) was inserted upstream of exon 1. d) After Cre-mediated recombination in *E. coli*, one loxP site remained upstream of the first exon. e) At the 3' end of the first exon, a second neo cassette flanked by FRT sites (purple) and with an additional loxP site was inserted into the targeting vector

Each cloning step was verified by analysis of a specific restriction pattern. Respective gel documentation of each cloning step is given in the appendix 5.7A.3. A representative result for Spe I digestion of the entire targeting vector is depicted in Figure 10. The complete targeting vector contained 3 restriction sites for Spe I (Figure 10 a). Therefore, Spe I digestion was supposed to result in the generation of 3 DNA fragments (767 bp,

1480 bp and 10647 bp). As shown in Figure 10 b (lane 2), these fragments were detectable after Spe I digestion of the complete targeting vector. In comparison, the undigested vector was loaded in lane 1.

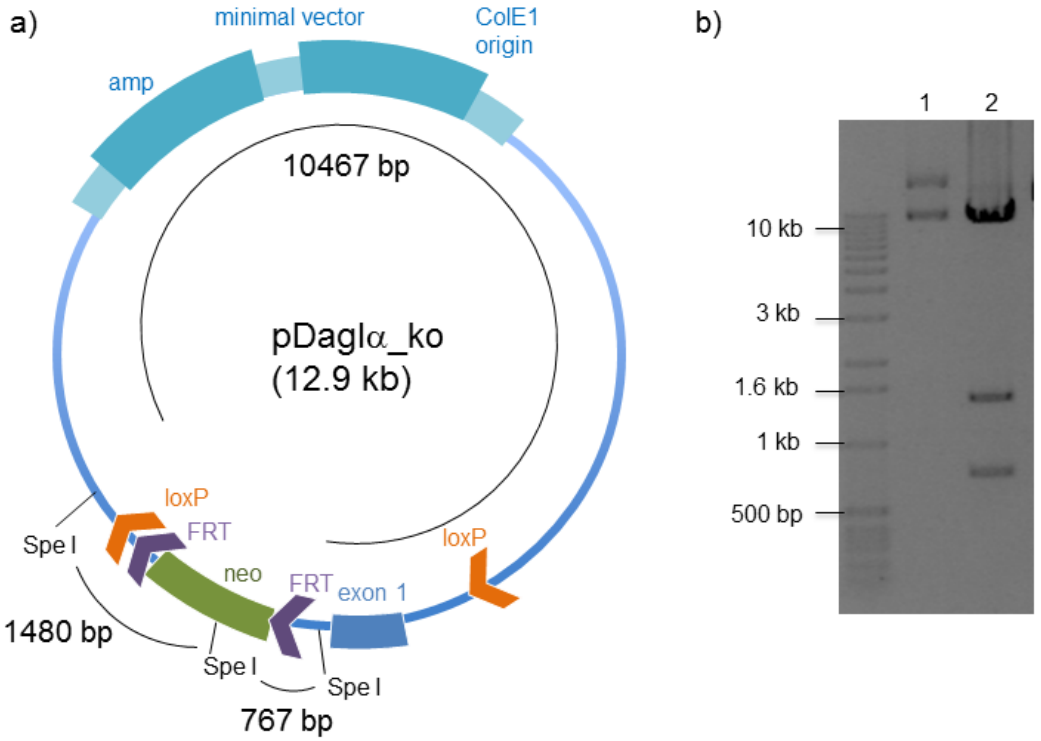

Figure 10: Analysis of a specific restriction pattern of the Daglα targeting vector. a) The Daglα targeting vector contained 3 restriction sites for Spe I, resulting in the generation of 3 DNA fragments upon Spe I digestion. Fragment sizes are indicated. b) Digestion of the complete targeting vector by Spe I resulted in the generation of the expected fragments. lane 1: undigested vector, lane 2: Spe I digested vector. amp: ampicillin resistance, loxP: loxP site, FRT: FRT site, neo: gene mediating neomycin resistance, pDaglα_ko: Daglα targeting vector

The orientation of the two loxP sites, as well as the location of the neo cassette was tested for accuracy by sequence analysis (Macrogen Corporation).

4.1.2 Screening strategies for targeted mutagenesis of the Daglα gene locus

For electroporation into ES cells, the targeting vector was digested with Sal I. Positive ES cell clones were selected via G418 resistance. Neomycin resistant ES cell clones were checked for homologous recombination at both ends of the targeting construct. Initial screening was performed using Southern blot. As shown in Figure 11, digestion of selected ES cell clones with Pst I resulted in a 4 kb fragment for the Daglα wild type locus. Upon homologous recombination at the 3' end, an additional restriction site for Pst I was used, resulting in a smaller fragment of about 3 kb. To exclude ectopic recombination, the

probe was located within a genomic region, which was not included in the targeting construct. ES cell clones that exhibited homologous recombination at the 3' end, were further analyzed for the presence of the loxP site upstream of exon 1. For this purpose, a PCR strategy was developed, as shown in Figure 11. A pair of primers (red arrows) flanking the loxP site generated a size specific PCR product. Thus, the unmodified wild type locus yielded a PCR product of about 630 bp, whereas the PCR product resulting from the targeted gene locus comprised about 680 bp. The size difference arose from the loxP sequence (34 bp) and two additional restriction sites (Not I and Xho I), which were inserted together with the loxP-flanked neo cassette and remained after Cre-mediated recombination. The Daglα targeting construct harboring the loxP site served as positive control, while DNA of the unmodified Daglα BAC clone RP23-13J22 was used as negative control.

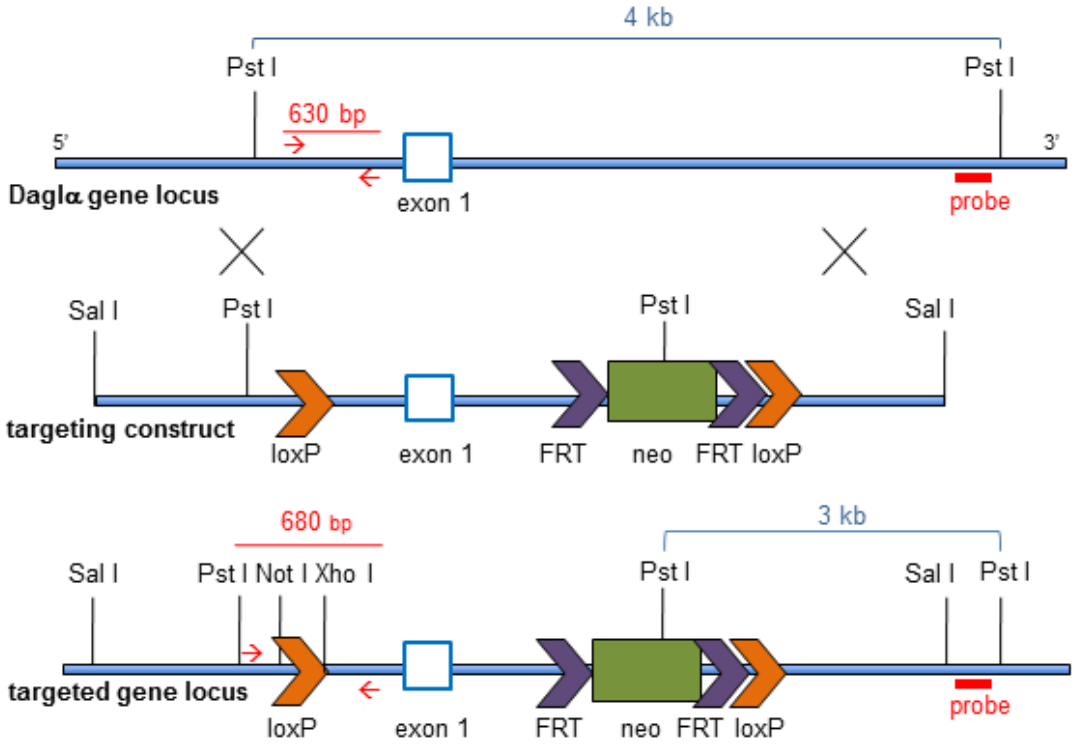

Figure 11: Targeted mutagenesis of the murine Daglα gene locus. Depicted are the wild type Daglα gene locus (top), the targeting construct (center) and the targeted gene locus (bottom). After homologous recombination, a loxP site (orange) upstream of the first exon and a FRT-flanked neo cassette (green) with an additional loxP site (orange) were inserted into the wild type Daglα gene locus. Prior to electroporation into ES cells, the targeting construct was digested with Sal I. Correct recombination was confirmed by Southern blot using the restriction sites for Pst I and the sequence-specific probe depicted in red. The resulting fragments are shown as blue brackets. Red arrows indicate the pair of primers used for verification of the 5' loxP site. The wild type gene locus (top) yielded a PCR product of about 630 bp. Insertion of the loxP site led to an extended PCR product of about 680 bp (bottom)

The targeting construct was introduced into murine ES cells via electroporation. Here, MPI2 ES cells on a 129Sv background and C57BL/6 derived Bruce4 ES cells were used.

Altogether about 700 ES cells clones were screened by Southern blot out of which 8 were positive for homologous recombination at the 3' end. Figure 12 a shows a representative Southern blot for Pst I digested ES cell DNA. Clone EP 226 # 31 displayed a wild type fragment at 4 kb and a fragment at 3 kb, indicating the modified allele. According to the targeting strategy (Figure 11) clone EP 226 # 31 was heterozygous for the targeted Daglα gene locus, whereas the other clones shown in Figure 12 a, displayed only the wild type fragment.

As explained earlier, screening of the targeted clones for the 5' loxP site was performed by PCR. The resulting PCR products of two representative ES cell clones are shown in Figure 12 b. Correctly recombined ES cell clones were heterozygous for the targeted allele. Thus, clone EP 225 # 153 and clone EP 226 # 83 displayed a wild type fragment (630 bp) and the loxP-containing fragment of the targeted locus at 680 bp.

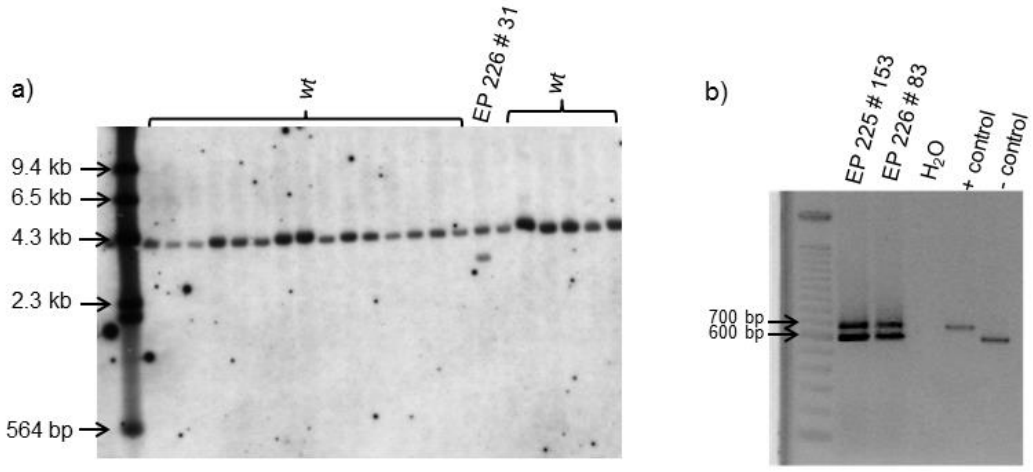

Figure 12: Verification of targeted ES cell clones for Daglα. a) Representative Southern blot for verification of homolgous recombination at the 3' end. All clones exhibited the wild type fragment at a size of 4 kb. Homologous recombination had occurred only in clone EP 226 # 31 and resulted in the expected restriction pattern of 4 kb (wild type locus) and 3 kb (targeted gene locus). b) Verification of the 5' loxP site by PCR. Simlar to the wild type DNA (- control), clone EP225 #153 and clone EP226 # 183 displayed a band at 630 bp. A second fragment with a size of 680 bp was produced from the loxP-containing allele. – control: unmodified BAC DNA, + control: Daglα targeting vector

All recombined clones identified by Southern blot are listed in Table 1. Verification of the 5' loxP site revealed complete homologous recombination for 4 out of 8 clones. These clones were used for subsequent injections into blastocysts.

Table 1: Summary of recombined ES cell clones for Daglα. All clones were tested for complete recombination by Southern blot and by PCR. Altogether, 4 clones were identified to harbor the complete targeting construct. EP: electroporation (continuous numbering of electroporations performed in the laboratory, # number of the respective clone)

Label	Genetic background	
EP181 # 68	129Sv	
EP181 # 137	129Sv	complete recombination
EP181 # 279	129Sv	
EP 225 # 140	C57BL/6	
EP 225 # 153	C57BL/6	complete recombination
EP 226 # 3	C57BL/6	complete recombination
EP 226 # 31	C57BL/6	
EP 226 # 83	C57BL/6	complete recombination

4.1.3 Generation of the Daglβ targeting vector

For the Daglβ gene locus, the same targeting strategy as described for Daglα was applied. The first exon of the gene and an upstream region of about 1.3 kb was flanked by loxP sites (Figure 13). For the generation of the targeting vector, the Red/ET technology (Genebridges™) was utilized. The BAC clone RP23-453H13 contained a fragment of the Daglβ gene locus and served as donor plasmid for the generation of the Daglβ subclone. The minimal vector was flanked by short DNA fragments, which were homolog to the Daglβ gene locus and confined the subcloning region. In addition, these short regions of homology contained restriction sites for Sal I. Homologous recombination between the modified minimal vector and the Daglβ BAC clone generated the Daglβ subclone. The targeting vector had a long homology arm upstream of exon 1 (7.4 kb) and a short homology arm distal of exon 1 (3.2 kb) (Figure 13 a-b). A loxP site upstream of the first exon was introduced by insertion and subsequent excision of a loxP-flanked neo cassette (Figure 13 c-d). Subsequently, a second selection cassette was inserted at the 3' end of exon 1. This FRT-flanked neo cassette facilitated neomycin-selection in the ES cell culture. Furthermore, the cassette contained a second loxP site at the 3' end. Thus, the insertion resulted in the loxP-flanked state for exon 1 and completed the conditional targeting vector for Daglβ (Figure 13 e).

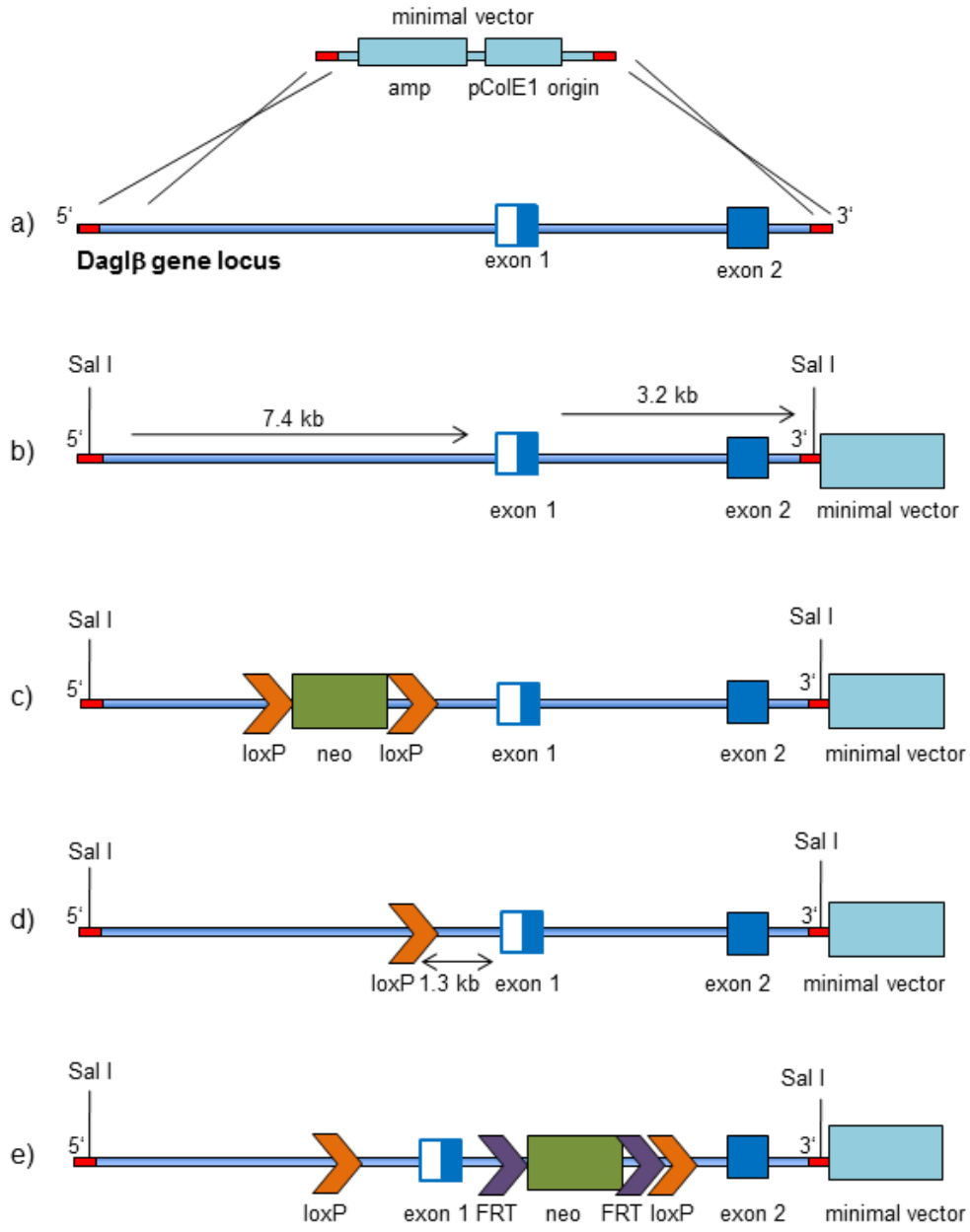

Figure 13: Cloning strategy for the conditional knockout targeting vector for Daglβ. As shown in a) a fragment of the Daglβ gene comprising the first and the second exon was subcloned into the minimal vector. b) The 5' homology arm included a sequence of about 7.4 kb, whereas the 3' homology arm downstream of exon 1 compassed 3.2 kb. At both sides, restriction sites for Sal I defined the subcloned sequence. c) A neo cassette (green) flanked by loxP sites (orange) was introduced upstream of the first exon. Subsequent Cre-mediated recombination in *E. coli* resulted in only a single loxP site, as shown in d). The following insertion of a neo cassette flanked by FRT sites (purple) with an additional loxP site at the 3' end completed the targeting vector (e)

As stated for the Daglα construct, the cloning of the Daglβ targeting vector was repeatedly checked by specific restriction pattern analysis. The corresponding gel documentation is found in the appendix 5.7A.5. A representative result of the targeting vector digested by Xho I is shown in Figure 14. The expected pattern of generated fragments is depicted in Figure 14 a. The targeting vector contained 4 restriction sites for Xho I, resulting in the generation of 4 DNA fragments upon Xho I mediated cleavage. These fragments were detectable on an agarose gel after Xho I digestion of the Daglβ targeting vector and subsequent gel electrophoresis (Figure 14 b, lane 2). The smallest fragment was detected at 187bp, although the staining of this fragment was comparably weaker. In lane 1 the undigested vector was loaded.

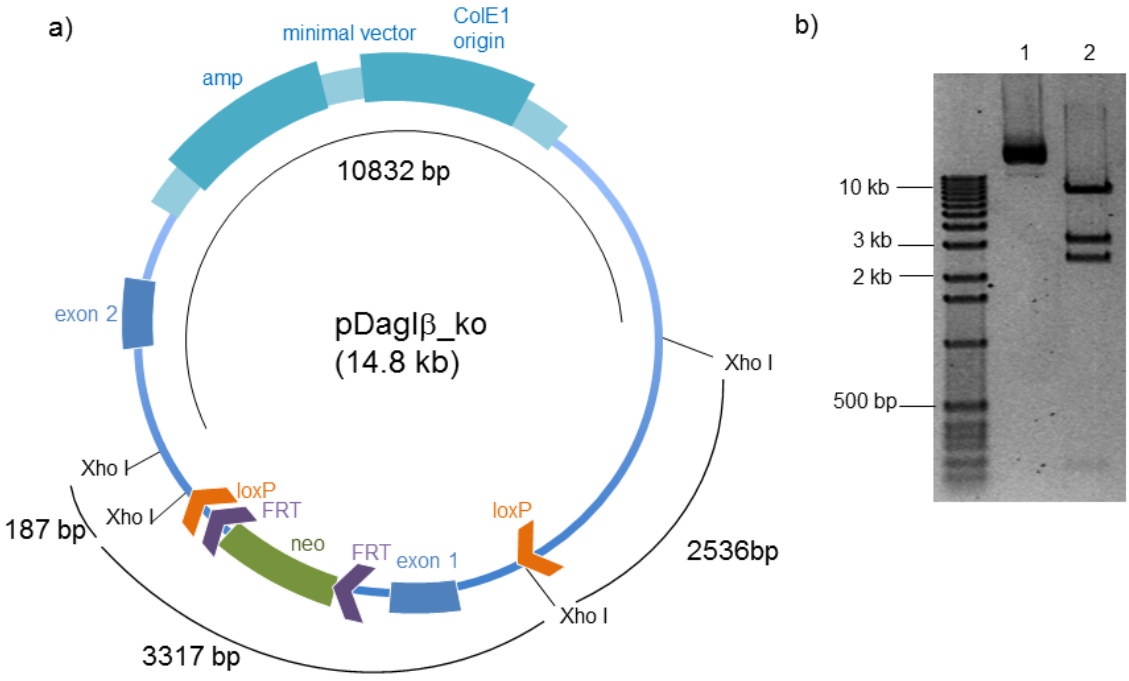

Figure 14: Analysis of a specific restriction pattern of the Daglβ targeting vector. a) The Daglβ targeting vector contained 4 restriction sites for Xho I, resulting in the generation of 4 DNA fragments upon Xho I digestion. Fragment sizes are indicated. b) Digestion of the complete targeting vector by Xho I resulted in the generation of the expected fragments. lane 1: undigested vector, lane 2: Xho I digested vector. amp: ampicillin resistance, loxP: loxP site, FRT: FRT site, neo: gene mediating neomycin resistance, pDaglβ_ko: Daglβ targeting vector

The orientation of the two loxP sites, as well as the location of the neo cassette was tested for accuracy by sequence analysis (Macrogen Corporation).

4.1.4 Screening strategies for targeted mutagenesis of the Daglβ gene locus

After digestion with Sal I, the targeting vector was electroporated into ES cells. Screening for homologous recombination was performed by Southern blot analysis based on the targeting strategy illustrated in Figure 15. Digestion of the Daglβ wild type gene locus with Nsi I generated a fragment of 5 kb. Due to the fact that the targeted Daglβ gene locus harbored the neo cassette (1.7 kb), the restriction pattern for Nsi I was altered. As a consequence, Nsi I digestion of the targeted gene locus resulted in a fragment of 6.7 kb. The sequence-specific probe shown in Figure 15 was directed against a genomic region outside of the targeting construct to ensure site-specific recombination. The ES cell clones identified by Southern blot were further analyzed for the presence of the 5' loxP site. The PCR strategy applied for this purpose was based on the same principle as explained for Daglα in section 4.1.2. Concerning the Daglβ gene locus, the expected PCR products had a size of about 700 bp for the wild type locus and 750 bp for the modified locus harboring the loxP site.

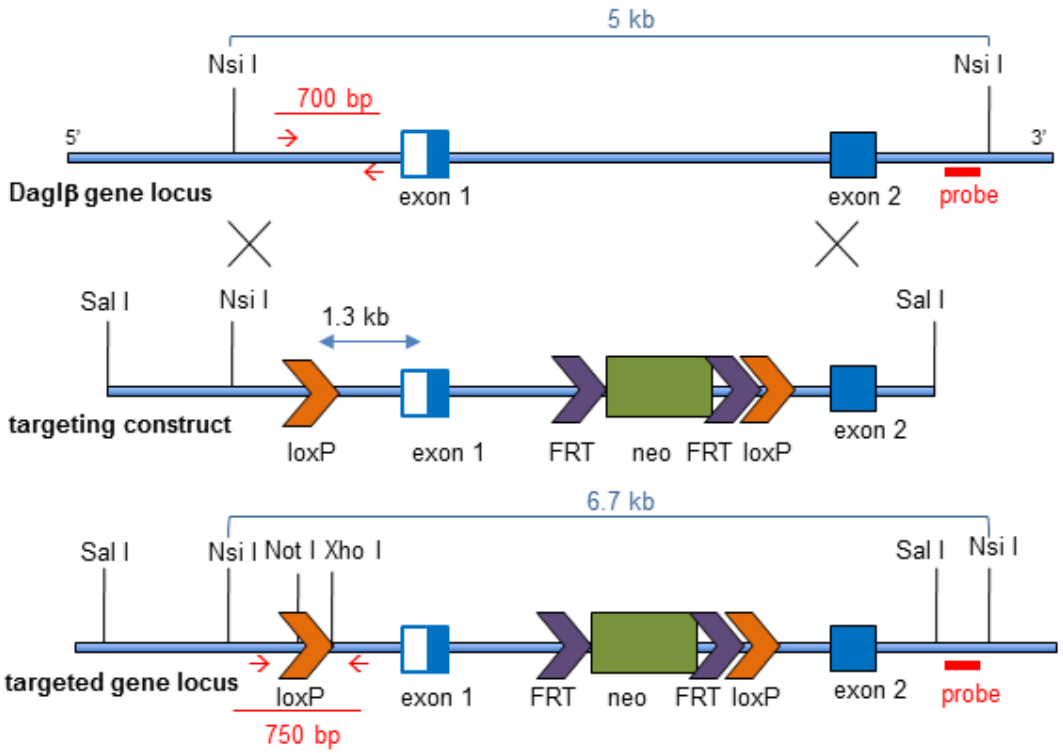

Figure 15: Targeted mutagenesis of the murine Daglβ gene locus. A part of the Daglβ wild type gene locus is illustrated in the upper scheme. The targeting construct (center) consisted of a loxP site (orange) upstream of exon 1 and a FRT-flanked neo cassette with an additional loxP site downstream of the first exon. For electroporation into ES cells, the targeting construct was digested by Sal I. Homologous recombination resulted in the targeted gene locus (bottom). Successful recombination was verified by Nsi I digestion and subsequent Southern blot using the probe shown in red. The primer pair (red arrows) for verification of the 5' loxP site yielded a PCR product of 700 bp (top) for the wild type locus and 750 bp for the targeted allele (bottom)

Fifteen electroporations were performed for the Daglβ targeting construct, using the ES cell lines MPI2 (129Sv) and Bruce4 (C57BL/6). All in all, 1260 ES cell clones were screened by Southern blot. Out of 390 MPI2 clones, no recombined ES cell clone was detected. In contrast, 7 ES cell clones on C57BL/6 background displayed the expected restriction pattern after Nsi I digestion. A representative Southern blot is depicted in Figure 16 a. Clone EP 1002 # 163 was heterozygous for the targeted gene locus with a wild type fragment at 5 kb and a fragment at 6.7 kb for the targeted allele. Subsequently, screening for the 5' loxP site was performed by PCR. A representative PCR result is shown in Figure 16 b. For clone EP 217 # 106, two PCR products of the expected sizes were detected. The Daglβ targeting construct comprising the 5' loxP site was taken as positive control. DNA of the BAC clone RP23-453H13 devoid of the loxP site served as negative control. Thus, this clone was heterozygous for the 5' loxP site.

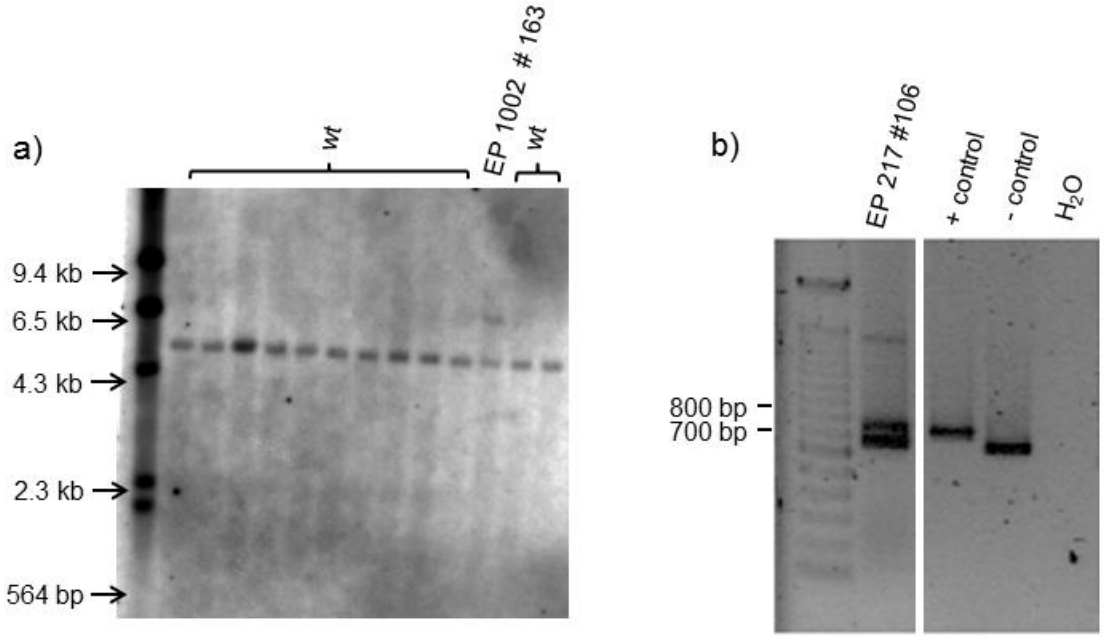

Figure 16: Verification of targeted ES cell clones for Daglβ. After Nsi I digestion, all clones displayed a wild type fragment of 5 kb. Clone EP 1002 # 163 additionally exhibited the restriction pattern for the targeted allele at 6.7.kb. b) PCR with primers flanking the 5' loxP site yielded two PCR products for clone EP 217 # 106. The lower fragment represented the wild type allele at 700 bp. The upper fragment (750 bp) resulted from the modified locus containing the loxP site. + control: Daglβ targeting construct, - control unmodified BAC DNA

A summary of the recombined ES cell clones is shown in Table 2. All clones were identified by Southern blot analysis and tested for the presence of the 5' loxP site by PCR. The completely recombined clones were subsequently used for blastocyst injections.

Table 2: Summary of recombined ES cell clones for Daglβ. All clones were tested by Southern blot for recombination at the 3' end and for the presence of the 5' loxP site by PCR. In 4 out of 7 clones identified by Southern blot, the 5' loxP site was detected. EP: electroporation (continuous numbering of electroporations performed in the laboratory, # number of the respective clone

Label	Genetic background	
EP185 # 38	C57BL/6	complete recombination
EP185 # 72	C57BL/6	
EP185 # 158	C57BL/6	
EP185 # 162	C57BL/6	
EP 217 # 106	C57BL/6	complete recombination
EP 1000 # 68	C57BL/6	complete recombination
EP 1002 # 163	C57BL/6	complete recombination

4.1.5 Generation of chimeric mice

Homologous recombinant ES cell clones were obtained for both targeting constructs, which were repeatedly injected into blastocysts. Injection of clone EP181 # 137 (Daglα, 129/Sv, fur color agouti) into C57BL/6 blastocysts yielded 6 chimeric animals (1 female, 5 male) that displayed a mixed fur color of black and agouti. A representative 129Sv/C57BL/6-chimera is shown in Figure 17 a. The degree of chimerism was judged by coat color and varied between 5 and 90 %. Furthermore, for clone EP226 # 3 (Daglα, C57BL/6, fur color black), two male chimeras (BalbC/C57BL/6) were obtained. These animals were identified by black and white brindled fur and displayed a degree of chimerism of about 50 and 85 %, respectively. One of these chimeras is depicted in Figure 17 b. Concerning the Daglβ targeting construct, one chimeric animal (BalbC/C57BL/6) was generated by blastocyst injection of clone EP 217 # 106 (Daglβ, C57BL/6, fur color black). The degree of chimerism of this animal was estimated around 85 %.

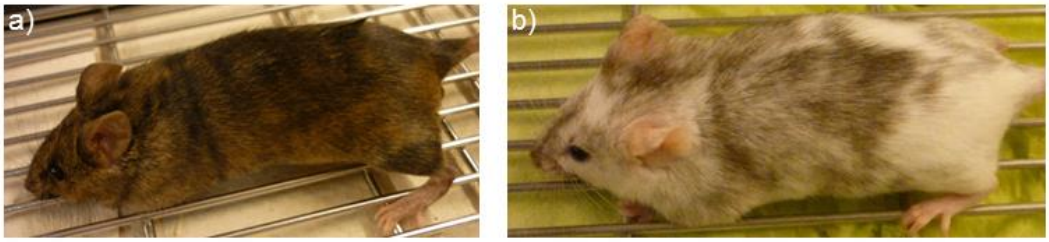

Figure 17: Chimeric animals obtained from blastocyst injection. a) Chimeric animals obtained from injection of 129/Sv ES cell clones into C57BL/6 blastocysts displayed black-agouti mixed fur. b) Injection of C57BL/6 ES cells into Balb/C blastocysts resulted in chimeras with black-white brindled fur

Chimeric animals were backcrossed with wild type mice on a C57BL/6 background. Successful germ-line transmission was indicated by the coat color of the offspring. For Daglα clones on a 129/Sv background, mouse pups with agouti-colored fur indicated germ-line transmission, whereas for Daglα clones on C57BL/6 background, germ-line transmission was revealed by black fur. Although the chimeric animal for the Daglβ targeting construct displayed a high percentage of chimerism, the genetic modification was not transmitted to its progeny. In contrast, germ-line transmission was successful for the Daglα targeting construct. The offspring of Daglα chimeric mice was analyzed for the genetic modification by Southern blot and PCR as exemplarily shown in Figure 18. Animals which had inherited the genetic modification exhibited a heterozygous genotype (wt/fl). Southern blot analysis revealed the same restriction pattern as for the corresponding ES cell clone. The wild type allele was detected as a fragment of 4 kb, whereas the targeted allele yielded a fragment of 3 kb (Figure 18 a). Screening for the 5’ loxP site yielded two PCR products for heterozygous animals (wt/fl), indicating the presence of the 5’ loxP site in the targeted allele (Figure 18 b).

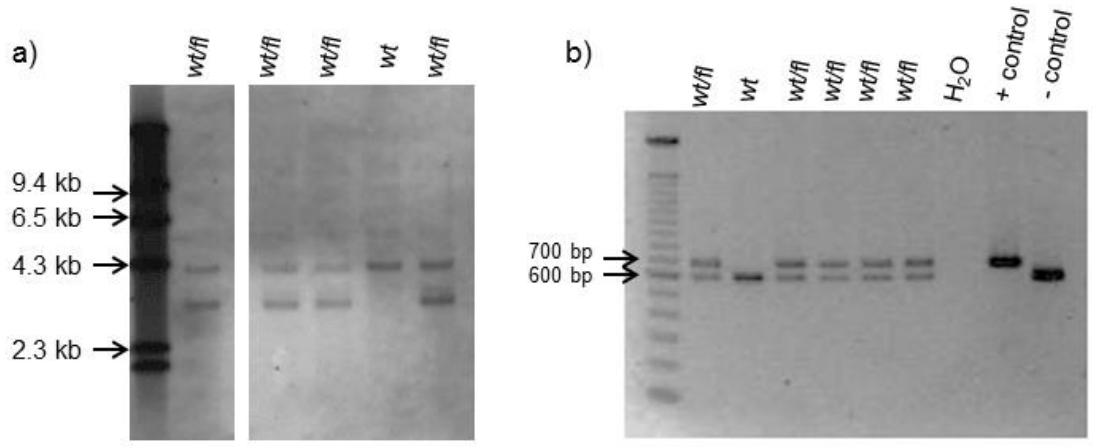

Figure 18: Germ-line transmission of the Daglα targeting construct. To confirm germ-line transmission of the genetic modification, the progeny of chimeric mice was analyzed by Southern blot (a) and by PCR (b). Offspring that had inherited the genetically engineered allele, displayed a heterozygous genotype (wt/fl). wt: wild type allele; fl: floxed allele. – control: unmodified BAC DNA, + control: Daglα targeting vector. For the corresponding targeting strategies see section 4.1.2

4.1.6 Establishment of conditional knockout mouse lines for Daglα

The neo cassette present in the targeting construct was necessary to mediate G418-resistance and thus to select recombined ES cell clones. To exclude possible alterations in gene expression, the neo cassette was removed from the genome after selection. Thus, subsequent to the verification of germ-line transmission, the offspring of chimeric mice was mated with FLP-deleter mice (C57BL/6 genetic background). In this mouse strain, the FLP recombinase is expressed under the human β–actin promotor (Rodríguez et al. 2000). Inheritance of the FLP recombinase thus leads to a ubiquitous deletion of the FRT-flanked neo cassette. The PCR strategy applied for the analysis of the resulting genotype is shown in Figure 19. To obtain PCR products of different sizes, the primers were placed at both ends of the neo cassette. The unmodified wild type allele was supposed to yield a PCR product of 443 bp, whereas the targeted allele harboring the neo cassette would produce a fragment of about 2.1 kb. After FLP recombination, the targeted allele devoid of the neo cassette generated a PCR product of 570 bp. Heterozygous floxed Daglα mice ($Dagl\alpha^{wt/fl}$) were mated with FLP-deleter mice and subsequently checked for FLP-mediated recombination.

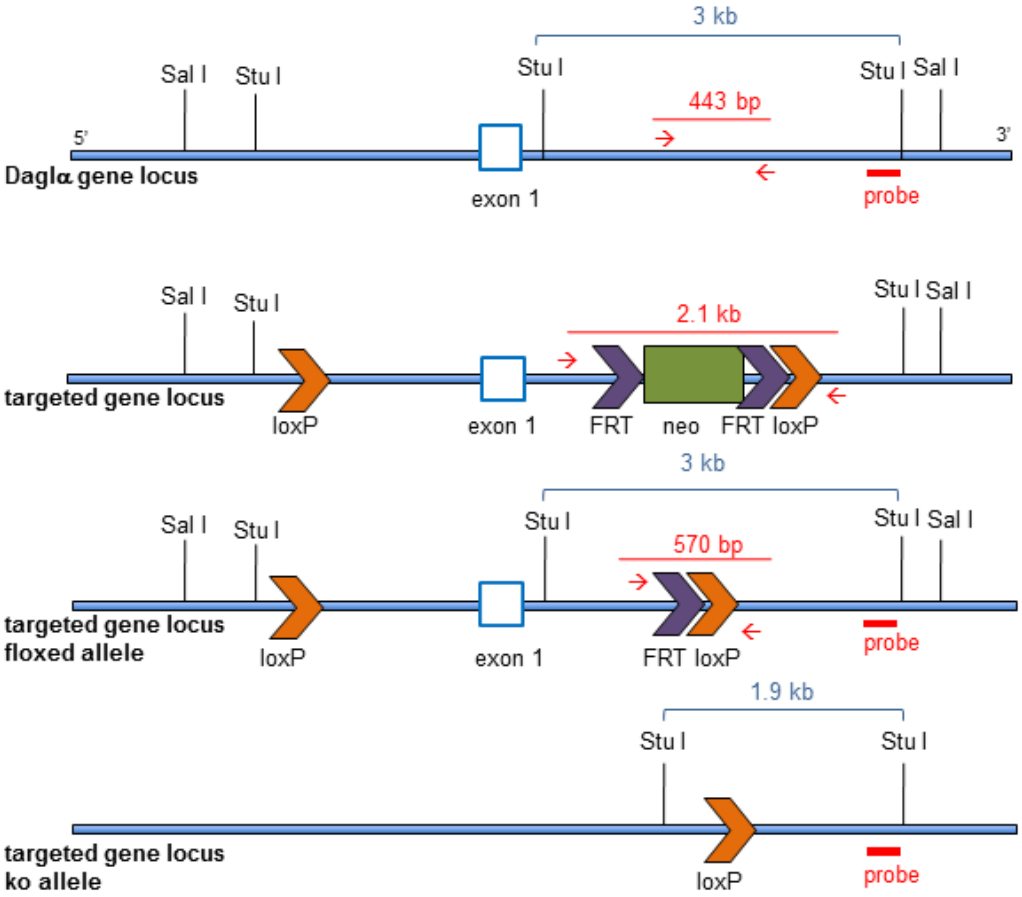

Figure 19: Strategies for the verification of FLP- and Cre-mediated recombination in Daglα knockout mice. Confirmation of FLP-mediated recombination by PCR: Dependent on the genotype, PCR with a primer pair (red arrows) flanking the neo cassette generated PCR products of different sizes. The wild type allele (top) led to a PCR product of 443 bp, whereas the presence of the neo cassette in the targeted gene locus (center) generated a fragment of 2.1 kb. After FLP-mediated recombination (bottom), a PCR fragment of 570 bp was generated. Verification of Cre-mediated recombination by Southern Blot: After Stu I digestion, the Southern blot probe detected a 3 kb fragment for the wild type (top) as well as for the floxed allele (center). Cre-mediated recombination led to an excision of the floxed genomic region, thereby decreasing the expected fragment length to 1.9 kb

Figure 20 a exemplarily illustrates the PCR results for 3 heterozygous animals (Daglα$^{wt/fl}$). Due to the hemizygous breeding of the FLP-deleter mice, only a part of the offspring inherited the FLP recombinase and FLP-mediated recombination occurred in these animals. This was indicated by a PCR product of 570 bp as shown in Figure 20 a in the first and the third lane. In the second lane, only the wild type fragment was observed. This animal was negative for the FLP recombinase and thus FLP-mediated recombination did not occur. However, the animal tested here was expected to be heterozygous for the modified gene locus including the neo cassette. Therefore, the PCR fragment indicating the presence of the neo cassette (2.1 kb) should also be detectable in this mouse. However, the neo cassette was not detected in heterozygous animals by this PCR

strategy. In contrast, this fragment was generated, when DNA samples from homozygous animals were tested, in which both alleles contained the neo cassette (Figure 20 b).

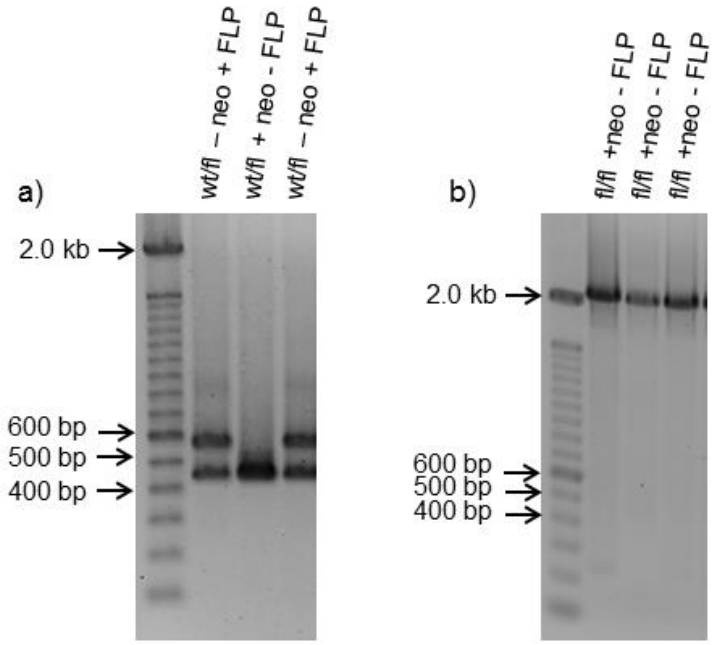

Figure 20: Verification of FLP-mediated recombination by PCR. PCR results for heterozygous animals are exemplarily shown in a). The wild type fragment (443 bp) was amplified for all samples. A second fragment at 570 bp was amplified for samples applied in the first and the third lane. A PCR product at this size indicated successful FLP-mediated recombination. For the results shown in the second lane, no fragment at a size of 2.1 kb was detected, although the neo cassette was present for one allele. b) Homozygous floxed animals were tested by PCR for the presence of the neo cassette. Here, a fragment of 2.1 kb was produced, whereas a wild type fragment was not detectable. wt: wild type, fl: floxed, neo: neomycin-cassette, FLP: FLP recombinase

Offspring which was positive for FLP-mediated recombination was further bred with several Cre-expressing mouse lines. To obtain a constitutive knockout of Daglα, the Pgk1-Cre line (Lallemand et al. 1998) was utilized. As Cre activity would lead to the excision of the floxed gene region, another strategy for verification of the resulting sequence had to be established, as explained in Figure 19. DNA samples, prepared from mouse tail biopsies, were digested with Stu I prior to Southern blot analysis. The unmodified wild type Daglα locus was subsequently detected as a 3 kb fragment. After successful Cre-mediated recombination, a fragment of 1.9 kb was detected. A representative Southern blot for the verification of Cre-mediated recombination is shown in Figure 21. The DNA fragments of a wild type animal Daglα$^{wt/wt}$ (left lane), a heterozygous knockout animal (Daglα$^{wt/ko}$, center) and a homozygous knockout animal (Daglα$^{ko/ko}$, right lane) are depicted. The wild type fragment was detected at 3 kb. After Cre-mediated recombination of the targeted allele, a second fragment at 1.9 kb was produced.

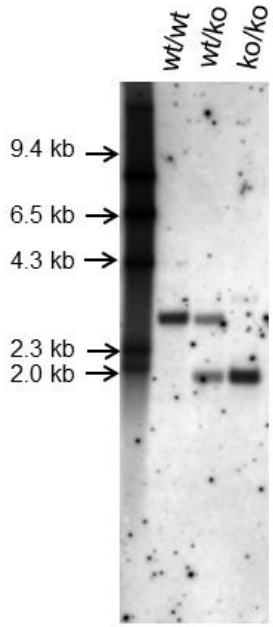

Figure 21: Verification of Cre-mediated recombination by Southern blot after Stu I digestion. A single fragment of 3 kb presented the wild type Daglα gene locus (left lane). DNA analysis of a heterozygous knockout animal (center) resulted in two fragments (wild type fragment of 3 kb, knockout fragment of 1.9 kb). A homozygous knockout animal (right lane) displayed a single fragment at 1.9 kb. wt: wild type, ko: knockout. The corresponding Southern blot strategy was introduced in Figure 19

4.1.7 Quantitative expression analysis

As shown in Figure 21, Cre activity resulted in the excision of the floxed gene region. As a next step, the functionality of the knockout was demonstrated by TaqMan gene expression analysis. If successful, the knockout strategy would completely erase mRNA transcription of the Daglα gene. The TaqMan assay used was purchased from Applied Biosystems (Mm00813830_m1). The location of the corresponding probe (green) is schematically presented in Figure 22. The probe is directed against the cDNA sequence of exon 8 and 9.

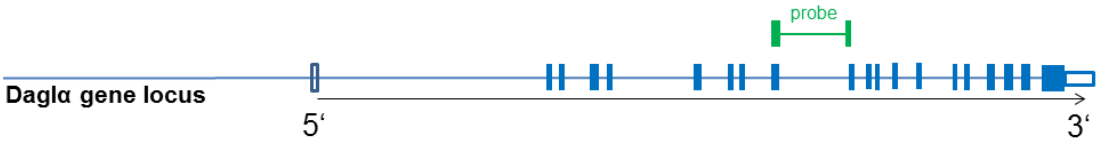

Figure 22: Schematic illustration of the Daglα TaqMan assay Mm00813830_m1. This assay was used to analyze the Daglα gene expression level in Daglα knockout animals. The probe spans the exon junction between exon 8 and 9. (Source: http://bioinfo.appliedbiosystems.com/genome-database)

For verification of the Daglα knockout, RNA was isolated from 3 different brain parts of a homozygous knockout animal (Daglα$^{ko/ko}$) and a wild type animal (Daglα$^{wt/wt}$). After

transcription into cDNA, the samples were analyzed by TaqMan. Two independent experiments were performed (Daglα$^{ko/ko}$ n = 2, Daglα$^{wt/wt}$ n = 2). The gene expression level of 18sRNA served as housekeeping control. In Figure 23 a representative result of a performed TaqMan assay is visualized. In wild type brain tissue, Daglα cDNA was detected from cycle 24 onwards (average Ct value 24.35), whereas in knockout brain tissue Daglα cDNA was detected later than cycle 34 (average Ct value 34.8), indicating a virtual absence of Daglα mRNA. Ct values greater than 35 approach the sensitivity limits of the real time PCR system and correspond to less than 10 copies of the target molecule (see: manufacturer's protocol of TaqMan gene expression assays, Applied Biosystems by Life Technologies). Therefore, the expression level of the Daglα gene in the Dagla$^{ko/ko}$ animal was close to the dection limit.

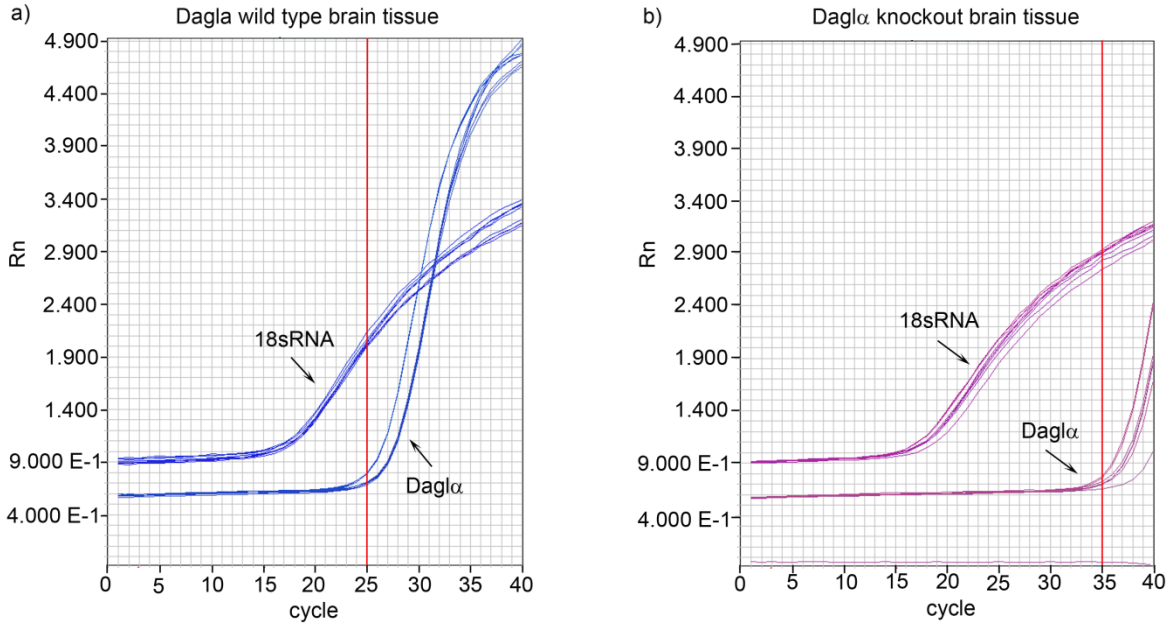

Figure 23: Representative amplification plots of Daglα wild type and knockout brain tissue. 18sRNA served as housekeeping control. In wild type brain tissue Daglα cDNA was detected from cycle 24 onwards (average Ct value 24.35). In brain tissue of the tested Daglα$^{ko/ko}$ animal, Daglα cDNA was detected later than cycle 34 (average Ct value 34.8), indicating a strong reduction in Daglα mRNA. Rn: Reporter fluorescence at cycle n

4.1.8 Measurement of 2-AG levels

DAGLα is the main 2-AG synthesizing enzyme in the adult brain. The complete loss of Daglα gene function will thus result in decreased 2-AG levels. The corresponding DAGLβ enzyme is still present in Daglα knockout animals. This enzyme is downregulated after development. Therefore, it accounts only for a minor part of 2-AG synthesis. Besides the gene expression analysis of Daglα in the respective knockout animals, the measurement of 2-AG levels in the brain was an important indicator for a functional knockout. Determination of 2-AG content in a Daglα$^{ko/ko}$ animal was performed by Dr. Ermelinda

Lomazzo and Dr Laura Bindila, members of the group of Prof. Beat Lutz (Institute of Physiological Chemistry, Johannes Gutenberg University Medical Center, Mainz). Figure 24 shows the results obtained for the measurement in hippocampal tissue. Hippocampal tissue of 5 wild type animals served as control tissue. On average the wild type tissue contained 23,2 nmol 2-AG per gram tissue. In hippomcampal tissue of the tested Daglα$^{ko/ko}$ animal 2.43 nmol 2-AG per gram tissue were detected. This indicates a strong reduction of 2-AG synthesis in the tested Daglα$^{ko/ko}$ animal.

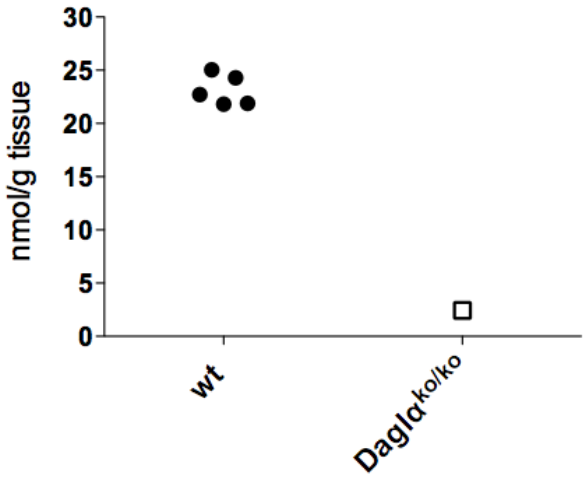

Figure 24: 2-AG level in Daglα$^{ko/ko}$ hippocampus compared to wild type tissue. Knockout of the Daglα gene led to a pronounced decrease in 2-AG content in the Daglα$^{ko/ko}$ animal. wt: wild type, n = 5, Daglα$^{ko/ko}$: n = 1

Subsequent to the molecular validation of the Daglα knockout, a group of homozygous Daglα$^{ko/ko}$ animals was subjected to a set of behavioral tests, which initiated the behavioral phenotyping of this new mouse line. The results are introduced in the following sections.

4.1.9 Behavioral analysis of Daglα$^{ko/ko}$ mice

Daglα$^{ko/ko}$ mice were viable, healthy and fertile and were apparently not different from their wild type littermates. To reveal potential effects of the Daglα knockout on locomotion and anxiety-related behavior, the open field test was performed. In addition, the fear conditioning paradigm was conducted. This paradigm was chosen, because it was already well described that $CB_1^{ko/ko}$ mice show a deficit in fear extinction (Marsicano et al. 2002; Kamprath et al. 2006). The fear conditioning model was thus performed with $CB_1^{ko/ko}$ animals to validate already published data and subsequently with a group of Daglα$^{ko/ko}$ animals. Daglα$^{ko/ko}$ mice were intitially tested for acute pain-perception in the hot plate test, because altered pain sensitivity could influence the outcome of the fear conditioning model.

4.1.9.1 Open field test

The open field test is a behavioral paradigm, which is commonly used to assess general locomotor activity, exploratory and anxiety-related behavior in rodents (Gould et al. 2009).

The general movement of wild type and Daglα$^{ko/ko}$ animals was monitored for 30 min. (Figure 25 a). A two-way ANOVA did not reveal a significant main effect for *genotype* ($F_{1,14}$ = 0.9374, p = 0.3494). A significant main effect for *time* ($F_{5,70}$ = 29.02, p < 0.0001) was detected, as the time spent moving decreased during the test session. The analysis of the distance travelled in the open field did not reveal a significant main effect for *genotype* ($F_{1,14}$ = 1.371, p = 0.2612) (Figure 25 b), but again a significant effect for *time* ($F_{5,70}$ = 25.15, p < 0.0001) was detected. The number of rearings was recorded during the test session and served as an indicator of exploratory behavior (Figure 25 c). Again, both groups behaved in a similar way and a two-way ANOVA did not detect a significant effect for *genotype* ($F_{1,14}$ = 0.07156, p = 0.7930). However, the exploratory activity of both groups increased after the first 5 min in the arena, statistical analysis revealed a significant main effect again for *time* ($F_{5,70}$ = 5.626, p = 0.0002). Another parameter evaluated in the open field test is the time that the animal spends in the center of the arena. A two-way ANOVA detected a significant main effect for *genotype* ($F_{1,14}$ = 4.967, p = 0.0427). Except for the first 5 min of the test session, Daglα$^{ko/ko}$ animals spent less time in the center compared to wild type animals. However, after 20 min of the test period a significant difference was detected between Daglα$^{ko/ko}$ and wild type animals (p < 0.05) (Figure 25 d).

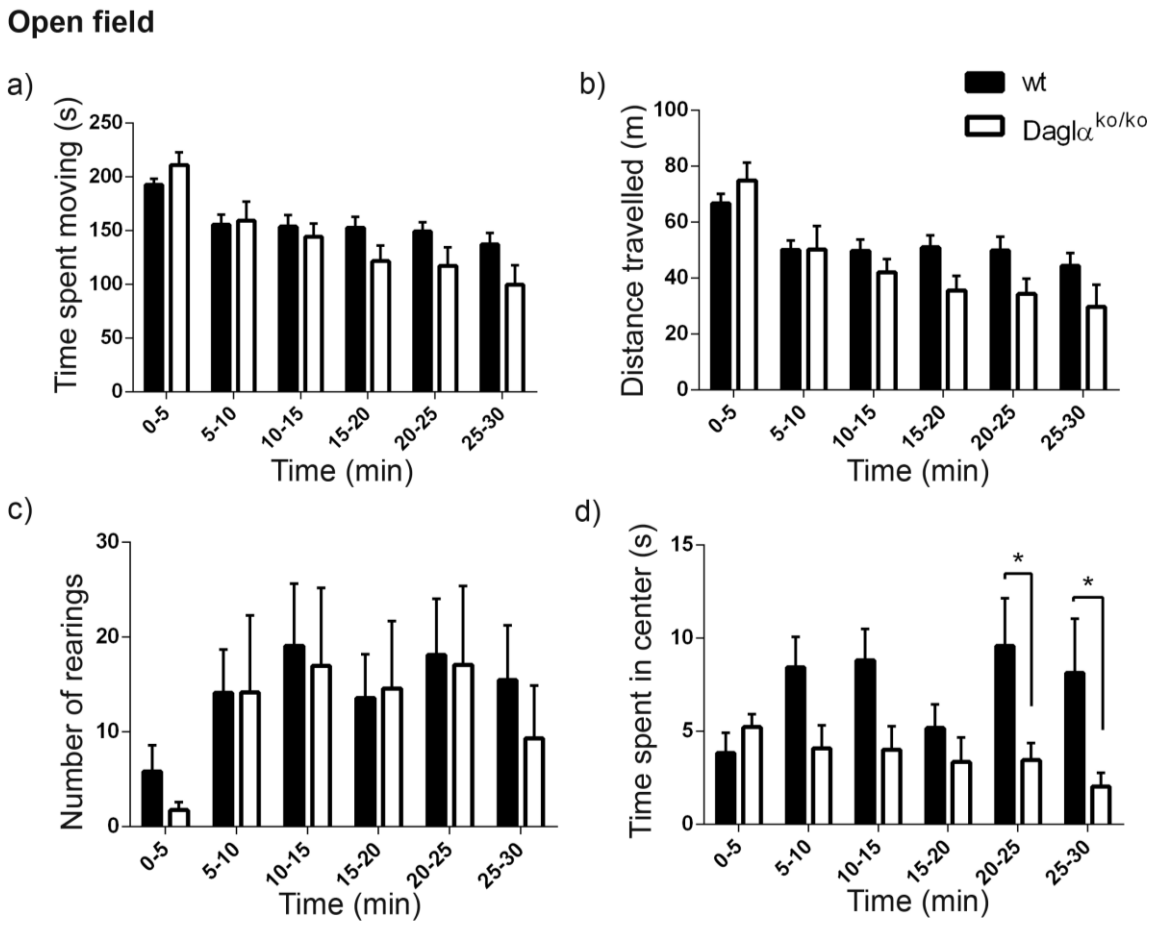

Figure 25: Open field test. a) and b) Concerning the general movement and the distance travelled during the session, the activity of Daglα$^{ko/ko}$ animals did not differ from wild type animals. c) Among the two different groups (Daglα$^{ko/ko}$ vs. wild type) no significant difference in the number of rearings was detected. d) Except for the first 5 min in the open arena, Daglα$^{ko/ko}$ mice spent less time in the center. A significant difference was detected between 20-25 min and 25-30 min. Daglα$^{ko/ko}$animals: n = 8, wild type animals: n = 8, Statistical analysis: two-way ANOVA, Bonferroni's post-hoc test, values represent mean ± SEM, between group comparison * $p < 0.05$, wt: wild type

4.1.9.2 Hot plate test

Acute thermal nociception of Daglα$^{ko/ko}$ animals was measured in the hot plate test. As depicted in Figure 26, the pain reaction of Daglα$^{ko/ko}$ mice was comparable to wild type mice. Statistical analysis did not reveal a significant difference between the two groups ($p = 0.3854$).

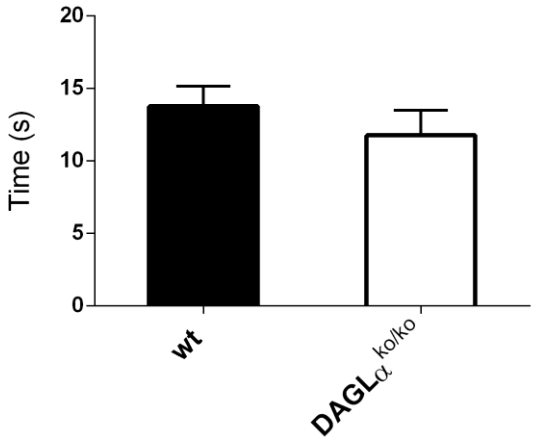

Figure 26: Hot plate test. Daglα$^{ko/ko}$ animals and wild type C57BL/6 animals were tested for acute thermal nociception. The latency of the first pain reaction (shaking of the hind-paw) was measured. Daglα$^{ko/ko}$animals: n = 8, wild type animals: n = 8, Statistical analysis: Student's t-test, values represent mean ± SEM, wt: wild type

4.1.9.3 Fear conditioning paradigm

Fear conditioning with an electric foot-shock as unconditioned stimulus was followed by several sessions of fear extinction, which were performed on day 1 to 3 and day 6 and 7 after the conditioning trial (see section 3.6.6.3). Between-session extinction considers the decline in freezing behavior between single extinction trials. Within-session extinction describes the decline in freezing that occurs within a single extinction trial.

Figure 27 serves to illustrate the experimental analysis of the complex paradigm. During the fear conditioning and extinction trials, the animal's movements were recorded by a vibration-sensitive platform. The vibration was measured in g (gram body weight) as a force, which acts on the vibration sensor at a certain point in time. The recordings are illustrated as peaks in a diagram, as shown in Figure 27. During the fear conditioning trial, the tone was presented for 20 s (Figure 27 a). The electric foot-shock was applied between the 18th and the 20th second. The animals reacted with twitching or jumping, which was detected by the vibration sensor and was visible as an increase in peak amplitudes. During the following extinction trials, freezing behavior of the animals was analysed. Periods of activity were indicated by peaks exceeding twice the baseline level

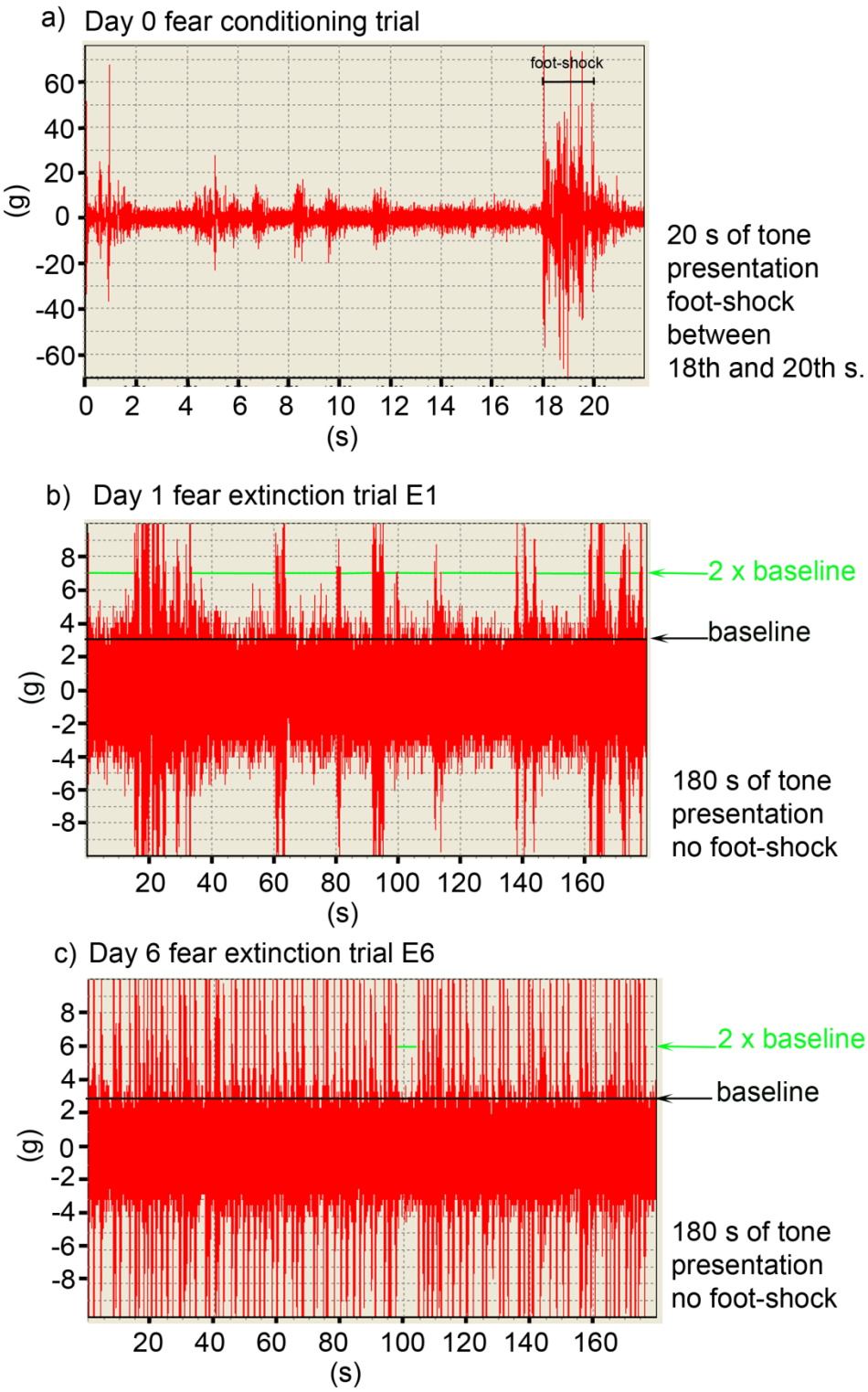

Figure 27: Freezing analysis in the fear conditioning paradigm. a) Fear conditioning was performed at day 0. A tone (9 kHz, 80 dB) was presented for 20 s. An electric foot-shock (0.7 mA) was applied between the 18th and the 20th s. The animal's movements were recorded by a vibration-sensitive platform and measured in gram (g). Increased movement was detected upon application of the foot-shock. b) At extinction trial E1 the animal reacted with freezing (green line). c) The time period spent freezing gradually reduced as the extinction trials were repeated. At extinction trial E6, no freezing was detectable, indicating between session extinction. Note the different scales of the y-axis (a-c)

(2 x baseline). Behavior was considered as freezing, if the amplitude of the peaks remained below this threshold for more than 2 s. In an extinction trial, the tone was presented for 180 s without applying a foot-shock. Figure 27 b illustrates the pattern of an animal's movement at extinction trial E1. The green line indicates periods of immobility (freezing) during the test session. In comparison, these periods were basically absent at extinction trial E6, as shown in Figure 27 c, indicating between-session extinction.

Both, $CB_1^{ko/ko}$ and $Daglα^{ko/ko}$ animals were tested in the fear conditioning paradigm in comparison to respective groups of wild type animals. Behavioral data were analysed for between-session extinction and within-session extinction. The respective results are presented in the following sections.

4.1.9.3.1 Between-session extinction

During the first 20 s of the different extinction trials, $CB_1^{ko/ko}$ animals displayed a slightly increased freezing behavior compared to wild type controls (Figure 28 a). However, at extinction trial E6 and at the recall trail R, both groups had reached the same level of freezing. A two-way ANOVA did not detect a significant effect for *genotype* ($F_{1,16} = 1.936$, $p = 0{,}1831$). A significant effect for *time* ($F_{4,64} = 14.82$, $p < 0.0001$) was detected and indicated the decline in freezing over time. Similar results were obtained for $Daglα^{ko/ko}$ animals. No main effect for *genotype* was detected ($F_{1,15} = 0.5761$, $p = 0.4596$). $Daglα^{ko/ko}$ animals and wild type animals displayed between-session-extinction and reached the same level of freezing in the recall trial R. A significant effect of *time* ($F_{4,60} = 13.56$, $p < 0.0001$) was detected (Figure 28 b).

If the whole period of tone presentation (180 s) was considered, a delay in between-session extinction for $CB_1^{ko/ko}$ animals, as well as for $Daglα^{ko/ko}$ animals became obvious. Both knockout lines sustained an elevated freezing level over several extinction trials, whereas wild type mice returned progressively to base-line levels (Figure 28 c and d). For both mouse lines, a two-way ANOVA revealed a significant main effect for *genotype* ($CB_1^{ko/ko}$: $F_{1,16} = 5.464$, $p = 0.0327$; $Daglα^{ko/ko}$: $F_{1,15} = 8.600$, $p = 0.0103$). In addition, a significant main effect for *time* ($CB_1^{ko/ko}$: $F_{4,64} = 14.31$, $p < 0.0001$; $Daglα^{ko/ko}$: $F_{4,60} = 27.67$, $p < 0.0001$) and *time* x *genotype* interaction was observed ($CB_1^{ko/ko}$: $F_{4,64} = 4.490$, $p = 0.0327$; $Daglα^{ko/ko}$: $F_{4,60} = 4.028$, $p = 0.0059$). Compared to their respective wild type control groups, $CB_1^{ko/ko}$ mice and $Daglα^{ko/ko}$ animals exhibited impaired extinction that differed significantly during trial sessions E2 ($CB_1^{ko/ko}$: $p < 0.05$, $Daglα^{ko/ko}$: $p < 0.01$) and E3 ($CB_1^{ko/ko}$: $p < 0.01$, $Daglα^{ko/ko}$ $p < 0.01$), respectively.

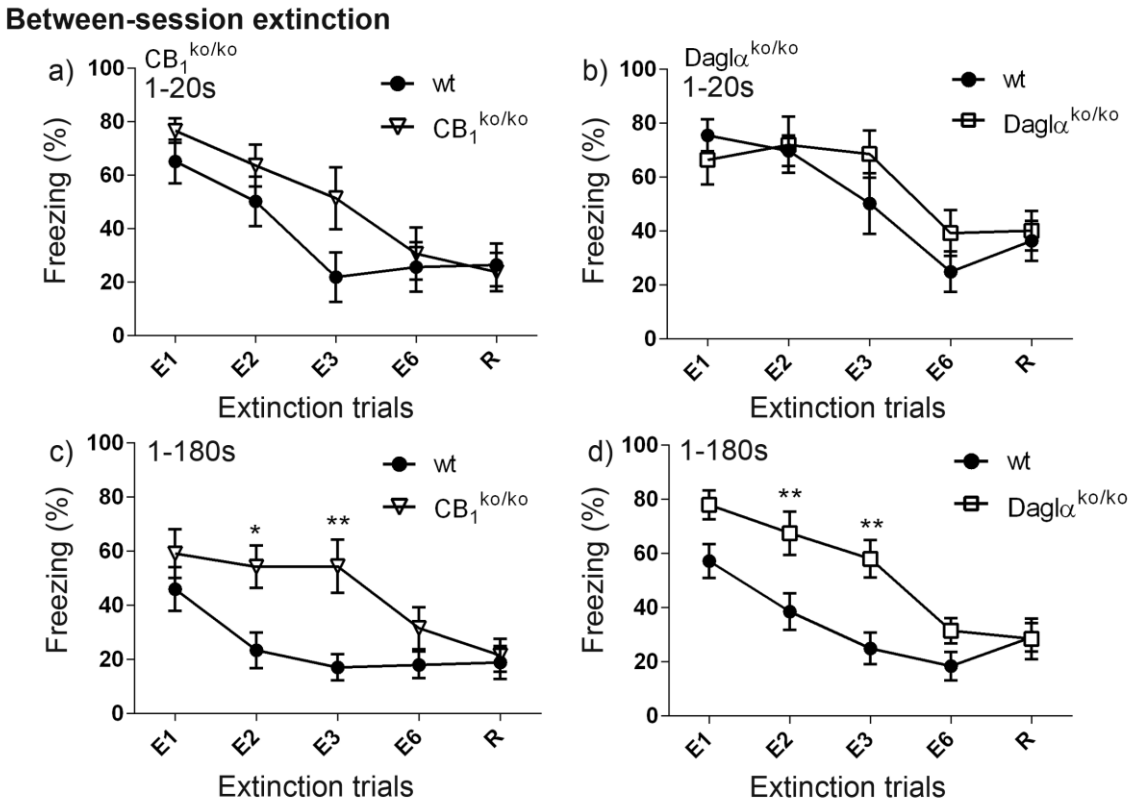

Figure 28: Fear extinction in $CB_1^{ko/ko}$ and $Dagl\alpha^{ko/ko}$ animals: Between-session extinction. a) and b): Analysis of the first 20 s of each extinction trial. $CB_1^{ko/ko}$ (a) and $Dagl\alpha^{ko/ko}$ (b) animals displayed between-session extinction, comparable to their respective control group. c)-d): Both knockout lines exhibited significantly impaired extinction in E2 and E3. $CB_1^{ko/ko}$: n = 9, wt: n = 9, $Dagl\alpha^{ko/ko}$: n = 8, wt: n = 9, Statistical analysis: two-way ANOVA, Bonferroni's post-hoc test, values represent mean ± SEM, between mouse line comparison * $p < 0.05$, ** $p < 0.01$, wt: wild type

The animals of both knockout lines exhibited between-session extinction. At extinction trials E6 and R, their respective freezing pattern reached levels comparable to wild type control animals. This was true for both time intervals that were considered (1-20 s, 1-180 s). However, if the whole time period of tone presentation was taken into account, the extinction was significantly delayed at extinction trial E2 and E3, compared to wild type control animals.

4.1.9.3.2 Within-session extinction

During the first extinction session E1, $CB_1^{ko/ko}$ animals displayed a similar extinction pattern as the wild type control animals (Figure 29 a). No significant main effect for *genotype* ($F_{1,16} = 1.178$, $p = 0.2939$) was detected, using two-way ANOVA. In contrast, a significant main effect for *time* was revealed ($F_{2,32} = 14.40$, $p < 0.0001$). For $Dagl\alpha^{ko/ko}$ animals, significance was observed for the main effects *genotype* ($F_{1,15} = 6.268$, $p = 0.0243$) and *time* ($F_{2,30} = 2.797$, $p = 0.0769$) compared to wild type animals. $Dagl\alpha^{ko/ko}$ animals reacted with increased freezing behavior after 120 s ($p < 0.05$) of tone presentation until the end of the test session at 180 s ($p < 0.01$) (Figure 29 b). In contrast,

wild type animals spent less time with freezing behavior as the tone persisted.

For the following extinction trials E2 and E3, a significant main effect for *genotype* was detected for the $CB_1^{ko/ko}$ group compared to the group of wild type animals (E2: $F_{1,16} = 9.199$, $p = 0.0079$; E3: $F_{1,16} = 11.57$, $p = 0.0036$). Similarly, a two-way ANOVA revealed a significant main effect for *genotype* on extinction trial E2 and E3 for the group of $Daglα^{ko/ko}$ animals (E2: $F_{1,15} = 7.885$, $p = 0.0132$; E3: $F_{1,15} = 11.93$, $p = 0.0035$). In contrast to $CB_1^{ko/ko}$ animals, $Daglα^{ko/ko}$ animals displayed impaired extinction already at extinction trial E1. At extinction trial E2, $CB_1^{ko/ko}$ mice maintained a high level of freezing throughout the test session ($p < 0.05$ after 120 s, $p < 0.01$ after 180 s) (Figure 29 c), which was also observed at extinction trial E3 (Figure 29 e). While the percentage of time spent freezing was below 20 % after 180 s of tone presentation in wild type mice, freezing behavior in $CB_1^{ko/ko}$ mice persisted at a high level ($p < 0.05$ after 120 s, $p < 0.01$ after 180 s) (Figure 29 e).

Concerning the within-session extinction of $Daglα^{ko/ko}$ animals, a sustained freezing behavior was detected upon persisting tone presentation (E2: $p < 0.05$ after 120 s until the end of the session after 180 s, E3: $p < 0.001$ after 120 s) (Figure 29 d and f). However, on extinction trial E3, a slight reduction in freezing was observed during the last third of tone presentation ($p < 0.05$ after 180 s). No significant main effect for *genotype* was detected at E6 for both mouse lines ($CB_1^{ko/ko}$ mice: $F_{1,16} = 2.194$, $0 = 0.1580$; $Daglα^{ko/ko}$ mice: $F_{1,15} = 3.397$, $p = 0.0852$). However, both knockout lines reacted with elevated (but not significant) freezing during the last third of the tone presentation, which was not observed in wild type mice (Figure 29 g and h).

The recall trial R was performed on day 7 after fear conditioning. The environmental conditions during this trial were adapted to the original fear conditioning trial by placing the animal back into the metal cage, where it had received the foot-shock. Two-way ANOVA did not reveal a significant main effect for *genotype* for this trial. This was true for both knockout strains ($CB_1^{ko/ko}$: $F_{1,16} = 0.09073$, $p = 0.7671$; $Daglα^{ko/ko}$: $F_{1,15} = 0.003897$, $p = 0.9511$) (Figure 29 i and j). The analysis of within-session extinction revealed that both knockout strains exhibited impaired fear extinction during prolonged tone presentation.

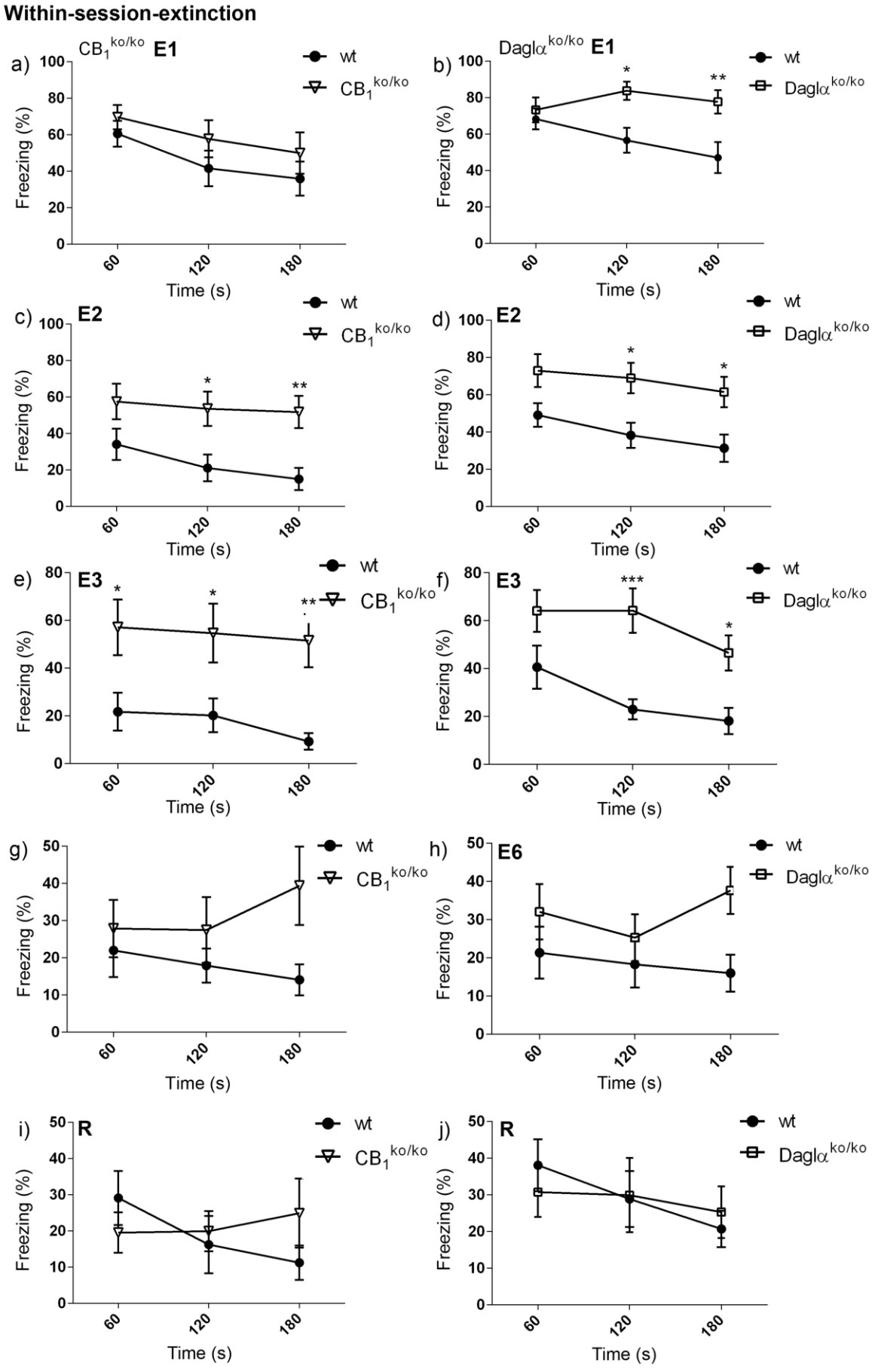
Within-session-extinction
a)
CB1ko/ko E1
wt
CB1ko/ko
Freezing (%)
Time (s)
b)
Daglαko/ko E1
wt
Daglαko/ko
Freezing (%)
Time (s)
c)
E2
wt
CB1ko/ko
Freezing (%)
Time (s)
d)
E2
wt
Daglαko/ko
Freezing (%)
Time (s)
e)
E3
wt
CB1ko/ko
Freezing (%)
Time (s)
f)
E3
wt
Daglαko/ko
Freezing (%)
Time (s)
g)
wt
CB1ko/ko
Freezing (%)
Time (s)
h)
E6
wt
Daglαko/ko
Freezing (%)
Time (s)
i)
R
wt
CB1ko/ko
Freezing (%)
Time (s)
j)
R
wt
Daglαko/ko
Freezing (%)
Time (s)

Figure 29: Fear extinction in $CB_1^{ko/ko}$ and $Daglα^{ko/ko}$ animals: Within-session-extinction. Within-session extinction describes the progression of freezing behavior during 180 s of tone presentation. The performance of $CB_1^{ko/ko}$ animals (a, c, e, g, i) and $Daglα^{ko/ko}$ animals (b, d, f, h, j) was analyzed compared to wild type animals. Each extinction trial was considered separately. $CB_1^{ko/ko}$: n = 9, wt n = 9, $Daglα^{ko/ko}$: n = 8, wt: n = 9, Statistical analysis: two-way ANOVA, Bonferroni's post-hoc test, values represent mean ± SEM, between mouse line comparison * $p < 0.05$, ** $p < 0.01$, *** $p < 0.001$, wt: wild type

4.2 Primary microglial cell cultures

The isolation of microglia performed within the scope of this work is described in the methods section 3.3.5. Primary cultures were generated from mouse brain cortices of 1-5 days old mice (C57BL/6). The resulting mixed glial cultures were cultivated until a confluent cell layer was formed. These cultures represented the starting material for the experiments performed with microglial cells.

In order to achieve the optimal yield of microglial cells from these mixed cultures, two different protocols were tested. On the one hand, microglia were enriched from the mixed cultures by different steps of trypsinization. This method was established by Saura and colleagues in 2003 (Saura et al. 2003) and is referred to as "trypsinization method" (see section 3.3.6.1). On the other hand, microglia were detached from the confluent layer by mechanical shaking of the cell culture flasks and subsequent collection from the supernatant. This method is referred to as "shaking method" (see section 3.3.6.2). Application of the "trypsinization-method" yielded on average 8×10^5 cells per cell culture flask (25 cm^2), whereas with the "shaking-method" around 3.3×10^4 cells were obtained. Thus, the yield of cells was comparably higher, when the "trypsinization-method" was used. In order to keep the numbers of used animals as low as possible, this method was applied for the collection of microglial cells from mixed glial cultures.

In Figure 30 microscopic images of the mixed glial culture before (a) and after trypsinization (b) are depicted. Before trypsinization, the mixed glial culture formed a confluent cell layer (Figure 30 a). After trypsinization, this layer was detached, but some cells were still found attached to the bottom of the cell culture flask. According to Saura and colleagues, a great majority of these cells are microglia, which are identifiable by CD11b expression (Saura et al. 2003), a surface marker molecule for microglial cells (Kettenmann & Hanisch 2011). This observation was subsequently confirmed by flow cytometry (see below). Hereby, viable cells can be discriminated from dead cells or cellular debris by the recognition of cell size (forward scatter, FSC) and granularity (sideward scatter, SSC). Damaged or dead cells are smaller than living cells and differ concerning their granularity. Based on these parameters, cellular debris can be distinguished from living cells. This is generally done by setting a "life gate" which includes living cells and separates them from dead or damaged cells (for detailed information see:

H.M. Shapiro 2003). Around 60 % of the collected cells were included in the “life gate”, as representatively shown in Figure 30 c and averaged for all performed experiments in Figure 30 e. For the identification of microglia within the “life gate”, the cells were stained with murine monoclonal antibodies against CD11b. On average, around 90 % of the cells in the life gate were positive for CD11b, as shown in Figure 30 e. A representative image of the CD11b-positive population is shown in Figure 30 d.

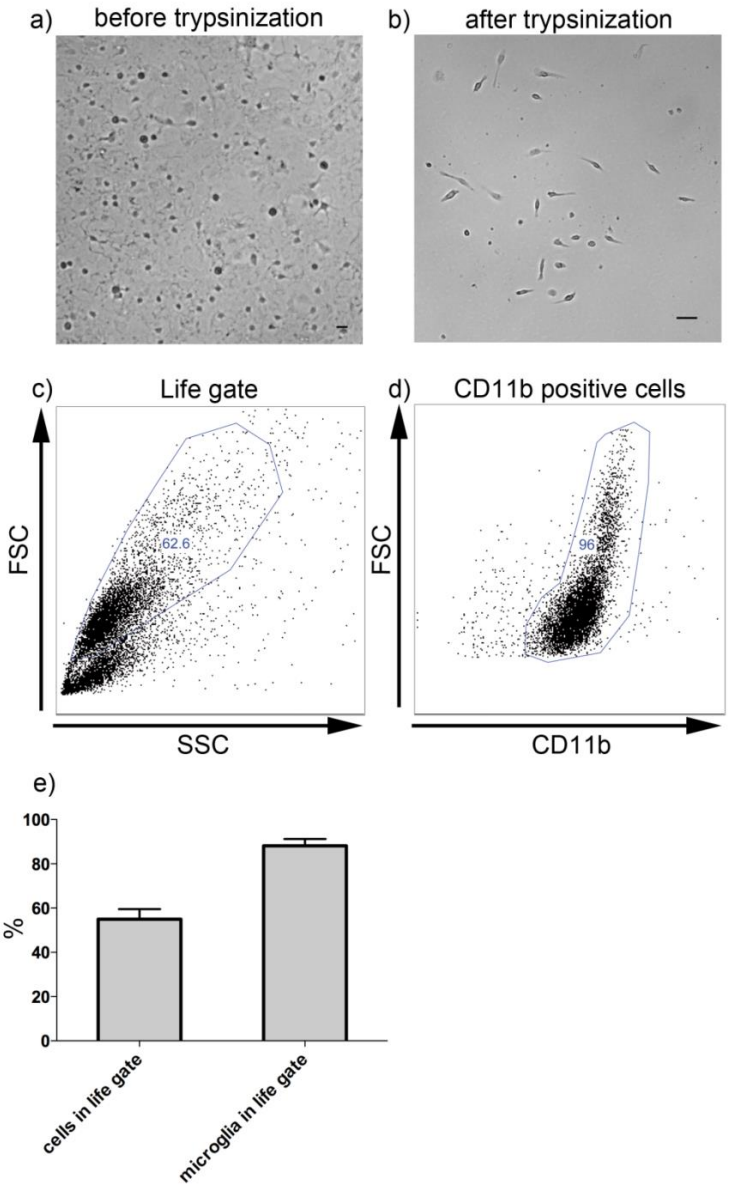

Figure 30: Establishment of the “trypsinization method” and flow cytometric analysis of primary microglia cultures. a)-d) Representative microscopic pictures and dot plots of the performed experiments. a) Confluent mixed glial culture. b) After mild trypsinization (0.12 % trypsin/EDTA, 15 min) microglial cells remained attached to the bottom of the flask and were collected after incubation with 0.25 % trypsin/EDTA for 5 min. Subsequent flow cytometric analysis of cell cultures was performed. Percentages of cell subsets included in the life gate and the cellular population pregated for CD11b expression are shown in c) and d) respectively. e) Summarized for the performed experiments, about 60 % of the total cell numbers recorded were included in the life gate. About 90 % of these cells were CD11b-positive and considered as microglia, scale bar in a) and b): 20 µm; FSC: forward scatter; SSC: sideward scatter

4.3 Stimulation experiments with primary microglial cells

Microglial cells are very versatile concerning their state of activity. The ability to adapt to different phases of an inflammatory process requires a high degree of flexibility on a molecular level (Hanisch & Kettenmann 2007). In the experiments described in the following, microglial cells were harvested by mild-trypsinization and re-plated into 24-well plates at a density of 1.5- 2 x 10^5 cells per well. After 24 h the cells were challenged with different stimuli to evoke a pro- or anti-inflammatory reaction. In order to have the ability to clearly define the respective state of activity, the experiments were aimed at identifying specific marker molecules for each state. A setup of different stimuli was used. LPS and IFNγ were utilized as pro-inflammatory substances, whereas IL-4, IL-10 and TGFβ served to elicit anti-inflammatory properties. In different experiments, the substances were used in combination or as single stimuli. Unless stated otherwise, the following concentrations and time periods were applied for the stimulation experiments: LPS (100 ng/ml, 16 h), IFNγ (20 ng/ml, 16 h), IL-4 (100 U/ml, 48 h), IL-10 (100 U/ml, 48h), TGFβ (20 ng/ml, 48 h). Each stimulation of each experiment was performed as triplicate (n = 3). Unstimulated cells served as controls.

4.3.1 Identification of marker molecules by flow cytometry

4.3.1.1 Intercellular Adhesion Molecule 1 (ICAM-1, CD54)

ICAM-1 is a cell surface glycoprotein involved in endothelial-leucocyte interaction and leucocyte extravasation (for review see Lee & Benveniste 1999; Long 2011). The expression of ICAM-1 on microglial cells is enhanced by LPS and IFNγ (Shrikant et al. 1995). In the present study, ICAM-1 expression by $CD11b^+$ microglia in response to different stimuli was assessed by flow cytometry. The results are illustrated in Figure 31. A representative dot plot of unstimulated control cells (Figure 31 a) presented the percentage of ICAM-1 expressing $CD11b^+$ cells in these cultures, whereas in Figure 31 b a LPS/IFNγ stimulated sample is shown. The quadrants were adjusted to the unstimulated control in a. Thus, the threshold for percentages of ICAM-1 expressing $CD11b^+$ cells was set below 1 %, as depicted in the upper right quadrant (0.61 %). In comparison, the percentages of ICAM-1^+ $CD11b^+$ cells increased to 47.2 % in these cultures upon stimulation with LPS/IFNγ (Figure 31 b). The upregulation of ICAM-1 expression was specific for samples stimulated with LPS/IFNγ, as illustrated in Figure 31 c. Here, the MFI (mean fluorescence intensity) values of ICAM-1 expression on microglial cells, pregated on CD11b are depicted as histograms. The upregulated expression level of ICAM-1 was

mirrored by an increase in the respective MFI value. Thus, MFI values of LPS/IFNγ stimulated samples shifted towards higher expression levels (red line), while cells stimulated with, IL-4 (blue), IL-10 (orange), IL-10/TGFβ (green) or TGFβ alone (yellow) expressed similar levels as the untreated control (grey, solid).

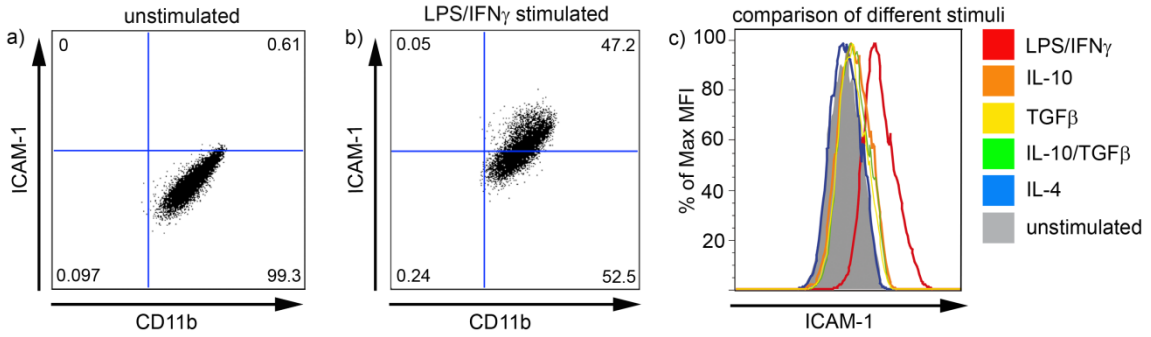

Figure 31: Analysis of ICAM-1 expression in microglial cells. Primary microglial cells where challenged with a set of different stimuli and subsequently analyzed for ICAM-1 expression by flow cytometry. a) Representative dot plot of an untreated control. Percentages of cell subsets are indicated in the respective quadrants. b) Representative dot plot of an LPS/IFNγ stimulated sample. c) Illustration of MFI values in a histogram revealed a shift towards higher expression levels of ICAM-1, which was specifically detected in LPS/IFNγ treated cells

LPS and IFNγ were tested as separate stimuli or in combination (Figure 32). Although both substances increased ICAM-1 expression in microglia, the effect of IFNγ alone was more pronounced compared to stimulation with LPS alone (Figure 32 a). Statistical analysis was performed with the MFI values obtained by flow cytometric analysis. A one-way ANOVA revealed a significant main effect for *treatment* (Figure 32 a: $F_{4,10} = 29.95$, $p < 0.0001$; Figure 32 b: $F_{5,12} = 325.9$, $p < 0.0001$). LPS alone led to a moderate, but significant increase of ICAM-1 expression in microglia ($p < 0.05$), when compared to the unstimulated control. The effect of IFNγ treatment led to a 2-fold increase in ICAM-1 expression ($p < 0.001$) when compared to unstimulated control cells (Figure 32 a). However, as shown in Figure 32 b, the combination of both substances induced a 3-fold increase compared to the unstimulated control ($p < 0.001$).

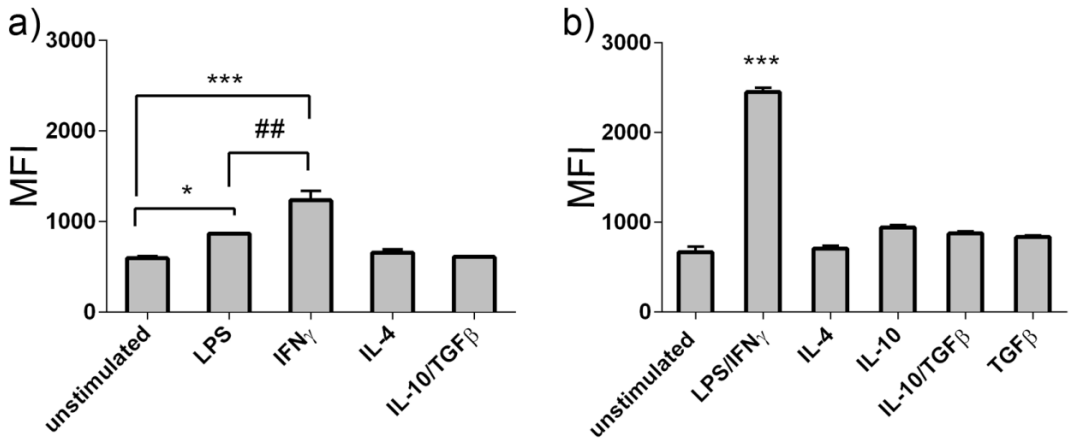

Figure 32: Analysis of stimulatory efficacy of LPS and IFNγ. Both substances were tested as separate stimuli (a) or in combination (b) and evoked an increase in ICAM-1 expression compared to untreated controls. a) The effect of IFNγ on ICAM-1 expression was significantly more pronounced, compared to LPS alone. b) The strongest effect on ICAM-1 expression was observed, when both substances were used in combination, resulting in a 3-fold increase compared to untreated controls. Statistical analysis: one-way ANOVA, Bonferroni's post-hoc test, values represent mean ± SEM, * $p < 0.05$ vs. untreated control, *** $p < 0.001$ vs. untreated control, ## $p < 0.01$ between different stimulations, MFI: mean fluorescence intensity

A significant upregulation of ICAM-1 in response to LPS/IFNγ stimulation was detected not only compared to the untreated control, but to all other stimulations tested ($p < 0.001$). This was an important aspect, because a unique marker molecule was supposed to react specifically to a certain stimulus.

4.3.1.2 Macrophage mannose receptor (MMR, CD206)

The expression of the macrophage mannose receptor (MMR) on alternatively activated macrophages is well described. As pattern recognition receptor it can recognize terminal mannose residues on the surface of invading pathogens and mediate their phagocytosis. In addition, this receptor is able to detect apoptotic cells and thus plays an important role in wound healing and tissue repair (for review see Fairweather & Cihakova 2009). Microglia have been reported to express MMR in the brain. Moreover, treatment of microglia with IL-4 leads to a robust increase of MMR expression over time (Zimmer et al. 2003). In order to test the suitability of the MMR as marker molecule for IL-4 stimulation, differrentially stimulated microglia were analyzed for their surface expression of MMR by flow cytometric analysis. The obtained data are summarized in Figure 33. Dot plots of unstimulated cells and cells stimulated with IL-4 are depicted in Figure 33 a and b, respectively. The quadrants were adjusted to the unstimulated control (a) and visualize increased percentages of MMR expressing cells to 67.4 % upon IL-4 stimulation (b). In Figure 33 c the MFI values for MMR expression on microglial cells, pregated for CD11b,

are depicted as histograms. A clear increase in MFI was detected for IL-4 treated cells (blue line), exclusively. The increase in MMR expression is visualized as a shift of the blue line towards higher fluorescence levels. In contrast, the MMR expression level was unaffected in cells stimulated with IL-10 (orange), TGFβ (yellow), IL-10/TGFβ (green) or LPS/IFNγ (red).

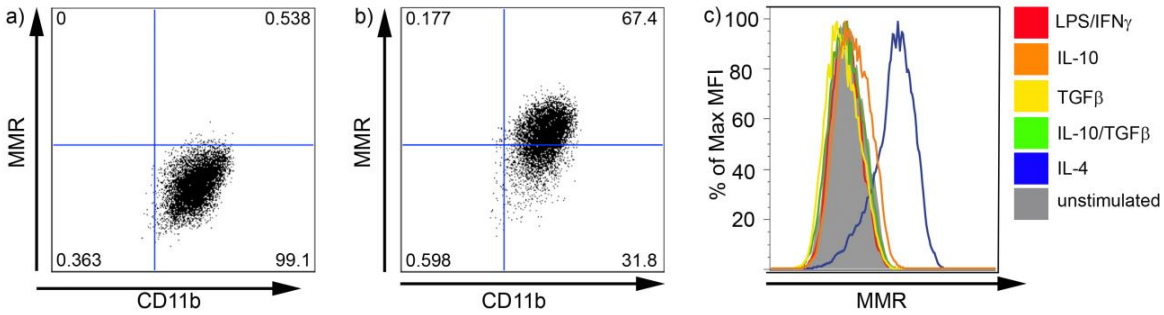

Figure 33: Analysis of MMR expression in microglial cells. Primary microglial cells where challenged with a set of different stimuli and subsequently analyzed for MMR expression by flow cytometric analysis. a) Representative dot plot of an untreated control. Percentages of cell subsets are indicated in the respective quadrants. b) Representative dot plot of an IL-4 stimulated sample. c) Illustration of MFI values as histograms. The increase in MMR expression was specifically detected in IL-4 treated samples

Increased MMR surface expression as a cellular response to IL-4 was well detectable in microglial cells after a stimulation period of 48 h (Figure 34 a). Even after an extended stimulation (72 h), the MMR was upregulated in IL-4 treated samples, whereas other stimulations did not affect MMR expression levels (Figure 34 b). LPS and IFNγ stimulation had no effect on the expression level of MMR. Both substances were tested in combination (Figure 34 a) or separately (Figure 34 b).

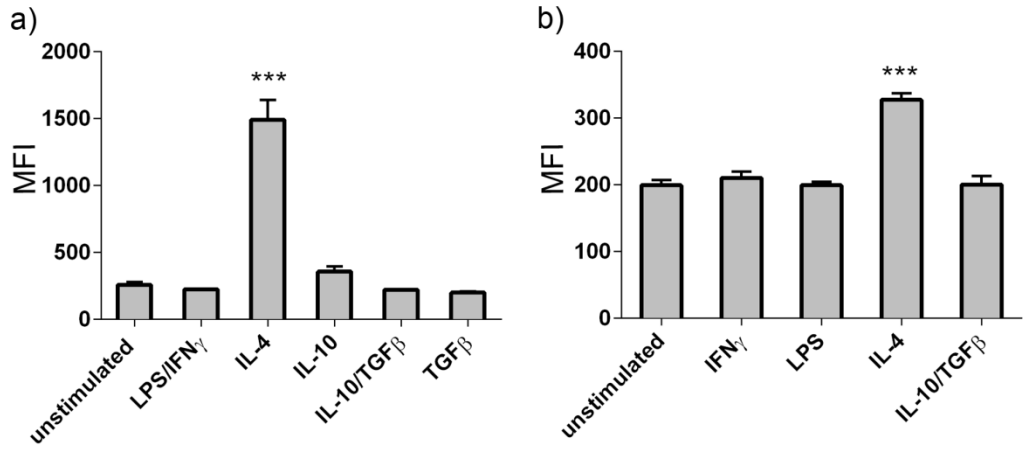

Figure 34: Effect of different stimuli on MMR surface expression on microglial cells. a) Stimulation of microglia with IL-4 (100 U/ml) for 48 h led to a pronounced increase in MMR surface expression. Compared to untreated controls, the expression level was elevated more than 3-fold. b) Separate stimulation of LPS and IFNγ had no effect on MMR expression. Extended IL-4 stimulation (72 h) led to a sustained upregulation of MMR. Statistical analysis: one-way ANOVA, Bonferroni's post-hoc test, values represent mean ± SEM, *** $p < 0.001$ vs. untreated control, MFI: mean fluorescence intensity

A one-way ANOVA of the MFI values obtained by flow cytometric analysis revealed a significant *treatment* effect (Figure 34 a: $F_{5,12} = 64.31$, $p < 0.0001$; Figure 34 b: $F_{4,10} = 35.28$, $p < 0.0001$). After IL-4 stimulation for 48 h, a significant upregulation of MMR was detected ($p < 0.001$) when compared to the untreated control (Figure 34 a). This effect persisted even, if the incubation time was extended to 72 hours ($p < 0.001$), as shown in Figure 34 b. The upregulation of MMR was significant and specific for IL-4 stimulation ($p < 0.001$).

According to the results summarized in Figure 33 and Figure 34, the MMR was considered to be a suitable marker for effective IL-4 stimulation. Besides ICAM-1 and MMR, additional surface molecules associated with an enhanced costimulatory capacity of antigen presenting cells were tested by flow cytometry. A representative summary of the respective molecules is depicted in Figure 35. Expression levels of CD86 (Figure 35 a) and CD40 (Figure 35 b) were influenced by LPS/IFNγ stimulation, whereas elevated levels of CD80 where detectable after IL-10 stimulation (Figure 35 b).

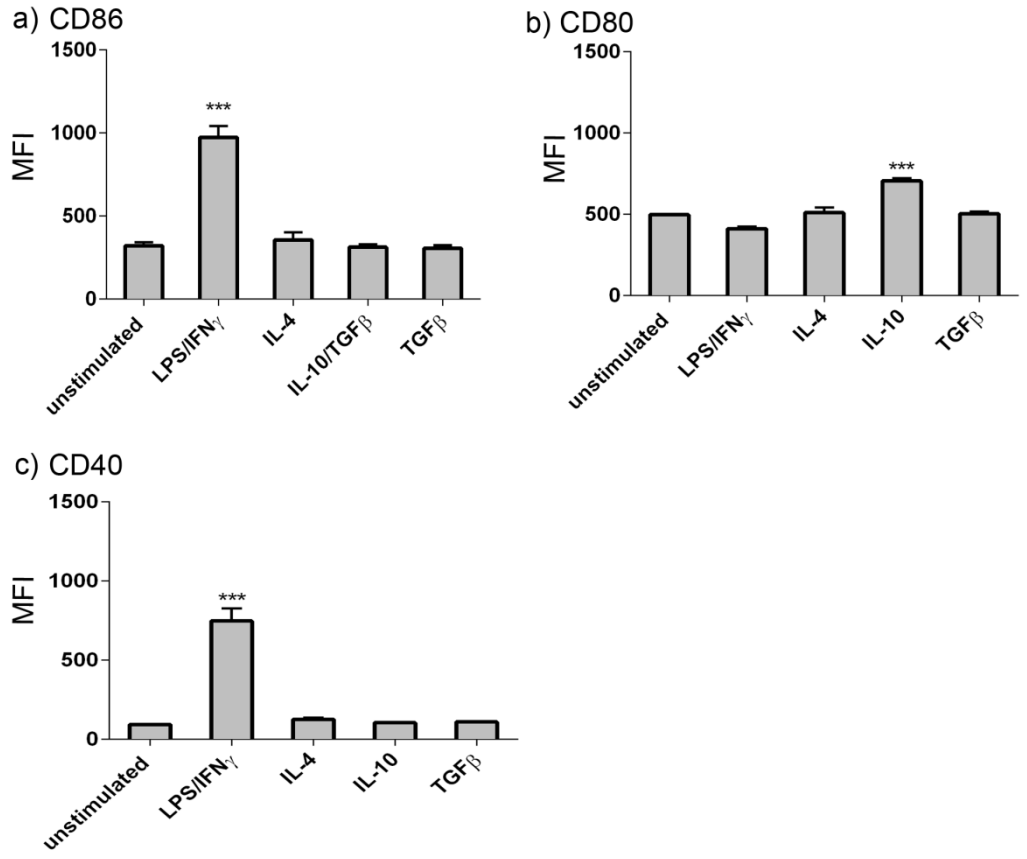

Figure 35: Surface marker molecules associated with activation of microglia cells tested by flow cytometry. a) Compared to untreated controls, CD86 expression was found to be upregulated after stimulation with LPS/IFNγ, whereas IL-10 stimulation led to an increased expression of CD80 in microglia (b). c) Enhanced expression of CD40 was detected after LPS/IFNγ stimulation. Statistical analysis: one-way ANOVA, Bonferroni's post-hoc test, values represent mean ± SEM,*** $p < 0.001$ vs. untreated control, MFI: mean fluorescence intensity

One-way ANOVA detected significant *treatment* effects for each molecule tested: CD86 (Figure 35 a: $F_{4,9} = 49.56$, $p < 0.0001$), CD80 (Figure 35 b: $F_{4,10} = 31.59$, $p < 0.0001$) and CD40 (Figure 35 c: $F_{4,10} = 64.39$, $p < 0.0001$). The expression of the costimulatory molecules CD86 and CD40 (Figure 35 a and c) was significantly upregulated in response to LPS/IFNγ stimulation, when compared to untreated controls ($p > 0.001$). In contrast, their respective expression pattern remained unaffected by other stimulations. The costimulatory molecule CD80 displayed a different response to the applied stimuli (Figure 35 b). Except for IL-10 stimulation, which had a significant effect on CD80 expression in microglia ($p < 0.001$) compared to unstimulated controls, no other stimulus applied had an influence on CD80 expression.

Besides the assessment of distinct marker molecules by flow cytometry, the cell culture supernatants of stimulated microglial cells were collected and analyzed by ELISA for different cytokine release patterns. The corresponding results are shown in the following section.

4.3.1.3 Identification of marker molecules by ELISA

4.3.1.3.1 Release of pro-inflammatory cytokines

The adaptation of different states of activity is accompanied by a change in cytokine release. Activated microglia are capable of releasing large amounts of pro-inflammatory cytokines in response to the appropriate stimulus (for review see Colton & Wilcock 2010). LPS/IFNγ stimulation increased the release of the pro-inflammatory cytokines IL-6 and TNFα. As illustrated in Figure 36, a one-way ANOVA revealed a significant *treatment* effect for IL-6 (Figure 36 a: $F_{5,12} = 465.5$, $p < 0.0001$). Compared to untreated controls, microglia challenged with LPS/IFNγ produced large amounts of this cytokine ($p < 0.001$) (Figure 36 a). In the case of TNFα, a significant treatment effect was detected as well (Figure 36 b: $F_{5,12} = 19.34$, $p < 0.0001$). LPS/IFNγ led to the release of detectable amounts of TNFα which represented a significant difference compared to untreated cells ($p < 0.001$). Otherwise, TNFα was undetectable.

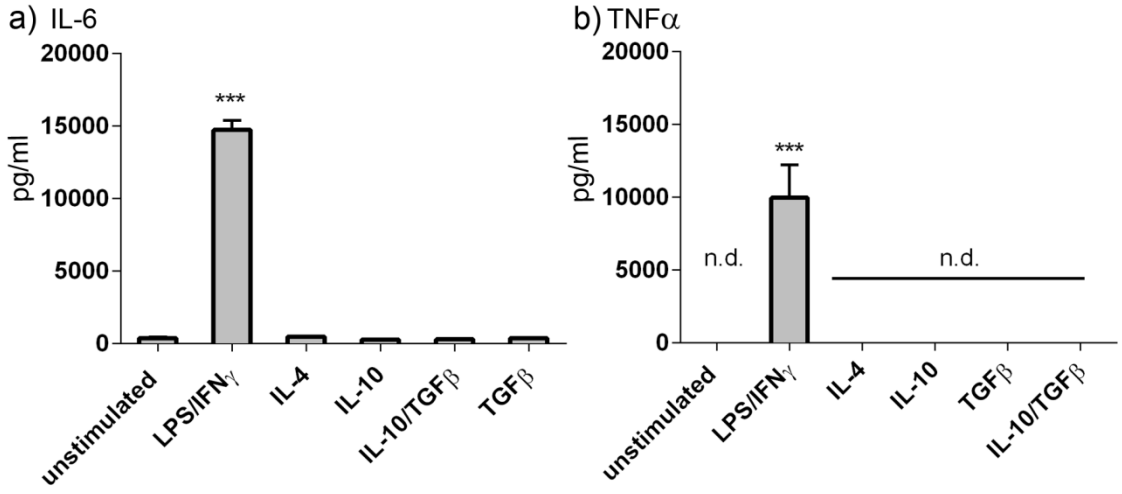

Figure 36: Release of pro-inflammatory cytokines of microglia in response to LPS/IFNγ stimulation. High levels of IL-6 (a) and TNFα (b) were detected in cell culture supernatants of microglia stimulated with LPS/IFNγ. Statistical analysis: one-way ANOVA, Bonferroni's post-hoc test, values represent mean ± SEM, *** $p < 0.001$ vs. untreated control, n.d. = not detected

Additional ELISA assays were performed in order to detect the pro-inflammatory cytokines IL-1β and IL-12 or the chemokine ligand CCL17, which was shown to by produced upon IL-4 stimulation in macrophages (Mantovani et al. 2004). However, neither IL-1β and IL-12, nor CCL17 production was detected in supernatants of differentially stimulated microglia.

Literature research on possible marker molecules that are specifically regulated by IL-10 and/or TGFβ stimulation revealed the hepatocyte growth factor (HGF) as putative candidate. HGF is released by microglial cells upon stimulation with TGFβ and serves as

chemotactic signal for oligodendrocyte migration (Lalive et al. 2005). The supernatants of stimulated microglia contained HGF, as depicted in Figure 37. Initially, a TGFβ concentration of 10 ng/ml was used, which corresponds to the concentration used by Lalive and colleagues (10 ng/ml, 48 h). Subsequently, performed ELISA measurements revealed that the highest amount of HGF was released by microglia stimulated with TGFβ, as shown in Figure 37 a. Nevertheless, a one-way ANOVA did not detect a significant *treatment* effect ($F_{4,10} = 0.9934$, $p = 0.4546$). As a next step, the TGFβ concentration used for stimulation was increased to 20 ng/ml. Hence, a significant effect for *treatment* was detected by one-way ANOVA (Figure 37 b: $F_{5,12} = 26.84$, $p < 0.001$). Compared to the untreated control, TGFβ stimulation significantly increased HGF release in microglial cells ($p < 0.001$).

In order to investigate the reliability and reproducibility of HGF as marker for TGFβ stimulation, microglia were harvested at different time points after isolation. The microglia used in Figure 37 b were collected and re-plated at day 24 after isolation and exhibited a clear-cut release-pattern for HGF. In contrast, microglia harvested at day 20 post isolation showed a completely different picture (Figure 37 c). A *treatment* effect was not observed here ($F_{5,11} = 2.829$, $p = 0.07$). The expected release-pattern was restored for microglia harvested later than day 26 post isolation, as representatively shown in Figure 37 d. A one-way ANOVA revealed a significant effect for *treatment* ($F_{4,15} = 65.22$, $p < 0.0001$). TGFβ stimulation led to a significant release of HGF, compared to untreated control cells ($p < 0.001$).

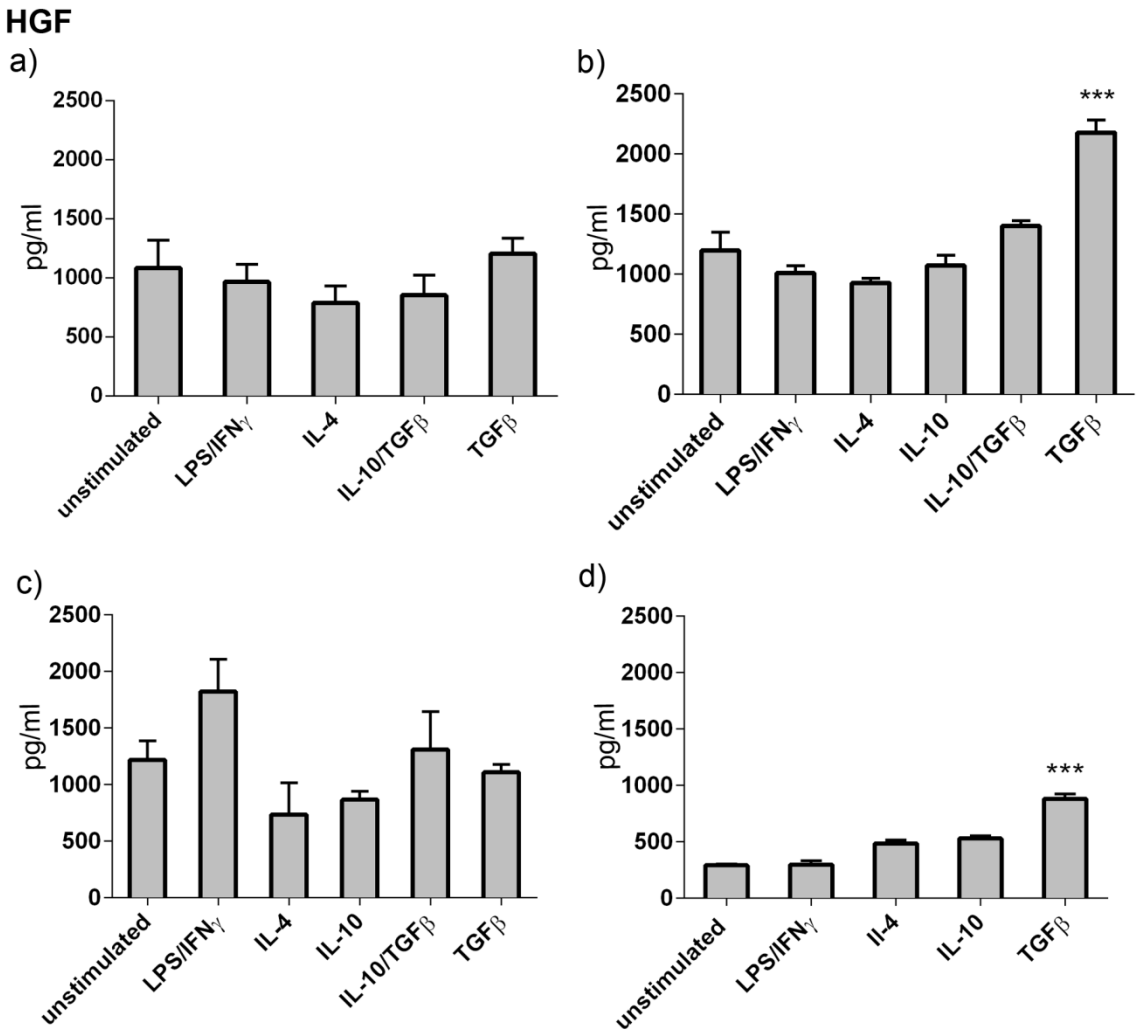

Figure 37: ELISA measurement of cell culture supernatants for HGF release by stimulated microglia. a) Stimulation with TGFβ at a concentration of 10 ng/ml was insufficient to evoke a significant release of HGF. b) Increased TGFβ concentrations (20 ng/ml) yielded a significant increase in HGF release. c) The release pattern was changed in microglia harvested prior to 24 days in culture. TGFβ was the strongest stimulus for HGF release in microglia harvested later than day 24 in culture (b and d) Statistical analysis: one-way ANOVA, Bonferroni's post-hoc test, values represent mean ± SEM, *** $p < 0.001$ vs. untreated control

In summary, the utilization of HGF release as marker for a TGFβ-induced phenotype is possible, if the variability of HGF release is taken into account. As a sensitive marker, HGF is only suitable for microglia harvested later than day 24 in culture. It should be noted here that the release of IL-6 and TNFα upon LPS/IFNγ stimulation was reproducible and did not depend on the age of harvested microglia.

As another method, quantitative real-time RT-PCR was used for the search of marker molecules whose expression was supposed to be specifically regulated by one of the applied stimuli. The results obtained by this method are introduced in the next section.

4.3.1.4 Identification of marker molecules by RT-PCR

Stimulation of macrophages by LPS and/or IFNγ leads to the induction of the pro-inflammatory M1 subtype. One of the unambiguous hallmarks of this phenotype is the production of reactive oxygen species by the inducible nitric oxide synthase (iNOS). In contrast, the alternative phenotype M2a is inducible by treatment with IL-4 and is characterized by elevated transcription levels of arginase 1 (Arg1), chitinase-3-like-3 (Ym1) and the molecule found-in-inflammatory-zone 1 (FIZZ1). All these elements are involved in tissue repair and wound healing (for review see: Martinez et al. 2009). Similar activation states accompanied by the same reactions on gene expression level were stated for microglia (Colton & Wilcock 2010).

In order to elaborate the mRNA levels for these molecules in stimulated microglia, quantitative real time RT-PCR was performed. Figure 38 illustrates the expression levels of the indicated genes for different stimuli. The respective gene expression levels were normalized to the expression level of the housekeeping gene GAPDH and were plotted on the y-axis. In unstimulated controls, the expression levels of the genes were mainly below the detection limit. Thus, instead of calculating the fold expression of the respective genes, this way of presentation was favored.

The induction of iNOS in microglial cells as a consequence of LPS/IFNγ stimulation was clearly detectable as depicted in Figure 38 a. A one-way ANOVA performed with the obtained ΔCt values clearly indicated a significant *treatment* effect on the expression of iNOS (Figure 38 a: $F_{4,10} = 14.67$, $p < 0.0001$). Compared to untreated controls, mRNA levels of iNOS were significantly elevated in response to LPS/IFNγ stimulation ($p < 0.01$). Concerning FIZZ1, Arg1 and Ym1, statistical analysis of the ΔCt values revealed a significant *treatment* effect for each of the genes, respectively (Figure 38 b: $F_{4,10} = 23.3$, $p < 0.0001$; Figure 38 c: $F_{4,10} = 93.21$, $p < 0.0001$ Figure 38 d: $F_{4,10} = 199.8$, $p < 0.0001$). The mRNA of FIZZ1 was exclusively detectable in response to IL-4 treatment ($p < 0.001$) (Figure 38 b). The same result was obtained for Ym1 ($p < 0.001$) (Figure 38 d). In the case of Arg1, the concentration of the corresponding mRNA was at the border of detection limit in LPS/IFNγ-, IL-10- and TGFβ treated samples. In contrast, IL-4 stimulation induced a significant increase in Arg1 mRNA levels ($p < 0.001$) (Figure 38 c).

In addition to the genes depicted in Figure 38, genes of other putative marker candidates for IL-10 or TGFβ stimulation were tested by TaqMan analysis, as for example, P2ry12 and Tlr1 (De Simone et al. 2010; Williams et al. 2002; Olson & Miller 2004). In contrast to the genes depicted here, these genes did not provide reliable results for any of the applied stimulations.

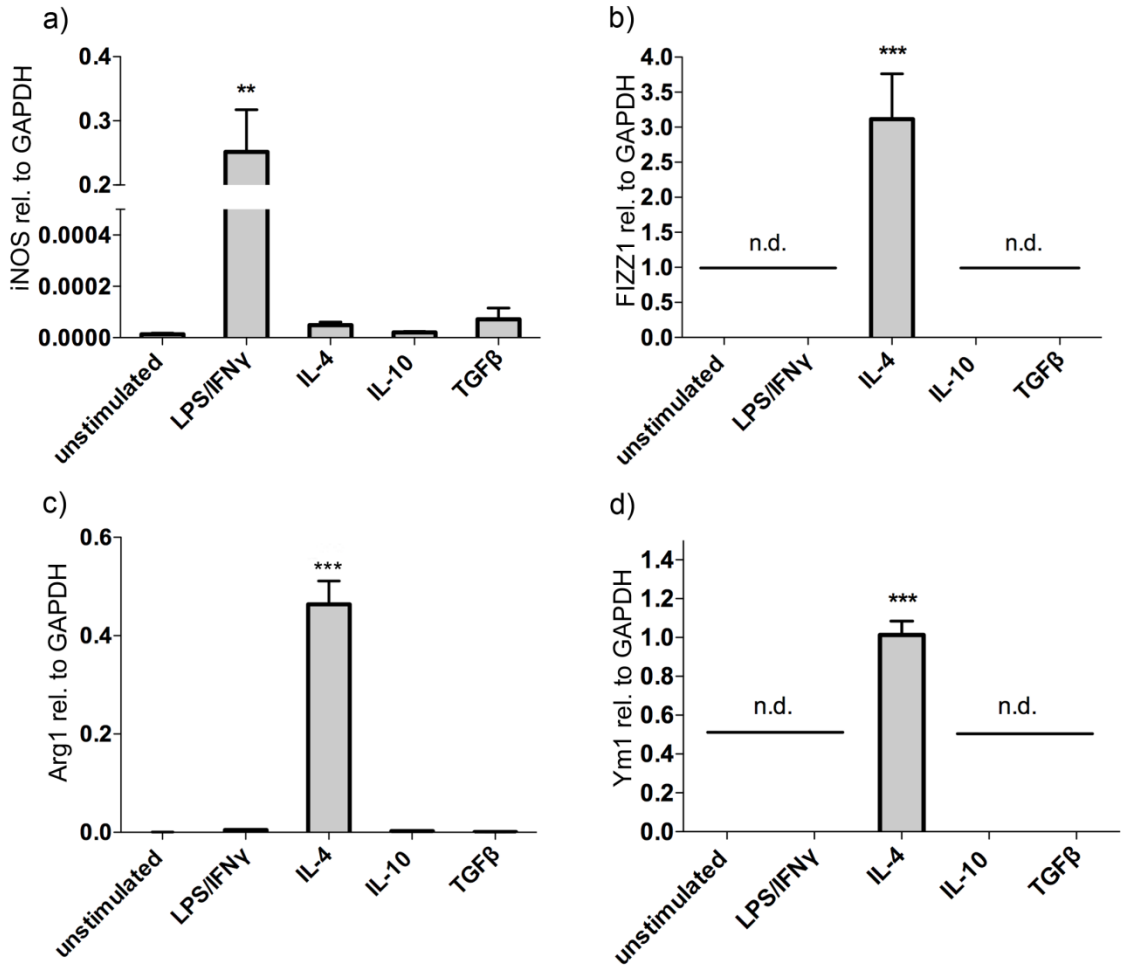

Figure 38: Quantitative gene expression analysis by real-time RT-PCR. Stimulated microglia were tested for altered gene expression of a) iNOS b) FIZZ1, c) Arg1 and d) YM1, Statistical analysis: one-way ANOVA, Bonferroni's post-hoc test, values represent mean ± SEM, ** $p < 0.01$ vs. untreated control, *** $p < 0.001$ vs. untreated control, n.d. = not detected

In summary, LPS and IFNγ elevated surface expression of ICAM-1, induced gene expression of iNOS and the release of pro-inflammatory cytokines such as IL-6 and TNFα. Challenging microglia with IL-4 resulted in elevated surface expression of MMR and induced gene expression of FIZZ1, Arg1 and Ym1. Treatment of microglia with TGFβ produced a significant increase in HGF release, even though this effect involved a kinetic component. Apart from that, IL-10 and TGFβ, applied separately or in combination, did not reveal significant effects on any of the molecules tested. The respective results were comparable to the untreated controls. An exception was found in CD80, which was upregulated in response to IL-10 stimulation as detected by flow cytomtry.

These preliminary studies were a prerequisite for the subsequent array-based gene expression profiling that was performed in collaboration with Prof. Dr. Joachim Schultze (Laboratory for Genomics and Immunoregulation, LIMES Institute, Bonn).

4.3.2 Gene expression profiling of differentially stimulated microglia

For gene expression profiling, the set of stimuli was narrowed down to the essentials, as a large amount of cells was required. Therefore, the substances which were supposed to yield the broadest impact on gene expression were chosen. Thus, microglia were subjected to LPS/IFNγ, IL-4 and TGFβ stimulation, as described before. The following experimental procedures were conducted by the group of Prof. Dr. Joachim Schultze at the LIMES Institute in Bonn. In order to maximize the purity of the obtained culture, the stimulated cells were sorted by a FACS Aria III cell sorter. Subsequent to RNA extraction and preparation of cRNA, microarray-based gene expression profiling was performed in order to identify a set of responsive genes. A list of the respective genes is found in the appendix. An overview of the numbers of genes that were differentially expressed in response to a certain stimulus is given as a Venn diagram in Figure 39. The most dramatic change in gene expression was evoked by LPS/IFNγ. Altogether 1558 genes were differentially expressed. About 125 and 121 genes were reactive to IL-4 and TGFβ, respectively. Some genes were found to be responsive to more than one specific stimulus. Corresponding numbers are depicted in the overlapping regions of the diagram.

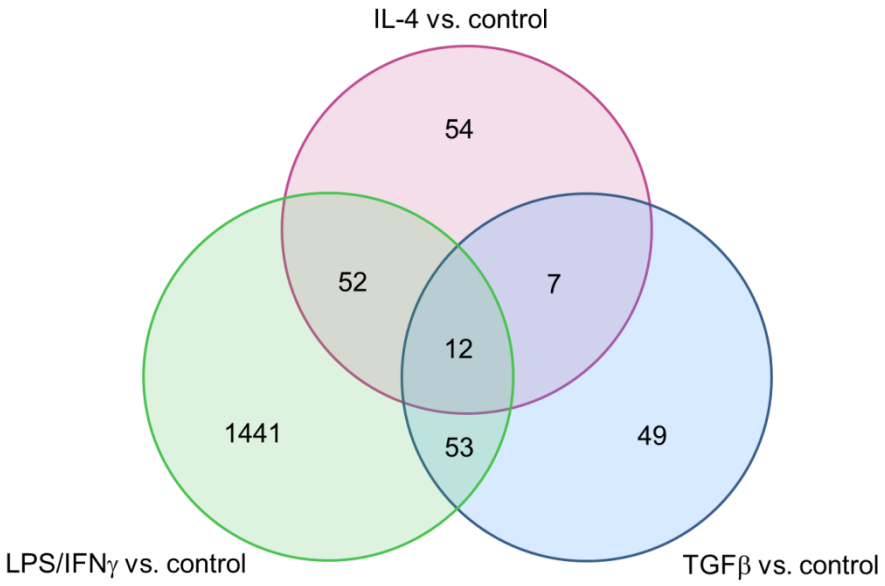

Figure 39: Venn diagram of genes affected by the different stimuli. Respective numbers depict the amount of genes that were responsive to one or more stimuli. The Figure was kindly provided by Dr. Thomas Ulas, Laboratory for Genomics and Immunoregulation, LIMES Institute

Among the differentially expressed genes, those related to the ECS were in the focus of interest. Figure 40 illustrates the activity patterns for the respective genes. Some gene names are listed more than once, because different probes for the same gene were used.

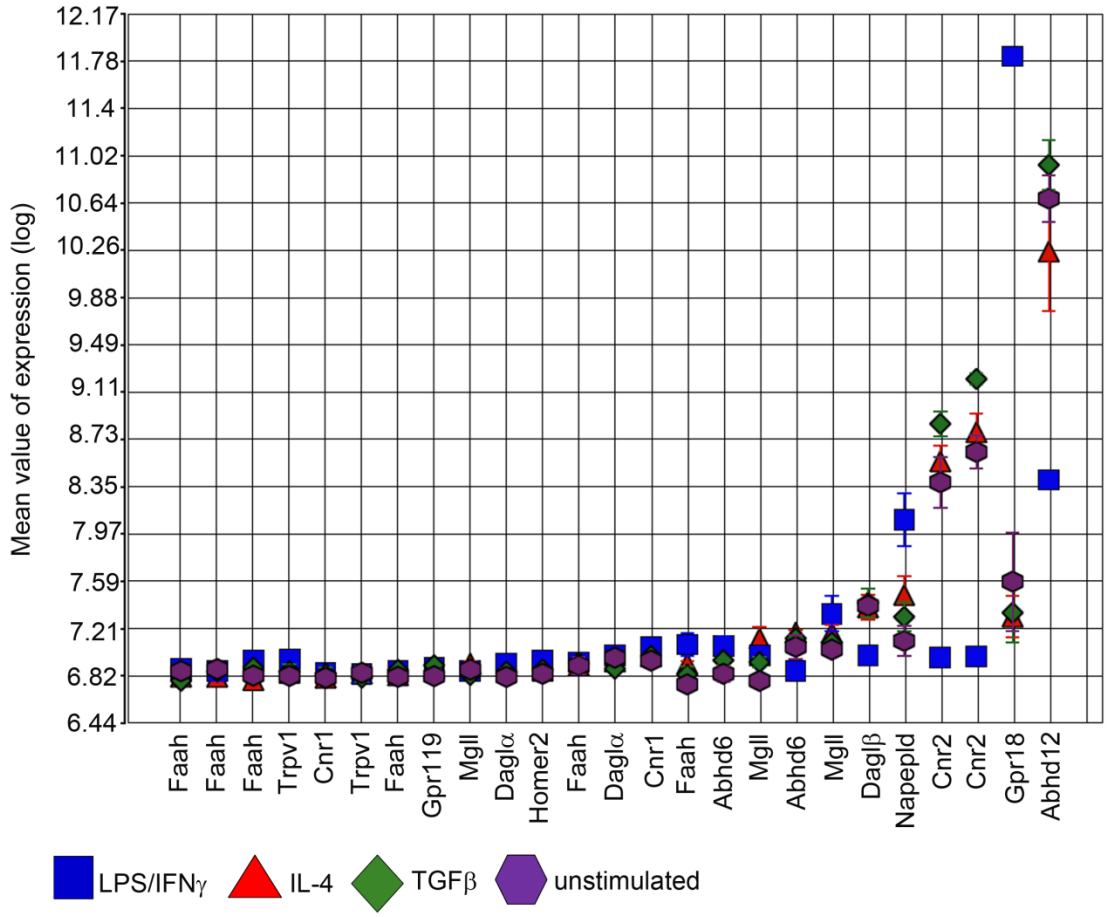

Figure 40: Expression patterns of genes related to the endocannabinoid system. The different expression levels in response to the applied stimuli are depicted as follows: LPS/IFNγ in blue, IL-4 in red, TGFβ in green, unstimulated in purple. Stimulus-dependent regulations were detected for Napepld, Daglβ, Cnr2, Gpr18 and Abhd12. Faah: Fatty-acid-amide hydrolase, Trpv1: transient receptor potential vanilloid type-1, Cnr1: Cannabinoid receptor 1, Gpr119: G-protein coupled receptor 119, Mgll: monoacyl glycerol lipase, Daglα: diacylglycerol lipase α, Homer2: homer homolog 2, Abhd6: Aβ-hydrolase 6, Daglβ: diacylglycerol lipase β, Napepld: N-arachidonoyl-phoshatidylethanolamine phospholipase D, Cnr2: cannabinoid receptor 2, Gpr18: G-protein coupled receptor 18, Abhd12: Aβ-hydrolase 12. The Figure was kindly provided by Dr. Thomas Ulas, Laboratory for Genomics and Immunoregulation, LIMES Institute

Gene expression data were analyzed using Partek Genomic Suite Microarray Analysis Software (Partek Inc.) and were kindly provided by Dr. Thomas Ulas (Laboratory for Genomics and Immunoregulation, LIMES Institute, Bonn).

Several genes including Faah, Trpv1, Cnr1, Gpr119, Mgll, Daglα, Homer2 and Abhd6 were unaffected by the different stimulations. The respective mean expression levels did not significantly differ from the unstimulated control. In contrast, statistical analysis revealed significant differences in gene regulation for Daglβ, Napepld, Cnr2, Gpr18 and Abhd12. While Daglβ ($p < 0.05$), Cnr2 ($p < 0.001$) and Abhd12 ($p < 0.01$) were downregulated in response to LPS/IFNγ stimulation, Napepld ($p < 0.05$) and Gpr18 ($p < 0.001$) displayed enhanced expression. Gpr18, the gene encoding the putative cannabinoid receptor GPR18 showed the strongest upregulation, leading to a 16-fold

enhanced expression of this receptor.

In contrast, the respective genes were less responsive to anti-inflammatory stimuli. IL-4 stimulation did not lead to significant changes in the respective expression pattern of any of the genes illustrated in Figure 40. Concerning the effect of TGFβ stimulation, Cnr2 was the only gene that displayed a significant upregulation in response to this stimulus ($p < 0.01$).

In general, the stimulatory impact on genes related to the ECS reflected the distribution of responsive genes in the Venn diagram depicted in Figure 39. Concerning the genes related to the ECS, the most pronounced effect on the respective gene expression levels was achieved in LPS/IFNγ stimulated microglia. IL-4 and TGFβ treatment did not lead to significant changes except for Cnr2, which was significantly upregulated upon TGFβ stimulation.

5 Discussion

The first aim of this thesis was to generate conditional knockout mouse lines for the two 2-AG synthesizing enzymes DAGLα and DAGLβ. Therefore, conditional knockout targeting vectors were generated and subsequently used for the generation of chimeric mice by blastocyst injection. Successful germline transmission was achieved for the Daglα targeting construct, resulting in the inheritance of the modified gene. Several cell type-specific and one constitutive knockout line were generated by selective breeding with different Cre-expressing mouse lines. The functionality of the knockout was analyzed by TaqMan assay and a set of preliminary behavioral tests was perfomed with the new mouse line.

The second aim was the characterization of different activation states in primary microglia. Within this project, the cultivation of primary microglia was established. In addition, these cells were challenged with a set of pro- or anti-inflammatory substances to evoke different states of activity. On order to facilitate the detection of the respective microglial phenotype, different methods were applied to identify characteristic marker molecules. Subsequent gene expression profiling of the differentially activated microglia was performed in collaboration with the group of Prof. J. Schultze (Laboratory for Genomics and Immunoregulation, LIMES Institute, Bonn) and revealed a set of responsive genes. The gene expression analysis was thereby focused on genes that are related to the ECS and will be discussed in the last section.

5.1 Generation of conditional knockout mice for Daglα and Daglβ

For the generation of the new mouse lines, targeting vectors for the respective gene had to be generated. The design of the targeting strategy was based on several considerations. First, both genes are composed of many exons (20 in the case of Daglα and 15 for Daglβ). The transmembrane domains, as well as the catalytically active region are encoded by more than 4 exons, respectively. An incomplete knockout can lead to a truncated version of the protein with incalculable properties (Müller 1999). To exclude this, a large sequence spanning the exons of the catalytic domain would have to be flanked by loxP sites. On the other hand, the efficiency of Cre-mediated recombination is inversely correlated with the distance between the loxP sites (Lakso et al. 1996). A comparatively convenient strategy for both genes involves the knockout of the first exon. Although this

exon is untranslated in the case of Daglα, it contains the transcription start point. Thus, for the approach described here, a sequence upstream from the respective first exon (870 bp for Daglα, 1.3 kb for Daglβ) and the first exon itself was included in the floxed region. This strategy was supposed to result in a complete loss of transcription. Important promotor elements for the transcription of Daglα are located at -450 bp and -200 bp relative to the transcription start point (Walker et al., 2009) and were thus included in the floxed sequence. In addition to two loxP sites, the targeting constructs contained a Frt-flanked neo cassette, which enabled positive selection in ES cells.

The targeting constructs were electroporated into MPI2 ES cells on a 129Sv background, as well as into C57BL/6 derived Bruce4 ES cells. Both ES cell lines were used in order to elevate the chance of germ-line transmission. In previous studies, most knockout mouse lines were generated using 129Sv-derived ES cells. However, it is known that the breeding efficacy of the 129Sv strain is low and the offspring often diplays abnormalities concerning anatomy, immunology and behavior. Many knockout lines had to be backcrossed to a C57BL/6 background for more than 10 generations to facilitate behavioral phenotyping (Seong et al. 2004). To circumvent this time consuming procedure, Bruce4 ES cells were preferentially used for blastocyst injection.

For the Daglα targeting construct, both ES cell lines demonstrated homologous recombination rates of 1 %, which is in line with other reports (Capecchi 1989; Seong et al. 2004). Altogether, 4 out of 8 clones displayed recombination for the entire construct. Concerning Daglβ, homologous recombination was undetectable in MPI2 ES cells. Due to the fact that the targeting construct was generated from C57BL/6 DNA, the different genetic background of the two strains could account for the absence of homologous recombination. The rate of recombination critically depends on the genetic background of the respective mouse strains. It has been shown that the recombination efficacy is around 20-fold decreased between non-isogenic mouse strains. In addition, the absolute frequencies of recombination are locus-dependent, as differences in chromatin structure can influence the accessibility of the required enzymatic machinery (Te Riele et al. 1992; Müller 1999). The recombination frequency of iso-genic DNA in Bruce4 ES cells occurred in around 0.8 % of the clones and was thus slightly lower for the Daglβ construct, compared to the Daglα targeting vector. Nevertheless, 4 out of 7 Daglβ clones displayed homologous recombination for the entire construct. Although repeated blastocyst injection was performed with these clones, only one chimeric animal was born. Altogether, this chimera provided more than 100 pups, but the genetic modification was not passed to its progeny. In contrast, germ-line transmission was achieved for the Daglα construct. Chimeric animals were obtained with both ES cell lines. Albeit, considerably more injections had to be performed for Bruce4 ES cell clones. While 3 injections of a MPI2

clone yielded 6 chimeric animals, 11 injections of Bruce4 ES cell clones had to be performed to obtain 2 chimeric animals. Compared to ES cells on a 129Sv background, C57BL/6 ES cell lines are known to be less efficient in producing genetically modified mice (Nagy et al. 1993). In addition, maintaining these cells in culture is more demanding and especially Bruce4 ES cells are susceptible to become aneuploid. Hence, the genetic instability reduces the germline transmission potency of this cell line (Longo et al. 1997; Hughes et al. 2007) and might account for the low efficiency of producing chimeric animals and thus germ-line transmission. Although work with Bruce4 ES cells involves some disadvantages, this cell line still represents a valuable tool for the generation of new mouse models. Due to the fact that the genomic sequence of the C57BL/6 mouse genome and the RPCI-23 C57BL/6J genomic BAC library is available *in silico*, convenient and sequence-specific targeting is possible (Osoegawa et al. 2000; Hughes et al. 2007). Moreover, the C57BL/6 strain is the best characterized inbred strain and mouse models on a C57BL/6 background allow the comparison with already described phenotypes (Skarnes et al. 2011). Yet, the genetic condition of the cells has to be tightly monitored and a suitable mouse line for blastocyst donation has to be utilized. Seong and colleagues reported considerable rates of germline transmission, when C57BL/6 ES cells were injected into co-isogenic blastocysts (Seong et al. 2004).

Meanwhile, new targeting techniques have been developed, which omit laborious ES cell culture. These systems involve the activity of zinc-finger nucleases or transcription activator-like effector nucleases, so-called TALENs, for sequence-specific DNA cleavage (Cui et al. 2011; Bogdanove & Voytas 2011). The enzymatic activity of these nucleases generates DNA double-strand breaks, which in turn activate the cell's own repair mechanisms. The enzymatic machinery responsible for DNA repair is then utilized to integrate DNA sequences by homologous recombination or to evoke small genetic modifications by non-homologous endjoining (NHEJ) (Cui et al. 2011; Bogdanove & Voytas 2011). The possibility to inject mRNA sequences for these nucleases together with the desired targeting construct into the pronuclei of murine one-cell embryos is a remarkable advantage. For the zinc-finger technology, homologous recombination rates of 1.7 to 4.5 % were reported. Nucleotide loss by NHEJ, which can be used to induce frame-shifts, occurred at even higher rates of up to 22 % (Meyer et al. 2010). However, the TALEN strategy is supposed to be more precise concerning sequence specificity (Mussolino & Cathomen 2012). Up to now, there is no conditional knockout reported that was generated by zinc-finger- or TALEN technology. Nevertheless, these techniques may facilitate a more rapid generation of the Daglβ knockout mouse line, because the targeting of ES cells is not necessary. Cui and colleagues reported the successful targeted integration of a 1.5 kb GFP-cassette, which was flanked by homology arms of about

800 bp (Cui et al. 2011). After adapting the homology regions of the developed Daglβ targeting construct, it probably could be used in the near future to generate conditional Daglβ knockouts by zinc-finger or TALEN methodology.

5.2 Daglα: knockout validation and tissue-specific knockout

The offspring of chimeric Daglα knockout animals was analyzed by PCR and Southern blot to check for the transmission of the genetic modification. Animals, which had inherited the genetic modification, were then subjected to selective breeding. First, mating with FLP-deleter mice led to the ubiquitous deletion of the FRT-flanked neo cassette. Neomycin-resistance was used as selection marker for the generation of the targeting construct and in ES cell culture. Nevertheless, it was shown that expression of the neo-gene can influence the expression of other genes in mammalian cells (Valera et al. 1994). Therefore, the neo-gene was removed by FLP-mediated recombination, which was then verified by PCR. The neo cassette was not detectable in heterozygous animals. Only homozygous animals, which contained the neo cassette in both alleles, displayed the expected fragment of about 2.1 kb. The wild type allele yielded a much smaller PCR product of about 443 bp. Due to the huge size difference of the two expected PCR products, one can assume that the wild type fragment was preferentially produced compared to the neo cassette-spanning fragment. Anyway, effective FLP-recombination was detectable by a fragment of 570 bp, which appeared after excision of the FRT-flanked neo cassette.

Offspring of FLP-expressing animals were mated with different Cre-expressing mouse lines. To obtain a ubiquitous deletion of the floxed gene region, the Pgk1-Cre strain was chosen. In this mouse strain the Cre recombinase is expressed under control of the Pgk1-promotor, which enables early and efficient excision of loxP-flanked sequences in all organs (Lallemand et al. 1998). Southern blot analysis revealed successful Cre-mediated recombination and confirmed the functionality of the loxP sites. Brain tissue of homozygous Pgk1-Cre animals was used for the validation of the Daglα knockout by mRNA-based TaqMan gene expression analysis. Compared to the mRNA levels of Daglα in wild type mice, the mRNA levels of homozygous Daglα Pgk1-Cre mice (hereupon referred to as Daglα knockout animals) were close to the detection limit, indicating a successful knockout of the gene. Although the 5’ loxP site was positioned upstream of a highly-conserved region proximal to the first exon, disturbing effects on Daglα gene expression can not be excluded in floxed animals. Due to the fact that the insertion of a loxP site might affect the respective gene expression, analysis of mRNA levels in floxed

animals is recommended (Birling et al. 2009). At the time of knockout validation, homozygous floxed animals were not available, but mRNA levels in Daglα$^{fl/fl}$ mice will be tested in the near future.

Loss of function of the Daglα gene was supposed to lead to a robust reduction in 2-AG synthesis, as DAGLα is the main 2-AG synthesizing enzyme in the adult organism. Due to enzymatic activity of the intact DAGLβ isoform, 2-AG is still present in Daglα$^{ko/ko}$ mice, albeit at remarkably reduced levels. Previous reports indicated a reduction of 2-AG levels of about 80 % in Daglα$^{ko/ko}$ animals (Gao et al. 2010). An extensive reduction in hippocampal 2-AG levels was also detected in the Daglα knockout mouse line presented here. However, so far only brain tissue of a single homozygous knockout animal was tested. To facilitate statistical validation of the reduced 2-AG levels, the numer of tested animals will have to be increased. Nevertheless, together these results strongly suggest that the applied gene targeting strategy has been successful in producing a loss-of-function Daglα allele.

In addition to the constitutive knockout, tissue-specific Daglα knockout mice were generated by mating Daglα$^{fl/fl}$ mice with appropriate Cre-expressing mouse lines. To specifically target cells of the myeloid lineage, the LysM-Cre line was utilized (Clausen et al. 1999). Mating with Syn1-Cre mice (Zhu et al. 2001) leads to neuron-specific deletion of Daglα expression. So far, these conditional mouse lines are still breeding. A first set of behavioral tests was performed with constitutive Daglα$^{ko/ko}$ mice. 2-AG mediated signaling plays a role in a variety of brain areas and in different neuronal circuits. Therefore, the effect of a constitutive Daglα knockout will become manifest in different neurological processes. In order to obtain first insights into possible behavioral alterations, a set of tests was performed with a group of Daglα$^{ko/ko}$ mice.

5.3 Behavioral phenotyping of Daglα$^{ko/ko}$ animals

The behavioral data discussed in this section are still preliminary, because the behavioral tests have to be repeated with a higher number of animals and separated gender analysis.

Daglα$^{ko/ko}$ animals appeared healthy, were fertile and initially not distinguishable from wild type littermates. Possible alterations in locomotor activity, novel environment exploration and anxiety-related behavior were assessed in an open field test. No deficits were detected in locomotion or exploratory behavior, indicated by the number of rearings. This observation is in line with a first report about a Daglα knockout mouse line (Gao et al. 2010), which also did not show changes here. Cannabimimetic activity of exogenous or

endogenous cannabinoids include a suppressive effect on motility, which is generally assessed by an open field test as part of the so-called tetrad assay (Martin et al. 1991; Onaivi 2002). Acute pharmacological blockage of the 2-AG degrading enzyme MAGL was shown to cause hypomotility in the tetrad assay (Long et al. 2009), thus indicating a typical cannabimimetic activity of 2-AG. Similar effects were detected for i.p. administered anandamide and THC (Fride & Mechoulam 1993; Crawley et al. 1993). Therefore, locomotion seems to be unaffected by reduced levels of 2-AG occurring in Daglα knockout mice, whereas elevated levels of 2-AG evoke hypomotility.

The open field test also serves to examine anxiety-related behavior. Anxious animals avoid the open area and tend to spend more time close to the walls or corners of the arena (Prut & Belzung 2003). Except for the first 5 min of the test session, Daglα$^{ko/ko}$ animals spent less time in the center of the arena compared to wild type conrols. A significant difference between the two groups was detected towards the end of the test session. While wild type animals started to familiarize with the environment and gradually spent more time in the open area, Daglα$^{ko/ko}$ animals seemed to be more cautious and reluctant, indicating anxious behavior. The ECS has been reported to influence emotional responses. Behavioral studies performed with CB_1 receptor knockout mice indicated increased anxiety-related behavior in various paradigms, such as the light-dark box or the plus maze test (Martin et al. 2002; Haller et al. 2004; Urigüen et al. 2004). Thus, the disrupted CB_1 signaling seemed to promote anxious behavior. Opposite effects were reported, when endocannabinoid levels were increased. Elevation of endogenous anandamide levels was achieved by pharmacological blockage of FAAH and led to reduced anxiety in behavioral tests. This effect was antagonized by the CB_1 antagonist rimonabant, demonstrating an involvement of the CB_1 receptor (Moreira et al. 2008). More recently, similar results were obtained for 2-AG. Inhibition of the 2-AG degrading enzyme MAGL reduced anxiety-related behavior. Interestingly, this effect seemed to involve CB_2 receptor signaling, as this effect was abolished by the pre-treatment of CB_2 antagonists or utilization of CB_2 knockout animals (Busquets-Garcia et al. 2011; Sciolino et al. 2011).

2-AG levels were remarkably reduced in hippocampal tissue of the Daglα knockout line presented here. As mentioned earlier, this result has to be further validated and extended to other brain regions. Nevertheless, these data indicate that reduced 2-AG signaling promotes anxiety.

To further investigate anxiety-related behavior in Daglα$^{ko/ko}$ mice the fear conditioning paradigm was chosen. The endocannabinoid system is an important modulator of pain responses (for review see Guindon & Hohmann 2009) and altered pain perception could influence the outcome of the fear extinction test. Therefore, the animals were tested for possible alterations in pain perception before the paradigm was started. A

hot plate test for acute thermal nociception did not reveal significant differences in pain responses in Daglα$^{ko/ko}$ mice. Similar results were reported earlier for Daglα$^{ko/ko}$ mice (Gao et al. 2010). Hot plate tests performed in mice, which were i.p. injected with 2-AG revealed a hypoalgesic effect of 2-AG (Mechoulam et al. 1995). Due to this finding one might argue that reduced 2-AG levels will lead to increased pain sensitivity. However, results obtained by exogenously administered endocannabinoids do not resemble physiological levels of these substances. Probably, the reduction of 2-AG in Daglα$^{ko/ko}$ mice is not pronounced enough to evoke an increased pain sensitivity. Additionally, compensatory effects of other endocannabinoids might also account for unaltered pain perception.

The fear conditioning paradigm is well accepted as a model for a variety of anxiety disorders prevailing in human society. Investigating behavioral characteristics and underlying neuronal mechanisms is of crucial importance for the development of effective treatment concepts of trauma- and other anxiety-related disorders. Among the scientific community different protocols are used for this paradigm. The one presented here is explained in detail in section 3.6.6.3. The analysis of the obtained data differentiates between-session extinction, which is achieved by consecutive exposure sessions and within-session extinction, which describes the decline of the fear response during a single exposure session. Between-session extinction is thought to be essential for long-lasting fear relieve (Craske et al. 2008). Elicited freezing behavior of the test subjects served as indicator for the degree of conditioned fear. In this context, it was already shown by previous studies that successful extinction of aversive memories is crucially dependent on CB_1 receptor signaling. Genetic ablation or pharmacological blockage of CB_1 receptor activation led to delayed between-session extinction, also termed long-term extinction and incapacity in achieving within-session extinction (short-term extinction). In contrast, acquisition and consolidation of aversive memories seemed to be independent of CB_1 receptor signaling (Marsicano et al. 2002; Plendl & Wotjak 2010).

Due to the fact that the activity of DAGLα is closely intertwined with the activity of the CB_1 receptor in the ECS, phenotypical similarities between the two knockout mouse lines are expected. To test this hypothesis, $CB_1^{ko/ko}$ and Daglα$^{ko/ko}$ animals were tested in parallel in the fear conditioning paradigm. Both knockout mouse lines displayed between-session extinction and reached similar base line freezing levels as wild type control animals. No difference between knockout and wild type animals was detected when exclusively the first 20 seconds of tone presentation were considered over the course of different extinction trials. A delay in between-session extinction became obvious, when the whole period of tone presentation was considered (180 s). This effect was most pronounced at extinction trials E2 and E3 in both knockout lines. This observation

contrasts the finding of Plendl and colleagues, who claimed that between-session extinction is dependent on intermittent tone presentations and cannot be achieved by a single tone presentation per day (Plendl & Wotjak 2010). The divergent observations might be ascribed to different mouse strains used for the behavioral testing. Plendl et al., used C57BL/6N $CB_1^{ko/ko}$ mice, whereas the tests presented here were performed with $CB_1^{ko/ko}$ mice on a C57BL/6J background (Zimmer et al. 1999). It was reported previously that in extinction tests, freezing of C57BL/6J mice declined significantly faster than the freezing of C57BL/6N mice (Stiedl et al. 1999).

Separate analysis of the extinction trials uncovered deficits of both, $CB_1^{ko/ko}$ and $Dagl\alpha^{ko/ko}$ mice in within-session extinction. At extinction trial E1, which was initiated 24 h after fear conditioning $CB_1^{ko/ko}$ mice displayed similar freezing behavior compared to wild type animals. This is in accordance with previous findings and indicates proper acquisition and early consolidation of memory (Marsicano et al. 2002). $Dagl\alpha^{ko/ko}$ mice showed impaired within-session extinction already on extinction trial E1. This finding raises the question, whether acquisition and early memory consolidation is affected in these animals. However, due to the low number of mice that were tested in the present study, the experiment has to be repeated with higher animal numbers to verify this observation. The role of 2-AG in acquisition and consolidation of memory has been investigated by pharmacological inhibition of MAGL. The authors did not observe an impact on memory formation by acute elevation 2-AG levels (Busquets-Garcia et al. 2011). Nevertheless, as these authors applied different tests than described here, and also acute elevation differs largely from constitutive downregulation, it cannot be excluded that reduced 2-AG levels affect early phases of memory creation.

Irrespective of these differences on extinction trial E1, $CB_1^{ko/ko}$ and $Dagl\alpha^{ko/ko}$ mice displayed a nearly superimposable behavior during the following sessions of extinction. Both mouse lines were significantly impaired in extinction of aversive memories. This observation was remarkable with respect to the fact that low levels of 2-AG are still present in $Dagl\alpha^{ko/ko}$ mice. Thus, the extend of reduction in 2-AG levels might already be sufficient to cause extinction impairment as seen in $CB_1^{ko/ko}$ animals. Unexpectedly, freezing behavior was elevated during the last third of tone presentation at extinction trial E6. Since this phenomenon was seen in both knockout lines, a random observation seems unlikely. Sustained freezing after fear incubation of several weeks was already observed in $CB_1^{ko/ko}$ animals. Although an initial decay of freezing had occurred, elevated freezing was evoked by a tone presentation 40 days after fear conditioning (Plendl & Wotjak 2010). However, in the paradigm discussed here, only 2 days without tone presentation preceded extinction trial E6. As mentioned before, repeated testing should be done to validate this observation.

The molecular mechanisms mediating extinction of aversive memories are complex. A first analysis of Daglα$^{ko/ko}$ mice in the fear conditioning paradigm predicts an important role for 2-AG in this context and supports the findings about an involvement of the CB_1 receptor. Nevertheless, the regulation of the ECS and the participation of different brain regions has to be further investigated. So far, it has been shown that 2-AG and AEA levels rise after the first extinction training in the basolateral amygdala (BLA), a brain region critically involved in the acquisition and expression of conditioned fear (Marsicano et al. 2002; Myers & Davis 2007). Yet, another study proposes that AEA and not 2-AG is important for altered synaptic transmission in the amygdala during processing of aversive memories (Azad et al. 2004). Besides the amygdala, other brain regions such as the hippocampus and the medial prefrontal cortex (mPFC) have been implicated in fear extinction processing. Kamprath and colleagues supposed that fear extinction involves a habituation-like component. By analysis of cell-type specific $CB_1^{ko/ko}$ animals they revealed that CB_1 receptor signaling in cortical glutamatergic synapses is essential for fear adaptation, which occurs upon repeated exposure to stressful events (Kamprath et al. 2006; Kamprath et al. 2009). Studies focusing on the effect of repeated homotypic stress point into the same direction. 2-AG levels in cortical brain regions were elevated after repeated stressor exposure, whereas glutamate release declined gradually (Rademacher et al. 2008; Patel & Hillard 2008). Patel and Hillard proposed a model, in which this mechanism of stress adaptation is mediated through an increased synthesis of 2-AG (Patel & Hillard 2008). Although many studies have been performed in this field, the exact mechanism underlying the processing of aversive memories remains elusive. Taking into account that retrograde endocannabinoid signaling is largely dependent on 2-AG produced by Daglα (Tanimura et al. 2010), the Daglα knockout mouse model represents a valuable tool for unraveling the ECS mediated process of fear extinction on a molecular level.

In conclusion, the conditional knockout mouse line for Daglα generated in this thesis opens up diverse possibilities to investigate the role of 2-AG signaling in a tissue specific manner. Nevertheless, the generation of the Daglβ knockout mouse line will be futher pursued, because a complete loss of 2-AG signaling will only be achieved by a doule knockout of Daglα and Daglβ.

5.4 Primary microglial cell cultures

The second aim of this thesis was focused on the establishment of primary microglial cell cultures, as well as on the induction and analysis of different activation states in this cell type. The microglial cells used in this work were primary cells, obtained from newborn C57BL/6 mice at postnatal days 1-5. Nowadays, a variety of murine microglial cell lines is available as for example BV-2 and N9 cell lines, which were generated by retroviral infection of primary microglia (Righi et al. 1989; Blasi et al. 1990). The highly proliferative cell line HAPI (highly aggressively proliferating immortalized) was obtained without genetic manipulation from primary rat microglia. However, the comparability of an immortalized cell line and primary cultures is still a controversial debate (Horvath et al. 2008; Henn et al. 2009; Stansley et al. 2012). Henn and colleagues compared primary cultures with the cell line BV-2 and sought to cover different aspects of microglial features. They detected a high degree of transcriptional overlap in response to pro-inflammatory stimuli and also similar capacities in cell-cell interactions. But the responsiveness to LPS was significantly weaker and cytokine production was partially impaired (Henn et al. 2009). A promising alternative to immortalized cell lines is represented by embryonic stem cell derived microglia (ESdM), which can be obtained from ES cells by a sophisticated differentiation protocol. ESdM are morphologically indistinguishable from primary microglia, display a similar expression pattern of surface receptors and are capable to phagocytose microsphere beads (Napoli et al. 2009; Beutner et al. 2010).

In order to characterize distinct activation states of microglia and to subject these differentially activated cells to comprehensive gene expression profiling, required highly sensitive cells. Primary microglia were the best choice for this purpose, because these cells are unaffected by genetic modification or artefacts of selection occurring in cell lines. Nevertheless, particularly with regard to the approved changes of the Animal Welfare Act (TierSchG), it is of special concern to keep the number of used animals as low as possible. For the establishment of a protocol, which assures the highest yield of microglia from mixed glial cultures, two different harvesting methods were tested. One of them was based on mechanical shaking, which led to an accumulation of microglia in the supernatant. The other one facilitated enrichment of microglia by different trypsinization steps. The best yield of microglia with respect to the amount of required starting material was achieved using the “trypsinization method”. Therefore, this technique was used for subsequent stimulation experiments that were performed in this project. Although the comparability of *in vivo* and *in vitro* data is limited, primary microglia cell cultures still represent the cell culture model, which is the most suitable to reflect physiological conditions. The ability of microglia to adopt different states of activation is preserved in these cells and enables the comprehensive investigation of this versatile cell type *in vitro*.

5.5 Different activation states of primary microglia

The occurrence of distinct activation states, such as a pro-inflammatory M1 subtype (classically activated), an anti-inflammatory M2a subtype (alternatively activated) and other subtypes with anti-inflammatory properties (acquired deactivated or M2b/M2c) has been reported for macrophages (Gordon 2003; Mantovani et al. 2004). A similar concept, which distinguishes between differentially activated subtypes of microglia has been proposed by other groups (Colton 2009; Varnum & Ikezu 2012).

One part of the project described here, focused on the polarization of primary microglia into distinct states of activity by challenging these cells with different pro- or anti-inflammatory substances. Furthermore, to facilitate a reliable identification of each state, a set of specific candidate marker molecules was tested, using different analytical methods. Treatment of microglial cells with pro-inflammatory substances such as LPS in combination with IFNγ resulted in a specific upregulation of ICAM-1, CD86 and CD40, as detected by flow cytometry. In addition, the production of the pro-inflammatory cytokines IL-6 and TNFα, as well as enhanced transcription of iNOS was induced. Concerning the experiments that were performed in this project, the upregulation of these molecules was reliable and specific to LPS/IFNγ stimulation. Simular results regarding LPS and/or IFNγ stimulated microglia were reported previously (Shrikant et al. 1995; Menèndez Iglesias et al. 1997; Stohwasser et al. 2000; Benveniste et al. 2004). Therefore, these molecules were considered to be uselful markers for the identification of the reactive pro-inflammatory “M1-like” subtype.

IL-4 stimulation was used to evoke an activation state with anti-inflammatory properties. Cell surface staining and subsequent flow cytometric analysis revealed a significant upregulation of the MMR in response to IL-4 treatment. In addition, mRNA levels of Arg1, Ym1 and FIZZ1 were specifically elevated. These findings are in accordance with previous reports and indicate the successful induction of the anti-inflammatory “M2a-like” activation state (Zimmer et al. 2003; Colton et al. 2006).

Stimulation of microglia with IL-10 and/or TGFβ was proposed to evoke an anti-inflammatory, here referred to as “M2c-like” phenotype, which is supposed to exhibit an anti-inflammatory profile distinct from that induced by IL-4 (Colton 2009). This hypothesis was tested in this study. Primary microglial cells were challenged with IL-10 and TGFβ alone or in combination. Subsequently, the expression levels of Toll-like receptor-1 (TLR-1) was tested, as the expression of these molecule was shown to be upregulated in response to IL-10 in human monocytes (Williams et al. 2002). However, these results could not be confirmed with primary microglial cells used here. Cell type and species differences might account for the lack of reproducibility. Other markers that were reported

to be upregulated in response to TGFβ stimulation in primary microglia, as for example the purinergic receptor P2ry12 (De Simone et al. 2010) and HGF (Lalive et al. 2005) were tested in this study as well. While no specific upregulation of P2ry12 upon TGFβ was detected, TGFβ stimulation evoked enhanced release of HGF, as determined by repeated ELISA measurement. Further testing is required to standardize the culture conditions, because the release pattern of HGF seems to involve a kinetic component. However, the present study is the first to report the HGF as possible marker molecule for a “M2c-like” subtype induced by TGFβ stimulation in primary microglia.

In macrophages and microglia a third subtype, which is associated with immunosuppressive properties, is often referred to as “deactivated” or “acquired deactivated” state (Gordon 2003; Mantovani et al. 2004; Colton 2009). The reason for difficulties to find suitable marker molecules for this subtype might be rooted in its function. The functioning of the pro-inflammatory “M1-like” subtype is associated with antigen presentation and massive release of different pro-inflammatory cytokines. Thus, these properties facilitate the identification of marker molecules of this subtype. The complexity of the reactive “M1-like” subtype was also mirrored by the abundance of induced genes upon LPS/IFNγ stimulation. This was revealed by comprehensive gene expression profiling performed in this project. Instead, the functioning of the “M2c-like” subtype is not supposed to be associated with antigen presentation and excessive cytokine release. Therefore, the set of typically regulated molecules might be reduced compared to the “M1-like” subtype - a fact that hamperes the search for marker molecules. This hypothesis is supported by the results of the conducted gene expression profiling. The impact of TGFβ stimulation on microglial gene expression was by far less pronounced than the impact of LPS/IFNγ stimulation. The effect of IL-10 on gene expression was tested in a study performed by Lang and colleagues. Albeit, they used primary macrophages and compared the effect of LPS alone and IL-10, they also observed that the number of genes induced by IL-10 was remarkably smaller compared to those induced by LPS (Lang et al. 2002).

Another aspect that has to be taken into account is the assumption that the classification of distinct phenotypes is - especially for activation states with anti-inflammatory properties - over simplified. For macrophages it has been proposed that anti-inflammatory activites are probably exerted by a continuum of phenotypes. Therefore, distinct anti-inflammatory subtypes are still controversially discussed (Gordon 2003; Mantovani et al. 2004; Mosser & Edwards 2008; Mantovani et al. 2013). Microglia are tissue specific and therefore probably less versatile than pheripheral macrophages. Nevertheless, it is possible that these cells can adopt diverse anti-inflammatory phenotypes, dependent on the phase of an inflammatory response, the cytokine

environment and not at least regional properties.

Interesting results were obtained in this project for the costimulatory molecule CD80, which was upregulated in response to IL-10 stimulation. In contrast, CD80 levels were unaffected by LPS/IFNγ treatment. Like CD86, CD80 is a costimulatory molecule present on antigen-presenting cells, such as dendritic cells. Both molecules play an important role in T-cell activation (for review see: Slavik et al. 1999), thus supporting pro-inflammatory activities. Although CD80 and CD86 are recognized by the same receptors, it was shown that they are not equally induced by the same stimuli. While CD86 was upregulated in response to LPS/IFNγ in primary murine microglial cultures, this was not observed for CD80 (Menèndez Iglesias et al. 1997). However, it was reported that CD80 was upregulated upon LPS/IFNγ stimulation in human microglia (Durafourt et al. 2012). Contrasting these findings, Sansom and colleagues proposed a model where CD80 plays a role in the restriction of T-cell activation. In that, regulatory T-cells interact with immature dendritic cells via CD80-CD152 interactions and thereby suppress T-cell activation in a non-inflammatory environment. Anti-inflammatory cytokines, such as IL-10 support this activity and prevent T-cell activation in the absence on an inflammatory stimulus (Sansom et al. 2003). Whether this model is applicable on microglial cells is of course arguable. Nevertheless, it would support the observation reported here that CD80 expression is enhanced in response to IL-10 stimulation. Microglia might act as regulators of T-cell activation under these conditions and thus promote the decay of an inflammatory reaction.

5.6 Differential expression of ECS-related genes in microglia

Comprehensive gene expression profiling performed within this work revealed that the combined application of LPS and IFNγ achieved the broadest impact on gene regulation in primary microglia. The subsequent phenotypic changes that were induced by these substances were well detectable, as described before. In comparison, the effect of IL-4 and TGFβ on gene transcription was by far less pronounced. Nevertheless, only a small proportion of regulated genes were commonly affected by IL-4 and TGFβ, pointing out distinct modulatory activities and supporting the idea of distinct activation states. The obtained lists of genes that were responsive to the respective stimulation represent an important source to analyze involved signaling pathways in detail in the near future.

As mentioned earlier, the regulation of genes that are related to the ECS was in the focus of this thesis. Gene expression profiling revealed a distinct expression pattern for several ECS-related molecules in differentially activated microglia. An overview of the

corresponding ECS components and of identified marker moelcules for the respective microglial activation state is given in Table 3.

Table 3: Regulation of ECS-related genes in differentially activated microglia. The subtypes "M1-like", "M2a-like" and "M2c-like" were induced by LPS/IFNγ, IL-4 or TGFβ stimulation, respectively. The sets of confirmed marker molecules and the responsive components of the ECS are listed below. LPS: Lipopolysaccharide, IFNγ: interferon γ, IL-4: interleukin-4, TGFβ: transforming growth factor β, ICAM-1: intercellular adhesion molecule-1, CD80/CD40: costimulatory molecules, TNFα: tumor necrosis factor α, IL-6: interleukin-6, iNOS: inducible nitric oxide synthase, MMR: macrophage mannose receptor, YM1: chitinase-3-like-3, FIZZ1: found-in-inflammatory-zone 1, Arg1: arginase 1, HGF: hepatocyte growth factor, CB_2: cannabinoid receptor 2, DAGLβ: diacylglycerol lipase β, ABHD12: Aβ-hydrolase 12, NAPE-PLD: N-arachidonoyl-phosphatidylethanolamine specific phospholipase D, GPR18: G-protein coupled receptor 18; ⬆ upregulated compared to unstimulated control, ⬇ downregulated compared to unstimulated control, ÷ no change compared to unstimulated control

	"M1-like" LPS/IFNγ		**"M2a-like" IL-4**		**"M2c-like" TGFβ**	
Marker molecules	ICAM-1	⬆	MMR	⬆	HGF	⬆
	CD80/CD40	⬆	Ym1	⬆		
	TNFa	⬆	FIZZ1	⬆		
	IL-6	⬆	Arg1	⬆		
	iNOS	⬆				
ECS related components	CB_2	⬇	CB_2	÷	CB_2	⬆
	DAGLβ	⬇	DAGLβ	÷	DAGLβ	÷
	ABHD12	⬇	ABHD12	÷	ABHD12	÷
	NAPE-PLD	⬆	NAPE-PLD	÷	NAPE-PLD	÷
	GPR18	⬆	GPR18	÷	GPR18	÷

The responsive genes encode key components of the ECS. Changes in the expression level of NAPE-PLD and DAGLβ were detected. These enzymes are responsible for the synthesis of the two main endocannabinoids AEA and 2-AG. Moreover, the expression of 2 cannabinoid receptors, CB_2 and GPR18, and ABHD12, a 2-AG degrading enzyme, were altered.

LPS/IFNγ stimulation had a stronger impact on gene expression levels than other stimuli in microglia. On closer consideration it becomes obvious that the genes encoding DAGLβ, the CB_2 receptor and ABHD12 were regulated in a similar way. Their respective expression levels were diminished in response to LPS/IFNγ. This is an interesting aspect, as all these components are closely related to 2-AG signaling. CB_2 expression was down regulated under pro-inflammatory conditions, while 2-AG production might have remained homeostatic with less synthesis and less degradation. In contrast, the gene encoding NAPE-PLD was upregulated in response to LPS/IFNγ, just as the newly identified

cannabinoid receptor GPR18, which can be activated by a metabolite of NAPE-PLD-produced AEA.

IL-4 stimulation did not result in significant changes in genes that encode components of the ECS. In contrast, TGFβ stimulation enhanced CB_2 receptor expression in primary microglia. The regulation of the CB_2 receptor in immune cells is definitely the aspect, which has been most intensively studied by others. Nevertheless, it is still not completely understood. It is generally assumed that CB_2 is not or only marginally expressed in healthy brain tissue (Munro et al. 1993; Galiègue et al. 1995a; Carlisle, et al. 2002). Cultured primary microglial cells are in a "primed", responsive state and express detectable amounts of CB_2 (Becher & Antel 1996; Carlisle, et al. 2002; Walter et al. 2003). It has also been reported that fully activated microglia occurring in brain tissue of patients suffering from multiple sclerosis or Alzheimer's disease express CB_2 (Benito et al. 2003; Yiangou et al. 2006). Therefore, CB_2 receptor upregulation is thought to be associated with the activation process of microglia under inflammatory conditions. In contrast, *in vitro* studies revealed that pro-inflammtory stimuli such as IFNγ alone did not affect CB_2 levels or, in the case of LPS, even reduced its expression in microglia (Carlisle, et al. 2002; Maresz et al. 2005). This observation is in line with the results reported here and supports the idea that CB_2 activation promotes rather immunosuppressive activities. However, it might also be possible, that CB_2 is upregulated in a short time frame during the process of activation to promote proliferation and migration to lesion sites, as this has been shown to occur in a 2-AG dependent manner (Walter et al. 2003; Carrier et al. 2004). Arranging these reports with the obtained data in this work, the following scenario might be possible: Downregulation of the CB_2 receptor would occur during the reactive pro-inflammatory phase of an immune response. A second wave of CB_2 expression would be induced in a later phase of inflammation coinciding with the switch to an immunosuppressive "M2a- or M2c-like" subtype. However, discrepancies of *in vivo* and *in vitro* data as well as differences in stimulation protocols complicate the generation of a consistent picture.

A completely different induction pattern was observed here for the newly identified cannabinoid receptor GPR18. The expression level of the corresponding gene was strongly elevated in response to LPS/IFNγ in primary microglia. Similar results were reported for macrophages. Takenouchi and colleagues observed an upregulation of Gpr18 mRNA levels in pertioneal macrophages and RAW264.7 macrophages upon LPS/IFNγ stimulation, while IL-4 treatment had no effect (Takenouchi et al. 2012). GPR18 can be activated by NaGly, which is a metabolite of AEA and the most efficacious agonist (McHugh et al. 2010). But also AEA and - to a lesser extent - 2-AG are able to activate GPR18 (McHugh et al. 2012). Addition of NaGly effectively induced apoptosis in macrophages (Takenouchi et al. 2012). It was proposed that NaGly might serve as an

immunosuppressive mediator, which reduces the number of pro-inflammatory M1 macrophages by inducing apoptosis (Takenouchi et al. 2012). Up to now, these observations were not verified in microglia and this study is the first to report enhanced GPR18 expression in LPS/IFNγ treated primary microglia. However, the interpretation of Takenouchi and colleagues supports the general view that the ECS exerts beneficial functions during the course of an immune response by balancing pro-and anti-inflammatory reactions.

In conclusion, gene expression profiling of differentially activated microglia revealed that each substance induced a distinct pattern of gene regulation. The obtained data will provide helpful insights into the function of different microglia subtypes on the level of gene expression. Some genes encoding components of the ECS were shown to be responsive to different stimuli and underline an important role of the ECS in immune regulation. Nevertheless, further research has to be performed. Comprehensive analysis of the gene structure and corresponding promotor elements of CB_2 and GPR18, for example, could provide important data, which might reveal the link between the signaling pathways elicited by different stimulants and the phenotypical outcome.

5.7 Conclusion and outlook

The ECS acts as regulator in numerous physiological processes, both in the CNS and in peripheral organs. Comprehensive research has identified several receptors and a set of endogenous ligands, which exhibit different affinities to each of the receptors. One part of this study aimed at generating conditional knockout mouse models for the 2-AG synthesizing enzymes DAGLα and DAGLβ. Different experiments concerning the generation of conditional targeting vectors, validation strategies and a first set of behavioral tests performed with $Daglα^{ko/ko}$ animals was outlined. The generation of the Daglβ knockout mouse line is still pending. New targeting techniques, as the TALEN methodology present promising and time saving tools, which might be used for the generation of this mouse line in the near future. DAGLα is the main 2-AG producing enzyme in the adult CNS. Utilization of the new mouse model will facilitate the elaboration of a comprehensive working profile of 2-AG in this area. Preliminary behavioral data indicate a role of 2-AG in anxiety and extinction of aversive memories. Additional tests, as for example the light-dark test or the elevated plus maze could further confirm and validate this phenotype. In addition, endogenous levels of a broader spectrum of endocannabinoids should be measured to reveal possible compensatory mechanisms. Cell-type specific knockout of Daglα in neurons as well as in myeloid cells is ongoing.

These approaches will provide important insights not only into the role of 2-AG signaling in neuronal circuits, but also in terms of microglia behavior, as these cells are supposed to be the main source of endocannabinoids under neuroinflammatory conditions (Stella 2009a).

In the second part of the project, the cultivation of primary microglial cultures was established and different activation states were induced. Comprehensive analysis verified marker molecules that can be used for the identification of these subtypes. Gene expression profiling of polarized microglia yielded different sets of responsive genes. These sets provide important starting points for the analysis of signaling mechanisms that are induced upon different stimulations. Genes encoding components of the ECS were shown to be differentially expressed. Futher reseach projects will have to be performed to analyze the role of the ECS in more detail. Therefore, differentially activated microglia could be challenged with exogenously applied cannabinoids *in vitro* and the effect of cannabinoids on microglial phenotypes could be analyzed. Moreover, neuron-microglia co-cultures represent a valuable tool to investigate the role of the ECS in neuron microglia crosstalk under different pro-or anti-inflammatory conditions.

In conclusion, this thesis provides two different tools: On the one hand, the conditional Daglα knockout mouse line and on the other hand, the protocol for cultivation, polarization and identification of different microglial phenotypes. Both tools will advance the research of the endocannabinoid field. The conditional Daglα knockout mouse line allows a universal application in different contexts and microglial cultures will provide further insights into the ECS under neuroinflammatory conditions.

Bibliography

Abush, H. & Akirav, I., 2010. Cannabinoids modulate hippocampal memory and plasticity. *Hippocampus*, 20(10), pp.1126–38.

Azad, S.C. et al., 2004. Circuitry for associative plasticity in the amygdala involves endocannabinoid signaling. *The Journal of neuroscience : the official journal of the Society for Neuroscience*, 24(44), pp.9953–61.

Banks, W.A. & Erickson, M.A., 2010. The blood–brain barrier and immune function and dysfunction. *Neurobiology of Disease*, 37(1), pp.26–32.

Battista, N. et al., 2012. The role of endocannabinoids in gonadal function and fertility along the evolutionary axis. *Molecular and cellular endocrinology*, 355(1), pp.1–14.

Becher, B. & Antel, J P, 1996. Comparison of phenotypic and functional properties of immediately ex vivo and cultured human adult microglia. *Glia*, 18(1), pp.1–10.

Bell, R.L. et al., 1980. Diglyceride lipase: a pathway for arachidonate release from human platelets. *Advances in prostaglandin and thromboxane research*, 6(7), pp.219–24.

Benito, C. et al., 2003. Cannabinoid CB 2 Receptors and Fatty Acid Amide Hydrolase Are Selectively Overexpressed in Neuritic Plaque-Associated Glia in Alzheimer ' s Disease Brains, 23(35), pp.11136–11141.

Benveniste, E. N., Nguyen, V.T. & Wesemann, D.R., 2004. Molecular regulation of CD40 gene expression in macrophages and microglia. *Brain behavior and immunity*, 18(1), pp.7–12.

Berghuis, P. et al., 2007. Hardwiring the brain: endocannabinoids shape neuronal connectivity. *Science (New York, N.Y.)*, 316(5828), pp.1212–6.

Beutner, C. et al., 2010. Generation of microglial cells from mouse embryonic stem cells. *Nature Protocols*, 5(9), pp.1481–1494.

Bilkei-Gorzo, A. et al., 2005. Early age-related cognitive impairment in mice lacking cannabinoid CB1 receptors. *Proceedings of the National Academy of Sciences of the United States of America*, 102(43), pp.15670–5.

Birling, M.-C., Gofflot, F. & Warot, X., 2009. Site-specific recombinases for manipulation of the mouse genome. *Methods In Molecular Biology Clifton Nj*, 561, pp.245–263.

Bisogno, T. et al., 2000. N-acyl-dopamines: novel synthetic CB(1) cannabinoid-receptor ligands and inhibitors of anandamide inactivation with cannabimimetic activity in vitro and in vivo. *The Biochemical journal*, 351 Pt 3, pp.817–24.

Bisogno, T. et al., 2003. Cloning of the first sn1-DAG lipases points to the spatial and temporal regulation of endocannabinoid signaling in the brain, 163(3), pp.463–468.

Blankman, J.L., Simon, G.M. & Cravatt, B. F., 2007. A comprehensive profile of brain enzymes that hydrolyze the endocannabinoid 2-arachidonoylglycerol. *Chemistry & biology*, 14(12), pp.1347–56.

Blasi, E. et al., 1990. Immortalization of murine microglial cells by a v-raf/v-myc carrying retrovirus. *Journal of Neuroimmunology*, 27(2-3), pp.229–237.

Bogdanove, A.J. & Voytas, D.F., 2011. TAL effectors: customizable proteins for DNA targeting. *Science (New York, N.Y.)*, 333(6051), pp.1843–6.

Bouaboula, M. et al., 1993. Cannabinoid-receptor expression in human leukocytes. *European journal of biochemistry / FEBS*, 214(1), pp.173–80.

Busquets-Garcia, A. et al., 2011. Differential role of anandamide and 2-arachidonoylglycerol in memory and anxiety-like responses. *Biological psychiatry*, 70(5), pp.479–86.

Capecchi, M.R., 1989. Altering the Genome Homologous Recombination. *Science*, 236(1987).

Carlisle, S.J., Marciano-Cabral, F., et al., 2002. Differential expression of the CB2 cannabinoid receptor by rodent macrophages and macrophage-like cells in relation to cell activation. *International Immunopharmacology*, 2(1), pp.69–82.

Carrier, E.J. et al., 2004. Cultured rat microglial cells synthesize the endocannabinoid 2-arachidonylglycerol, which increases proliferation via a CB2 receptor-dependent mechanism. *Molecular Pharmacology*, 65(4), pp.999–1007.

Clausen, B.E. et al., 1999. Conditional gene targeting in macrophages and granulocytes using LysMcre mice. *Transgenic research*, 8(4), pp.265–77.

Colton, C. et al., 1996. Species differences in the generation of reactive oxygen species by microglia. *Molecular and chemical neuropathology*, 28(1-3), pp.15–20.

Colton, C. A. et al., 2006. Expression profiles for macrophage alternative activation genes in AD and in mouse models of AD. *Journal of neuroinflammation*, 3(27).

Colton, C. A., 2009. Heterogeneity of microglial activation in the innate immune response in the brain. *Journal of neuroimmune pharmacology : the official journal of the Society on NeuroImmune Pharmacology*, 4(4), pp.399–418.

Colton, C. A. & Wilcock, D.M., 2010. Assessing activation states in microglia. *CNS & neurological disorders drug targets*, 9(2), pp.174–91.

Correa, F. et al., 2010. Anandamide enhances IL-10 production in activated microglia by targeting CB(2) receptors: roles of ERK1/2, JNK, and NF-kappaB. *Glia*, 58(2), pp.135–47.

Craske, M.G. et al., 2008. Optimizing inhibitory learning during exposure therapy. *Behaviour Research and Therapy*, 46(1), pp.5–27.

Cravatt, B. F. et al., 1996. Molecular characterization of an enzyme that degrades neuromodulatory fatty-acid amides. *Nature*, 384(6604), pp.83–87.

Crawley, J.N. et al., 1993. Anandamide, an endogenous ligand of the cannabinoid receptor, induces hypomotility and hypothermia in vivo in rodents. *Pharmacology Biochemistry and Behavior*, 46(4), pp.967–972.

Cui, X. et al., 2011. Targeted integration in rat and mouse embryos with zinc-finger nucleases. *Nature Biotechnology*, 29(1), pp.64–67.

Devane, W. A. et al., 1988. Determination and characterization of a cannabinoid receptor in rat brain. *Molecular Pharmacology*, 34(5), pp.605–613.

Devane, W. A. et al., 1992. Isolation and Structure of a Brain Constituent That Binds to the Cannabinoid Receptor. *Science*, 1558(10), pp.19–22.

Dinh, T. P. et al., 2002. Brain monoglyceride lipase participating in endocannabinoid inactivation. *Proceedings of the National Academy of Sciences of the United States of America*, 99(16), pp.10819–24.

Dinh, T. P., Kathuria, S. & Piomelli, D., 2004. RNA Interference Suggests a Primary Role for Monoacylglycerol Lipase in the Degradation of the Endocannabinoid 2-Arachidonoylglycerol, 66(5), pp.1260–1264.

Downer, E.J., 2011. Cannabinoids and innate immunity: taking a toll on neuroinflammation. *TheScientificWorldJournal*, 11, pp.855–65.

Durafourt, B. A. et al., 2012. Comparison of polarization properties of human adult microglia and blood-derived macrophages. *Glia*, 60(5), pp.717–27.

Eljaschewitsch, E. et al., 2006. The endocannabinoid anandamide protects neurons during CNS inflammation by induction of MKP-1 in microglial cells. *Neuron*, 49(1), pp.67–79.

Fairweather, D. & Cihakova, D., 2009. Alternatively activated macrophages in infection and autoimmunity. *Journal of Autoimmunity*, 33(3-4), pp.222–230.

Fiskerstrand, T. et al., 2010. Mutations in ABHD12 Cause the Neurodegenerative Disease PHARC : An Inborn Error of Endocannabinoid Metabolism. *The American Journal of Human Genetics*, 87(3), pp.410–417.

Fowler, C.J., 2012. Anandamide uptake explained? *Trends in pharmacological sciences*, 33(4), pp.181–5.

Fride, E. & Mechoulam, R., 1993. Pharmacological activity of the cannabinoid receptor agonist, anandamide, a brain constituent. *European journal of pharmacology*, 231(2), pp.313–4.

Galiègue, S. et al., 1995. Expression of central and peripheral cannabinoid receptors in human immune tissues and leukocyte subpopulations. *European journal of biochemistry / FEBS*, 232(1), pp.54–61.

Gao, Y. et al., 2010. Loss of retrograde endocannabinoid signaling and reduced adult neurogenesis in diacylglycerol lipase knock-out mice. *The Journal of neuroscience : the official journal of the Society for Neuroscience*, 30(6), pp.2017–24.

Gaoni, Y. & Mechoulam, R., 1964. Isolation, Structure, and Partial Synthesis of an Active Constituent of Hashish. *Journal of the American Chemical Society*, 86(8), pp.1646–1647.

Ginhoux, F. et al., 2010. Fate mapping analysis reveals that adult microglia derive from primitive macrophages. *Science (New York, N.Y.)*, 330(6005), pp.841–5.

Giulian, D & Baker, T.J., 1986. Characterization of ameboid microglia isolated from developing mammalian brain. *Journal of Neuroscience*, 6(8), pp.2163–2178.

Goncalves, M.B. et al., 2008. A diacylglycerol lipase-CB2 cannabinoid pathway regulates adult subventricular zone neurogenesis in an age-dependent manner. *Molecular and Cellular Neuroscience*, 38(4), pp.526–536.

Gordon, S., 2003. Alternative activation of macrophages. *Nature reviews. Immunology*, 3(1), pp.23–35.

Greter, M. & Merad, M., 2013. Regulation of microglia development and homeostasis. *Glia*, 61(1), pp.121–7.

Guindon, J. & Hohmann, A.G., 2009. The endocannabinoid system and pain. *CNS neurological disorders drug targets*, 8(6), pp.403–421.

Gulyas, A. I. et al., 2004. Segregation of two endocannabinoid-hydrolyzing enzymes into pre- and postsynaptic compartments in the rat hippocampus, cerebellum and amygdala. *The European journal of neuroscience*, 20(2), pp.441–58.

Haller, J. et al., 2004. Context-dependent effects of CB1 cannabinoid gene disruption on anxiety-like and social behaviour in mice. *European Journal of Neuroscience*, 19(7), pp.1906–1912.

Hanisch, U.-K., 2002. Microglia as a source and target of cytokines. *Glia*, 40(2), pp.140–55.

Hanisch, U.-K. & Kettenmann, H., 2007. Microglia : active sensor and versatile effector cells in the normal and pathologic brain. *Nature Neuroscience*, 10(11), pp.1387–1394.

Hansen, H.S. et al., 2000. N-Acylethanolamines and precursor phospholipids - relation to cell injury. *Chemistry and physics of lipids*, 108(1-2), pp.135–50.

Hanus, L et al., 2001. 2-arachidonyl glyceryl ether, an endogenous agonist of the cannabinoid CB1 receptor. *Proceedings of the National Academy of Sciences of the United States of America*, 98(7), pp.3662–5.

Henn, A. et al., 2009. The suitability of BV2 cells as alternative model system for primary microglia cultures or for animal experiments examining brain inflammation. *ALTEX Alternativen zu Tierexperimenten*, 26(2), pp.83–94.

Horvath, R.J. et al., 2008. Differential migration, LPS-induced cytokine, chemokine, and NO expression in immortalized BV-2 and HAPI cell lines and primary microglial cultures. *Journal of neurochemistry*, 107(2), pp.557–69.

Huang, S.M. et al., 2002. An endogenous capsaicin-like substance with high potency at recombinant and native vanilloid VR1 receptors. *Proceedings of the National Academy of Sciences of the United States of America*, 99(12), pp.8400–5.

Hughes, E.D. et al., 2007. Genetic variation in C57BL/6 ES cell lines and genetic instability in the Bruce4 C57BL/6 ES cell line. *Mammalian genome : official journal of the International Mammalian Genome Society*, 18(8), pp.549–58.

Idris, A.I. & Ralston, S.H., 2010. Cannabinoids and bone: friend or foe? *Calcified tissue international*, 87(4), pp.285–97.

Izzo, A. A. & Sharkey, K. A., 2010. Cannabinoids and the gut: new developments and emerging concepts. *Pharmacology & therapeutics*, 126(1), pp.21–38.

Jung, K. et al., 2005. Stimulation of Endocannabinoid Formation in Brain Slice Cultures through Activation of Group I Metabotropic Glutamate Receptors.*Molecular Pharmacology*, 68(5), pp.1196–1202.

Kamprath, K et al., 2009. Endocannabinoids mediate acute fear adaptation via glutamatergic neurons independently of corticotropin-releasing hormone signaling. *Genes brain and behavior*, 8(2), pp.203–211.

Kamprath, K. et al., 2006. Cannabinoid CB1 receptor mediates fear extinction via habituation-like processes. *The Journal of neuroscience : the official journal of the Society for Neuroscience*, 26(25), pp.6677–86.

Karlsson, M. et al., 1997. cDNA Cloning, Tissue Distribution, and Identification of the Catalytic Triad of Monoglyceride Lipase. *Journal of Biological Chemistry* , 272(43), pp.27218–27223.

Katona, I. & Freund, T. F., 2008. Endocannabinoid signaling as a synaptic circuit breaker in neurological disease. *Nature medicine*, 14(9), pp.923–30.

Kettenmann, H. & Hanisch, U.-K., 2011. Physiology of microglia. *Physiological reviews,* pp.461–553.

Kierdorf, K. et al., 2013. Microglia emerge from erythromyeloid precursors via Pu.1- and Irf8-dependent pathways. *Nature neuroscience*, 16(3), pp.273–80.

Klein, T.W., Friedman, H. & Specter, S., 1998. Marijuana, immunity and infection. *Journal of Neuroimmunology*, 83(1–2), pp.102–115.

Kontgen, F. et al., 1993. Targeted disruption of the MHC class II Aa gene in C57BL:6 mice. *International Immunology*, 5(8), pp.957–964.

Lakso, M. et al., 1996. Efficient in vivo manipulation of mouse zygote stage genomic sequences at the. *Proceedings of the National Academy of Sciences of the United States of America* , 93, pp.5860–5865.

Lalive, P.H. et al., 2005. TGF-beta-treated microglia induce oligodendrocyte precursor cell chemotaxis through the HGF-c-Met pathway. *European journal of immunology*, 35(3), pp.727–37.

Lallemand, Y. et al., 1998. Maternally expressed PGK-Cre transgene as a tool for early and uniform activation of the Cre site-specific recombinase. *Transgenic Research*, 7(2), pp.105–112.

Lang, R. et al., 2002. Shaping gene expression in activated and resting primary macrophages by IL-10. *Journal of immunology*, 169(5), pp.2253–63.

Ledeboer, A. et al., 2000. Interleukin-10, interleukin-4, and transforming growth factor-β differentially regulate lipopolysaccharide-induced production of pro-inflammatory cytokines and nitric oxide in co-cultures of rat astroglial and microglial cells. *Glia*, 30(2), pp.134–142.

Lee, S.C. et al., 1993. Cytokine production by human fetal microglia and astrocytes. Differential induction by lipopolysaccharide and IL-1 beta. *The Journal of Immunology,* 150(7), pp.2659–2667.

Lee, S.J. & Benveniste, E. N., 1999. Adhesion molecule expression and regulation on cells of the central nervous system. *Journal of neuroimmunology*, 98(2), pp.77–88.

Long, E.O., 2011. ICAM-1: getting a grip on leukocyte adhesion. *Journal of immunology*, 186(9), pp.5021–3.

Long, J.Z. et al., 2009. Selective blockade of 2-arachidonoylglycerol hydrolysis produces cannabinoid behavioral effects. *Nature chemical biology*, 5(1), pp.37–44.

Longo, L. et al., 1997. The chromosome make-up of mouse embryonic stem cells is predictive of somatic and germ cell chimaerism. *Transgenic Research*, 6(5), pp.321–328.

Lutz, B., 2007. The endocannabinoid system and extinction learning. *Molecular neurobiology*, 36(1), pp.92–101.

Mantovani, A. et al., 2013. Macrophage plasticity and polarization in tissue repair and remodelling. *The Journal of pathology*, 229(2), pp.176–85.

Mantovani, A. et al., 2004. The chemokine system in diverse forms of macrophage activation and polarization. *Trends in Immunology*, 25(12), pp. 677-86.

Maresz, K. et al., 2005. Modulation of the cannabinoid CB2 receptor in microglial cells in response to inflammatory stimuli. *Journal of neurochemistry*, 95(2), pp.437–45.

Marrs, W.R. et al., 2010. The serine hydrolase ABHD6 controls the accumulation and efficacy of 2-AG at cannabinoid receptors. *Nature neuroscience*, 13(8), pp.951–7.

Marsicano, G. et al., 2003. CB1 cannabinoid receptors and on-demand defense against excitotoxicity. *Science (New York, N.Y.)*, 302(5642), pp.84–8.

Marsicano, G. et al., 2002. The endogenous cannabinoid system controls extinction of aversive memories. *Nature*, 418(6897), pp.530–534.

Martin, B.R. et al., 1991. Behavioral, biochemical, and molecular modeling evaluations of cannabinoid analogs. *Pharmacology, biochemistry, and behavior*, 40(3), pp.471–8.

Martin, M. et al., 2002. Involvement of CB1 cannabinoid receptors in emotional behaviour. *Psychopharmacology*, 159(4), pp.379–387.

Martinez, F.O., Helming, L. & Gordon, S., 2009. Alternative Activation of Macrophages : An Immunologic Functional Perspective, *Annual review of Immunology,* 27, pp.451-83

Di Marzo, V., 2008. Targeting the endocannabinoid system: to enhance or reduce? *Nature reviews. Drug discovery*, 7(5), pp.438–55.

Matsuda, L.A. et al., 1990. Structure of a cannabinoid receptor and functional expression of the cloned cDNA. *Nature*, 346(6284), pp.561–564.

McHugh, D. et al., 2010. N-arachidonoyl glycine, an abundant endogenous lipid, potently drives directed cellular migration through GPR18, the putative abnormal cannabidiol receptor. *BMC Neuroscience*, 11(1),

McHugh, D. et al., 2012. Δ(9) -Tetrahydrocannabinol and N-arachidonyl glycine are full agonists at GPR18 receptors and induce migration in human endometrial HEC-1B cells. *British journal of pharmacology*, 165(8), pp.2414–24.

Mechoulam, R. et al., 1995. Identification of an endogenous 2-monoglyceride, present in canine gut, that binds to cannabinoid receptors. *Biochemical Pharmacology*, 50(1), pp.83–90.

Menèndez Iglesias, B. et al., 1997. Analysis of B7-1 and B7-2 costimulatory ligands in cultured mouse microglia: upregulation by interferon-gamma and lipopolysaccharide and downregulation by interleukin-10, prostaglandin E2 and cyclic AMP-elevating agents. *Journal of Neuroimmunology*, 72(1), pp.83–93.

Meyer, M. et al., 2010. Gene targeting by homologous recombination in mouse zygotes mediated by zinc-finger nucleases. *Proceedings of the National Academy of Sciences of the United States of America*, 107(34), pp.15022–15026.

Montecucco, F. & Di Marzo, V., 2012. At the heart of the matter: the endocannabinoid system in cardiovascular function and dysfunction. *Trends in pharmacological sciences*, 33(6), pp.331–40.

Moreira, F.A. et al., 2008. Reduced anxiety-like behaviour induced by genetic and pharmacological inhibition of the endocannabinoid-degrading enzyme fatty acid amide hydrolase (FAAH) is mediated by CB1 receptors. *Neuropharmacology*, 54, pp.141-50.

Mosser, D.M. & Edwards, J.P., 2008. Exploring the full spectrum of macrophage activation. *Nature reviews. Immunology*, 8(12), pp.958–69.

Muccioli, G.G. et al., 2007. Identification of a novel endocannabinoid-hydrolyzing enzyme expressed by microglial cells. *Journal of Neuroscience*, 27(11), pp.2883–2889.

Müller, U., 1999. Ten years of gene targeting: targeted mouse mutants, from vector design to phenotype analysis. *Mechanisms of development*, 82(1-2), pp.3–21.

Munro, S., Thomas, K.L. & Abu-Shaar, M., 1993. Molecular characterization of a peripheral receptor for cannabinoids. *Nature*, 365(6441), pp.61–65.

Murray, R.M. et al., 2007. Cannabis, the mind and society: the hash realities. *Nature neuroscienc*e , 8, pp. 886-95.

Mussolino, C. & Cathomen, T., 2012. TALE nucleases: tailored genome engineering made easy. *Current opinion in biotechnology*, 23(5), pp.644–50.

Myers, K.M. & Davis, M., 2007. Mechanisms of fear extinction. *Molecular psychiatry*, 12(2), pp.120–50.

Nagy, A. et al., 1993. Derivation of completely cell culture-derived mice from early-passage embryonic stem cells. *Proceedings of the National Academy of Sciences of the United States of America*, 90(18), pp.8424–8428.

Napoli, I., Kierdorf, K. & Neumann, H., 2009. Microglial precursors derived from mouse embryonic stem cells. *Glia*, 57(15), pp.1660–1671.

Neumann, H, Kotter, M.R. & Franklin, R.J.M., 2009. Debris clearance by microglia: an essential link between degeneration and regeneration. *Brain : a journal of neurology*, 132(Pt 2), pp.288–95.

Nimmerjahn, A., Kirchhoff, F. & Helmchen, F., 2005. Resting microglial cells are highly dynamic surveillants of brain parenchyma in vivo. *Science (New York, N.Y.)*, 308(5726), pp.1314–8.

Ohno-Shosaku, T., Tanimura, A. & Hashimotodani, Y., 2012. Endocannabinoids and Retrograde Modulation of Synaptic Transmission. *Neuroscientist*, 18(2), pp. 199-32.

Okamoto, Y. et al., 2004. Molecular characterization of a phospholipase D generating anandamide and its congeners. *The Journal of biological chemistry*, 279(7), pp.5298–305.

Olson, J.K. & Miller, S.D., 2004. Microglia initiate central nervous system innate and adaptive immune responses through multiple TLRs. *The Journal of Immunology*, 173(6), pp.3916–24.

Onaivi, E., 2002. *The Biology of Marijuana: From Gene to Behavior*, Taylor & Francis, London and New York, CRC Press.

Osoegawa, K. et al., 2000. Bacterial Artificial Chromosome Libraries for Mouse Sequencing and Functional Analysis. *Genome Research*, 10(1), pp.116–128.

Pandey, R. et al., 2009. Endocannabinoids and immune regulation. *Pharmacological research : the official journal of the Italian Pharmacological Society*, 60(2), pp.85–92.

Patel, S. & Hillard, C.J., 2008. Adaptations in endocannabinoid signaling in response to repeated homotypic stress: a novel mechanism for stress habituation. *European Journal of Neuroscience*, 27(11), pp.2821–2829.

De Petrocellis, L. & Di Marzo, V., 2009. An introduction to the endocannabinoid system: from the early to the latest concepts. *Best practice & research. Clinical endocrinology & metabolism*, 23(1), pp.1–15.

Plendl, W. & Wotjak, C. T., 2010. Dissociation of within- and between-session extinction of conditioned fear. *The Journal of neuroscience : the official journal of the Society for Neuroscience*, 30(14), pp.4990–8.

Ponomarev, E.D. et al., 2007. CNS-derived interleukin-4 is essential for the regulation of autoimmune inflammation and induces a state of alternative activation in microglial cells. *The Journal of neuroscience : the official journal of the Society for Neuroscience*, 27(40), pp.10714–21.

Ponomarev, E.D. et al., 2005. Development of a culture system that supports adult microglial cell proliferation and maintenance in the resting state. *Journal of immunological methods*, 300(1-2), pp.32–46.

Porter, A.C. et al., 2002. Characterization of a novel endocannabinoid, virodhamine, with antagonist activity at the CB1 receptor. *The Journal of pharmacology and experimental therapeutics*, 301(3), pp.1020–4.

Prescotts, S.M. & Majerus, P. W., 1983. Characterization of 1 , 2-Diacylglycerol Hydrolysis in Human Platelets.*Journal of Biological Chemistry*, 258(2), pp.764–69.

Prut, L. & Belzung, C., 2003. The open field as a paradigm to measure the effects of drugs on anxiety-like behaviors: a review. *European Journal of Pharmacology*, 463(1-3), pp.3–33.

Puffenbarger, R.A., Boothe, A.C. & Cabral, G.A., 2000. Cannabinoids inhibit LPS-inducible cytokine mRNA expression in rat microglial cells. *Glia*, 29(1), pp.58–69.

Rademacher, D.J. et al., 2008. Effects of acute and repeated restraint stress on endocannabinoid content in the amygdala, ventral striatum, and medial prefrontal cortex in mice. *Neuropharmacology*, 54(1), pp.108–16.

Raes, G. et al., 2002. Differential expression of FIZZ1 and Ym1 in alternatively versus classically activated macrophages. *Journal of Leukocyte Biology*, 71, pp.597–602.

Te Riele, H., Maandag, E.R. & Berns, A., 1992. Highly efficient gene targeting in embryonic stem cells through homologous recombination with isogenic DNA constructs. *Proceedings of the National Academy of Sciences of the United States of America*, 89(11), pp.5128–5132.

Righi, M. et al., 1989. Monokine production by microglial cell clones. *European Journal of Immunology*, 19(8), pp.1443–1448.

Rodríguez, C.I. et al., 2000. High-efficiency deleter mice show that FLPe is an alternative to Cre-loxP. *Nature genetics*, 25(2), pp.139–40.

Ryberg, E. et al., 2007. The orphan receptor GPR55 is a novel cannabinoid receptor. *British journal of pharmacology*, 152(7), pp.1092–101.

Saario, S.M. et al., 2005. Characterization of the sulfhydryl-sensitive site in the enzyme responsible for hydrolysis of 2-arachidonoyl-glycerol in rat cerebellar membranes. *Chemistry & biology*, 12(6), pp.649–56.

Sambrook, J., Fritsch, E.F. & Maniatis, T., 1989. Molecular Cloning: A Laboratory Manual. *Cold Spring Harbor Press*

Sambrook, J. & Russel, D.W., 2001. Molecular Cloning: Molecular Cloning: A Laboratory Manual. *Cold Spring Harbor Press*

Sansom, D.M., Manzotti, C.N. & Zheng, Y., 2003. What's the difference between CD80 and CD86? *Trends in Immunology*, 24(6), pp.313–318.

Saura, J., Tusell, J.M. & Serratosa, J., 2003. High-yield isolation of murine microglia by mild trypsinization. *Glia*, 44(3), pp.183–189.

Sciolino, N.R., Zhou, W. & Hohmann, A.G., 2011. Enhancement of endocannabinoid signaling with JZL184, an inhibitor of the 2-arachidonoylglycerol hydrolyzing enzyme monoacylglycerol lipase, produces anxiolytic effects under conditions of high environmental aversiveness in rats. *Pharmacological research : the official journal of the Italian Pharmacological Society*, 64(3), pp.226–34.

Seong, E. et al., 2004. To knockout in 129 or in C57BL/6: that is the question. *Trends in genetics : TIG*, 20(2), pp.59–62.

Shapiro, H.M. 2003. Practical Flow Cytometry, Fourth edition, John Wiley & Sons, Inc. Hoboken, New Jersey

Shrikant, P. et al., 1995. Intercellular adhesion molecule-1 gene expression by glial cells. Differential mechanisms of inhibition by IL-10 and IL-6. *The Journal of Immunology*, 155(3), pp.1489–1501.

Shrikant, P. & Benveniste, E N, 1996. The central nervous system as an immunocompetent organ: role of glial cells in antigen presentation. *The Journal of Immunology* , 157 (5), pp.1819–1822.

De Simone, R. et al., 2010. TGF-β and LPS modulate ADP-induced migration of microglial cells through P2Y1 and P2Y12 receptor expression. *Journal of Neurochemistry*, 115(2), pp.450–459.

Skarnes, W.C. et al., 2011. A conditional knockout resource for the genome-wide study of mouse gene function. *Nature*, 474(7351), pp.337–342.

Slavik, J.M., Hutchcroft, J.E. & Bierer, B.E., 1999. CD28/CTLA-4 and CD80/CD86 families: signaling and function. *Immunologic Research*, 19(1), pp.1–24.

Stansley, B., Post, J. & Hensley, K., 2012. A comparative review of cell culture systems for the study of microglial biology in Alzheimer's disease. *Journal of neuroinflammation*, 9(1), p.115.

Stella, N., 2009. Neuropharmacology Endocannabinoid signaling in microglial cells. *Neuropharmacology*, 56, pp.244–253.

Stella, N., 2011. Cannabinoid and cannabinoid-like receptors in microglia, astrocytes and astrocytomas. *Glia*, 58(9), pp.1017–1030.

Stiedl, O. et al., 1999. Strain and substrain differences in context- and tone-dependent fear conditioning of inbred mice. *Behavioural brain research*, 104(1-2), pp.1–12.

Stohwasser, R. et al., 2000. Biochemical analysis of proteasomes from mouse microglia: induction of immunoproteasomes by interferon-gamma and lipopolysaccharide. *Glia*, 29(4), pp.355–65.

Sugiura, T. et al., 1995. 2-Arachidonoylglycerol: A Possible Endogenous Cannabinoid Receptor Ligand in Brain. *Biochemical and Biophysical Research Communications*, 215(1), pp.89–97.

Takenouchi, R. et al., 2012. N-arachidonoyl glycine induces macrophage apoptosis via GPR18. *Biochemical and biophysical research communications*, 418(2), pp.366–71.

Tanimura, A. et al., 2010. The endocannabinoid 2-arachidonoylglycerol produced by diacylglycerol lipase alpha mediates retrograde suppression of synaptic transmission. *Neuron*, 65(3), pp.320–7.

Urigüen, L. et al., 2004. Impaired action of anxiolytic drugs in mice deficient in cannabinoid CB1 receptors. *Neuropharmacology*, 46(7), pp.966–73.

Valera, A. et al., 1994. Expression of the neomycin-resistance (neo) gene induces alterations in gene expression and metabolism. *Human Gene Therapy*, 5(4), pp.449–456.

Varnum, M.M. & Ikezu, T., 2012. The Classification of Microglial Activation Phenotypes on Neurodegeneration and Regeneration in Alzheimer's Disease Brain. *Archivum immunologiae et therapiae experimentalis*, 60 pp.251–266.

Voss, A.K., Thomas, T. & Gruss, P., 1998. Efficiency assessment of the gene trap approach. *Developmental dynamics an official publication of the American Association of Anatomists*, 212(2), pp.171–180.

Wake, H. et al., 2009. Resting microglia directly monitor the functional state of synapses in vivo and determine the fate of ischemic terminals. *The Journal of neuroscience : the official journal of the Society for Neuroscience*, 29(13), pp.3974–80.

Walter, L. et al., 2003. Nonpsychotropic cannabinoid receptors regulate microglial cell migration. *Journal of Neuroscience*, 23(4), pp.1398–1405.

Williams, L. et al., 2002. IL-10 expression profiling in human monocytes. *Journal of Leukocyte Biology*, 72(4), pp.800–9.

Witting, A. et al., 2004. P2X7 receptors control 2-arachidonoylglycerol production by microglial cells. *Proceedings of the National Academy of Sciences of the United States of America*, 101(9), pp.3214–3219.

Yang, I. et al., 2010. The role of microglia in central nervous system immunity and glioma immunology. *Journal of Clinical Neuroscience*, 17(1), pp.6–10.

Yiangou, Y. et al., 2006. COX-2, CB2 and P2X7-immunoreactivities are increased in activated microglial cells/macrophages of multiple sclerosis and amyotrophic lateral sclerosis spinal cord. *BMC neurology*, (6)12.

Zhu, Y. et al., 2001. Ablation of NF1 function in neurons induces abnormal development of cerebral cortex and reactive gliosis in the brain. *Genes & Development*, 15(7), pp.859–876.

Zimmer, A. et al., 1999. Increased mortality, hypoactivity, and hypoalgesia in cannabinoid CB1 receptor knockout mice. *Proceedings of the National Academy of Sciences of the United States of America*, 96(10), pp.5780–5.

Zimmer, H., Riese, S. & Régnier-Vigouroux, A., 2003b. Functional characterization of mannose receptor expressed by immunocompetent mouse microglia. *Glia*, 42(1), pp.89–100.

Zygmunt, P.M. et al., 1999. Vanilloid receptors on sensory nerves mediate the vasodilator action of anandamide. *Nature*, 400(6743), pp.452–7.

A Appendix

A.1 Primers Daglα

Primers used for cloning of the Daglα targeting construct. Respective cloning step, identifier and sequence are indicated.

Cloning step	Primer	Sequence 5'-3'
Subcloning	Subcloning_forward	GACTCAGCACAGTGGAGCTG GGCAGCAGGTGGGATAGATC AGATGATGCTGTCGACGCTCT CCTGAGTAGGACAAATC
	Subcloning_reverse	CAACTACAGTGGCTCTCACCT CTCATCTGTTTCCATCCAGCT GAGTGACCGTCGACTCACAGC TTGTCTGTAAGCGGATG
Insertion loxP-neo-loxP cassette	loxP-neo-loxP_fwd	ATGACCCCCTGTGCAGCTGCA GCTCTTAGCTTAGCCCCCATG TGACCTGAAATTAACCCTCACT AAAGGGCG
	loxP-neo-loxP_rev	GTTCTGGGTTGAGTCTGGGGA GTGGGTGGGAGCAGGCTTGC CCTTAGAGATAATACGACTCA CTATAGGGCTC
Insertion FRT-neo-FRT-loxP cassette	Frt-neo-FRT-loxP_fwd	AGGAGACTCAGAAGGGTATAG AGAAGTAGCCCAGGCTACGTC GTCCCTGGAATTAACCCTCAC TAAAGGGCG
	Frt-neo-FRT-loxP_rev	ACAATTCCCAGAAACCCAGTA GCACCGCCATCAACCAAGTGA AAGGAAGGTAATACGACTCAC TATAGGGCTC

Cloning step	Primer	Sequence 5'-3'
Sequencing	Dagla_seq_loxP1_fwd	GCAGGGTTTCACTTTCAGTC
	Dagla_seq_loxP1_rev	CCTACTCTCACCCTCCTCAA
	Dagla_seq_Exon1_fwd	GACCTGAAGGAGGGGAAC
	Dagla_seq_Exon1_rev	CCTGTCTTCCCTCACAGTAT
	Dagla_seq_frt_loxP_fwd	CTTGACATGGTTTGGAGTGA
	Dagla_seq_frt_loxP_rev	AGAAAGCGAAGGAGCAAAG
	Dagla+frtloxP3'_1 (ST7)	TCTAAGGGCAAGCCTGCT
	Dagla+frtloxP3'_3 (ST8)	TGCCATGCGTGTCACCAT
	Dagla+frtloxP3'_4 (ST9)	ATGGTGACACGCATGGCA
	Dagla+frtloxP3'_5 (ST10)	GAATAGGAACTTCGCGGC
	Dagla+frtloxP3'_6 (ST11)	ACCTGGCTCATGAGTCCT
	Dagla+frtloxP3'_8 (ST12)	GACAGGTCGGTCTTGACA
	Dagla+frtloxP3'_11 (ST13)	GACTGGGCACAACAGACA
	Dagla+frtloxP3'_13 (ST14)	CCAGTAGCCACAGAACCA
	Dagla: Seq.frtloxP_14	GGATTCATCGACTGTGGC
	Dagla: Seq.frtloxP_15	GCTCTGTGAAGTGGGACA
Southern blot probe	probe_a_fwd1	AGGAGGATTGGCCTCTGTT
	probe_a_rev1	TGGACGTCGTGACTTATGGA
	SBa_BamH1_fwd1	CTCCTTCCTCCTCTCATTGC
	SBa_BamH1_rev1	GGAAATCCCTGACCTTCGTA
5' loxP PCR	LoxPa_Xho_fwd1	CCTCCAGGCCTACAGAA
	LoxPa_Xho_rev1	CACCGGAGAACTGGTTTG
FLP-PCR	FLP_dela_fwd_01	TGAGGTTCTTGGTTGCTGTC
	FLP_dela_fwd_03	TGCTCTGTGAAGTGGGACAT

A.2 Primers Daglβ

Primers used for cloning of the Daglβ targeting construct. Respective cloning step, identifier and sequence are indicated.

Cloning step	Primer	Sequence 5'-3'
Subcloning	Subcloning_forward	CCTCCTTCTCAGACTCAGACT GACTGAGTCATCTGGACTCTC AGCATCAGGTCGACTCACAGC TTGTCTGTAAGCGGATG
	Subcloning_reverse	ACTCATGGCCAGGATGAGCAG GCACACAGGTGCTCCTGGAGA AGCTGATGGTCGACGCTCTCC TGAGTAGGACAAATC
Insertion loxP-neo-loxP cassette	loxP-neo-loxP_fwd	CAAACCTAGGTTACCTCTAATT CCTCCAGCAATTGACTGTAGC CAATTTTAATTAACCCTCACTA AAGGGCG
	loxP-neo-loxP_rev	AATTTTTGTTGTGCAAACCTTG TTCCTTGATTTAAAACTACTGA TTAAATTAATACGACTCACTAT AGGGCTC
Insertion FRT-neo-FRT-loxP cassette	Frt-neo-FRT-loxP_fwd	GTAAGTGAGGCCGCCGTGAG GGTGGGAGGCGCGCTGGTTA AGGCGACAAAAATTAACCCTC ACTAAAGGGCG
	Frt-neo-FRT-loxP_rev	ATTGTGCTCCGGGGGCGCGG TTGCCCCTTAAGCACCAAGAA GGCACGACTTAATACGACTCA CTATAGGGCTC
Sequencing	SeqDaglb1.loxPfwd	GCCCAGTATCAGGTTTGTC
	SeqDaglb1.loxPrev	ACACAAAGCTCGGTGAGC
	SeqDaglbex1fwd	ACCCAGACCTACGTCCTA
	SeqDaglbex1rev	TTTGTCACGTCCTGCACG

Cloning step	Primer	Sequence 5’-3’
	SeqDaglb2.loxPfrtfwd	CCGCTATCAGGACATAGC
	SeqDaglb2.loxPfrtrev	CACATTTCCCTCACGCTC
	probe_b_fwd1	TGCCTGCACCTATCTGTCTG
	probe_b_rev1	CCTTCCAAGTGCTGGGATTA
5’loxP PCR	Daglb_loxP_Xho_fwd1	GTCGTCTTGGTATCCTTAG
	Daglb_loxP_Xho_rev1	TACCACACCCATCCTGCA

A.3 Cloning of the Daglα targeting vector (gel documentation)

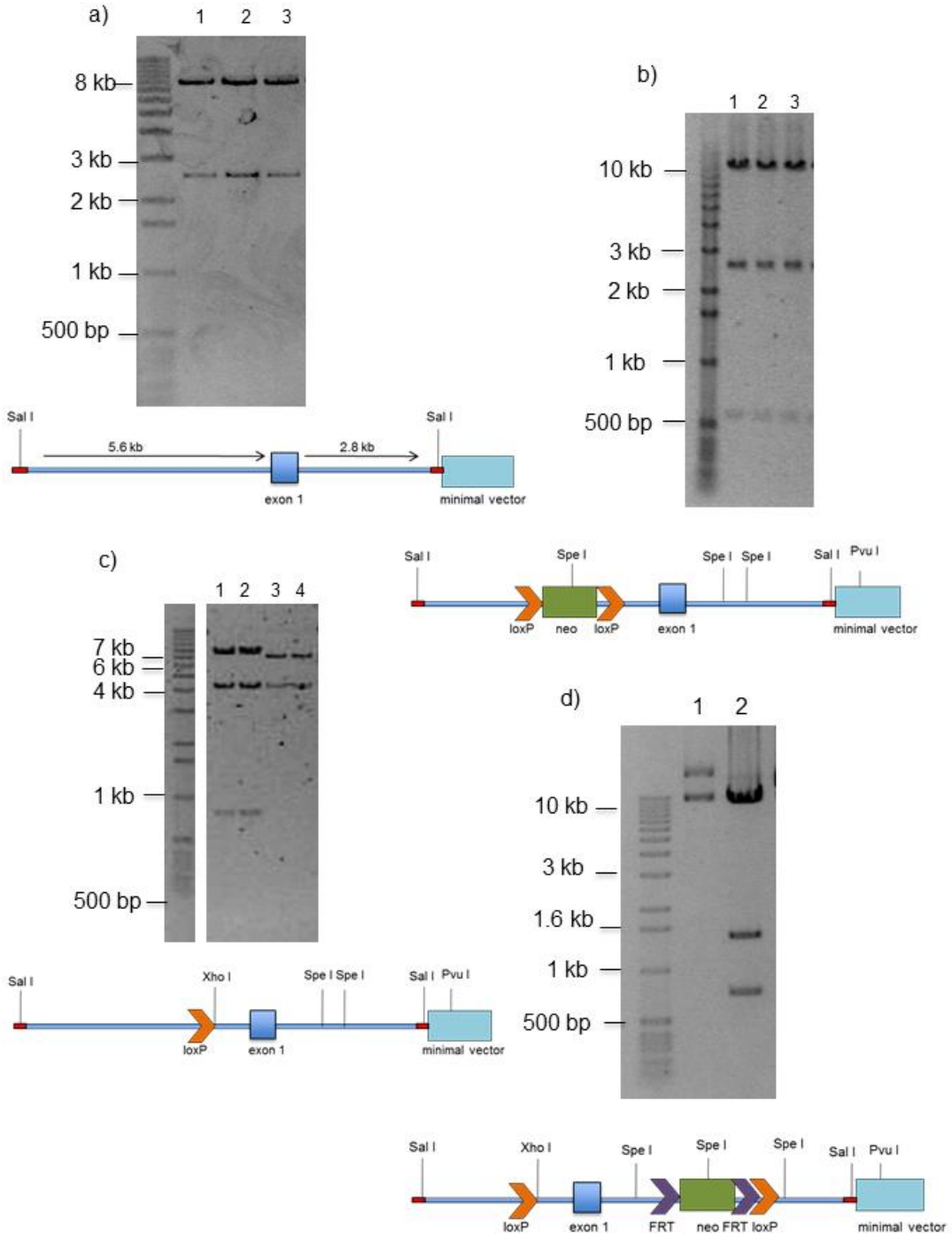

Figure 41: Restriction pattern analysis of the separate cloning steps for the Daglα targeting vector. a) Verification of correct sublconing. Restriction digestion with Sal I, expected fragments: 2.7 kb (minimal vector), 8.4 kb Daglα gene fragment. b) Restriction pattern for Spe I digestion after insertion of the loxP-flanked neo cassette. Expected fragments: 9554 bp, 2637 bp, 573 bp. c) Lane 1 and 2: Xho I/Pvu I digestion of the Daglα sublclone harboring the loxP-flanked neo cassette. Resulting fragments: 7396 bp, 4502 bp, 866 bp. Lane 3 and 4: Xho I/Pvu I digestion after excision of the neo cassette by Cre-mediated recombination. Resulting fragments: 6783 bp, 4320 bp. d) Restriction pattern analysis after insertion of the FRT-flanked neo cassette downstream of exon 1: Lane 1 undigested vector, lane 2: Spe I restriction pattern 10647 bp, 1480 bp 767bp

A.4 Vector card pDaglα_ko

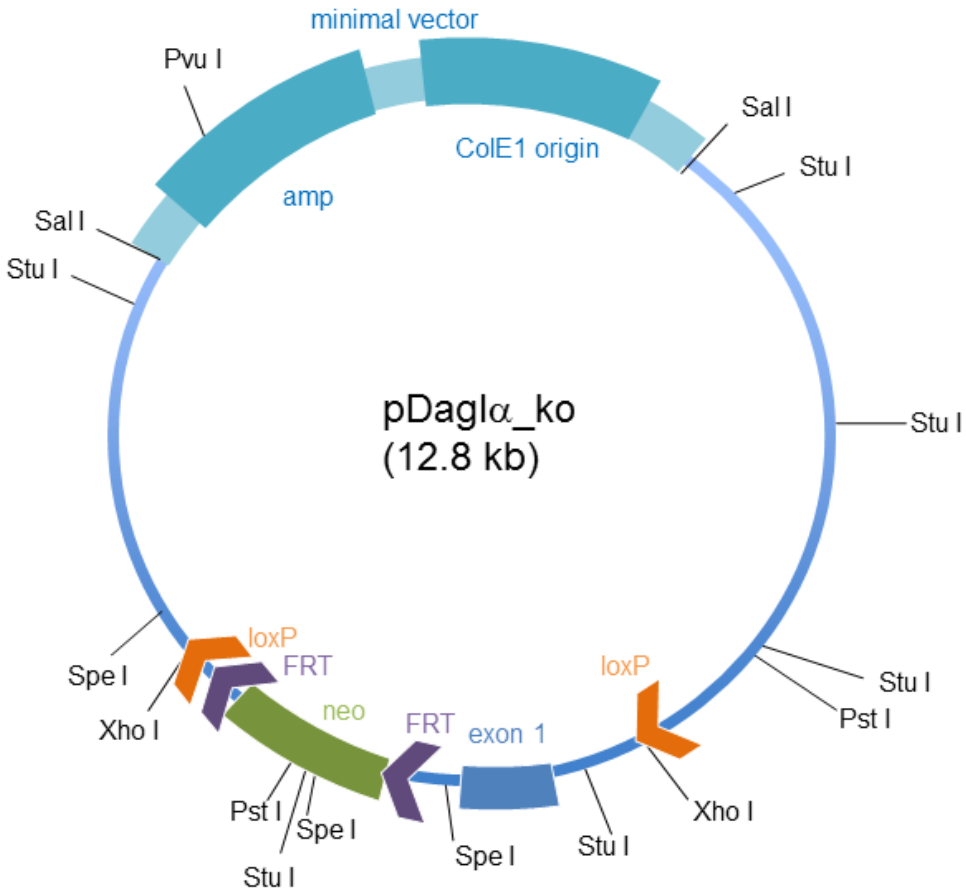

pDaglα_ko
Host: TOP10 *E.coli*
Antibiotic resistance: ampicillin, kanamycin
Backbone: minimal vector (Genebridges™)
amp: ampicillin resistance gene
ColE1 origin: origin of replication
loxP: loxP site
FRT: FRT site
neo: neomycin resistance gene

A.5 Cloning of the Daglβ targeting vector (gel documentation)

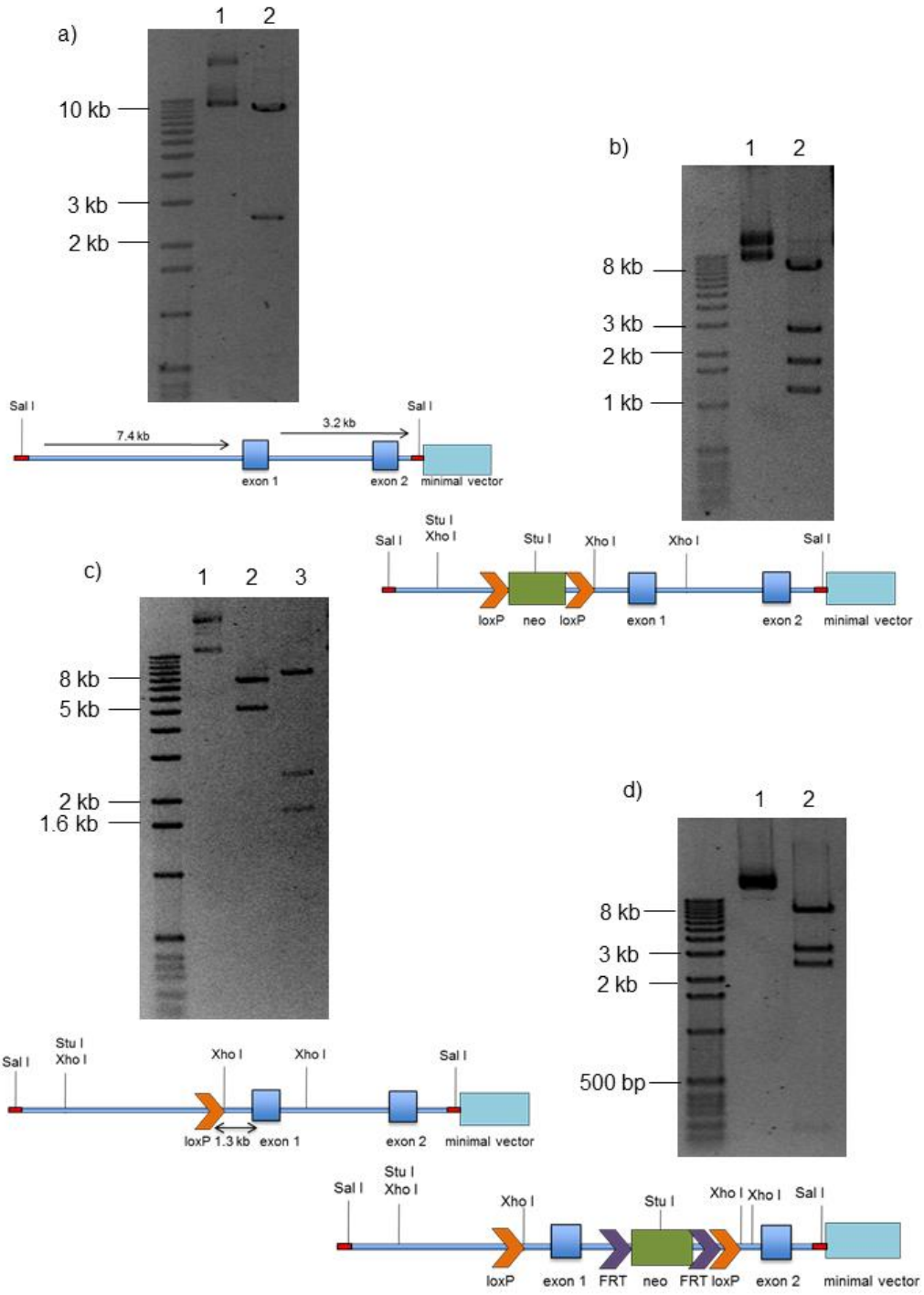

Figure 42: Restriction pattern analysis of the separate cloning steps for the Daglβ targeting vector. Undigested vectors are shown in lane 1, respectively. a) Lane 2: verification of correct subcloning by restriction digestion with Sal I. Expected fragments 2.7 kb (minimal vector), 10.4 kb (subcloned Daglβ gene fragment). b) Restriction pattern for Xho I/Stu I digestion after insertion of the loxP-flanked neo cassette. Expected fragments: 8832 bp, 2838 bp,1828 bp, 1248 bp. c) Restriction pattern after excision of the loxP-neo cassette by Cre-mediated recombination. Lane 2: Spe I digestion: 7946 bp, 5250 bp, lane 3: Xho I/Stu I digestion: 8830 bp, 2536 bp, 1828 bp. d) Restriction pattern after insertion of the FRT-flanked neo cassette. Xho I restriction pattern 10832 bp, 3317 bp, 2536 bp, 187 bp

A.6 Vector card pDaglβ_ko

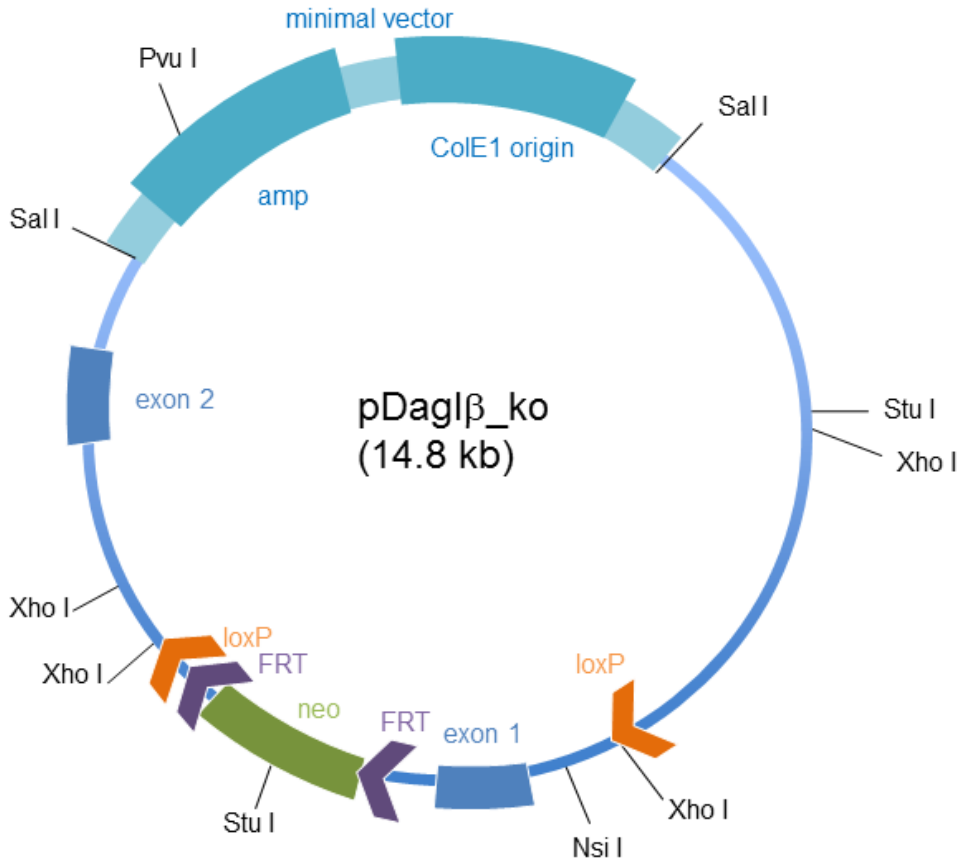

pDaglβ_ko
Host: TOP10 *E.coli*
Antibiotic resistance: ampicillin, kanamycin
Backbone: minimal vector (Genebridges™)
amp: ampicillin resistance gene
ColE1 origin: origin of replication
loxP: loxP site
FRT: FRT site
neo: neomycin resistance gene

A.7 PCR conditions

A.7.1 Red/ET cloning: amplification minimal vector template and selection cassettes

PCR setup (50 µl)

Sterile water	35 µl
10 µl Phusion buffer 5x	5 µl
Forward primer 100µM	1 µl
Reverse primer 100µM	1 µl
dNTPs 10mM	1 µl
Taq polymerase	1 µl
Respective template	1 µl

Cycling parameters

1 x	Initial denaturation	98°C	1 min
5 x	Denaturation	98°C	1 min
	Annealing	62°C	1 min
	Decrease temp. after first cycle 1°C every cycle		
	Elongation	72°C	2 min 30 s
30 x	Denaturation	98°C	1 min
	Annealing	57°C	1 min
	Elongation	72°C	2 min 30 s
1 x	Final elongation	72°C	10 min
	Cooling	4°C	∞

A.7.2 5’ loxP PCR Daglα, FLP PCR Daglα

PCR setup (20 µl)

Sterile water	8	µl
10 x GoTaq PCR mix	10	µl
Forward primer 100µM	0.5	µl
Reverse primer 100µM	0.5	µl

Cycling parameters (5’ loxP PCR)

1 x	Initial denaturation	95°C	30 s
30 x	Denaturation	95°C	30 s
	Annealing	60°C	1 min
	Elongation	68°C	1 min
1 x	Final elongation	68°C	5 min
	Cooling	4°C	∞

Cycling parameters (FLP PCR)

1 x	Initial denaturation	95°C	30 s
5 x	Denaturation	95°C	30 s
	Annealing	60°C	45 s
	Decrease temp. after first cycle 1°C every cycle		
	Elongation	68°C	2 min 15 s
30 x	Denaturation	95°C	30 s
	Annealing	55°C	45 s
	Elongation	68°C	2 min 15 s
1 x	Final elongation	68°C	10 min
	Cooling	4°C	∞

A.7.3 5’ loxP PCR Daglβ

PCR setup (50 µl)

Sterile water	41.25	µl
10 x PCR-buffer	5	µl
Forward primer (probe_a_fwd1, 100 µM)	1	µl
Feverse primer (probe_a_rev1, 100 µM)	1	µl
dNTPs (10mM)	1	µl
Taq polymerase	0.25	µl
Daglβ BAC DNA (1µg/µl)	0.5	µl

Cycling parameters

1 x	Initial denaturation	95°C	2 min
25 x	Denaturation	95°C	30 s
	Annealing	60°C	1 min
	Elongation	68°C	1 min
1 x	Final elongation	68°C	5 min
	Cooling	4°C	∞

A.8 Supplier information

Applichem	http://www.applichem.com/
Applied Biosystems	http://www.appliedbiosystems.com/
eBioscience	http://www.eBioscience.com/
Genebridges	http://www.genebridges.com/
Invitrogen	http://www.invitrogen.com/
Macrogen	http://www.macrogen.com/
Metabion	http://www.metabion.com/
Merck	http://www.merck.de/
New England Biolabs	http://www.neb.com/
Peqlab	http://www.peqlab.de/
Qiagen	http://www.qiagen.com/
R & D Systems	http://www.rndsystems.com/
Roche	http://www.roche.de/
Roth	http://www.carl-roth.de/
Sigma	http://www.sigmaaldrich.com

A.9 Databases

Ensembl genome browser	http://www.ensembl.org/index.html
Pubmed	http://www.ncbi.nlm.nih.gov/sites/entrez
UCSC genome browser	http://genome.ucsc.edu/

A.10 Gene lists

Genes regulated in response to LPS/IFNγ stimulation. The list contains only those genes, which were up- or down regulated more than 5-fold.

Gene Symbol	p-value LPS/IFNγ vs. Unstimulated	Fold change	direction of regulation
Cxcl9	0,000000006	196,935	LPS/IFNγ up vs unstimuliert
Edn1	0,000000009	6,51133	LPS/IFNγ up vs unstimuliert
AA467197	0,000000012	21,8861	LPS/IFNγ up vs unstimuliert
Pla2g15	0,000000074	-8,16129	LPS/IFNγ down vs unstimuliert
Upp1	0,000000097	22,3213	LPS/IFNγ up vs unstimuliert

Gene Symbol	p-value LPS/IFNγ vs. Unstimulated	Fold change	direction of regulation
Hdc	0,000000196	5,36764	LPS/IFNγ up vs unstimuliert
Lcn2	0,000000238	25,0955	LPS/IFNγ up vs unstimuliert
Rasa3	0,000000372	-5,96718	LPS/IFNγ down vs unstimuliert
Gna13	0,000000415	5,3434	LPS/IFNγ up vs unstimuliert
Timp2	0,000000439	-12,9755	LPS/IFNγ down vs unstimuliert
Il1a	0,000000448	8,01685	LPS/IFNγ up vs unstimuliert
Mmp13	0,000000467	60,1106	LPS/IFNγ up vs unstimuliert
Wdr20b	0,000000684	5,96725	LPS/IFNγ up vs unstimuliert
Cbr3	0,000000700	-5,28099	LPS/IFNγ down vs unstimuliert
Traf1	0,000000714	22,6156	LPS/IFNγ up vs unstimuliert
Serping1	0,000000718	5,16438	LPS/IFNγ up vs unstimuliert
LOC676420	0,000000761	-10,853	LPS/IFNγ down vs unstimuliert
Lrmp	0,000000781	-6,55502	LPS/IFNγ down vs unstimuliert
Lrrc8c	0,000000793	5,25804	LPS/IFNγ up vs unstimuliert
Ccrl2	0,000000924	8,02634	LPS/IFNγ up vs unstimuliert
Timd4	0,000000977	8,13945	LPS/IFNγ up vs unstimuliert
Gbp5	0,000001041	14,2051	LPS/IFNγ up vs unstimuliert
Traf1	0,000001060	23,0048	LPS/IFNγ up vs unstimuliert
Gas6	0,000001072	-25,8009	LPS/IFNγ down vs unstimuliert
Ptges	0,000001102	9,34913	LPS/IFNγ up vs unstimuliert
Serping1	0,000001109	5,24719	LPS/IFNγ up vs unstimuliert
A630077B13Rik	0,000001127	20,9652	LPS/IFNγ up vs unstimuliert
Nos2	0,000001299	5,01362	LPS/IFNγ up vs unstimuliert
Maged1	0,000001309	-6,6463	LPS/IFNγ down vs unstimuliert
Acot7	0,000001313	7,84605	LPS/IFNγ up vs unstimuliert
F730045P10Rik	0,000001350	27,1584	LPS/IFNγ up vs unstimuliert
Arl11	0,000001400	-6,25569	LPS/IFNγ down vs unstimuliert
Gbp1	0,000001477	22,4927	LPS/IFNγ up vs unstimuliert
Sesn1	0,000001682	-8,51438	LPS/IFNγ down vs unstimuliert
Ypel3	0,000001687	-11,1516	LPS/IFNγ down vs unstimuliert
Cd69	0,000001758	28,4359	LPS/IFNγ up vs unstimuliert
Zdhhc14	0,000001867	-13,4425	LPS/IFNγ down vs unstimuliert
Batf2	0,000002026	17,3107	LPS/IFNγ up vs unstimuliert
Ckb	0,000002265	-8,64977	LPS/IFNγ down vs unstimuliert
LOC641240	0,000002323	22,1468	LPS/IFNγ up vs unstimuliert
Hexa	0,000002612	-6,28893	LPS/IFNγ down vs unstimuliert
Smpdl3b	0,000002814	8,83506	LPS/IFNγ up vs unstimuliert
H2-Eb1	0,000003008	14,0159	LPS/IFNγ up vs unstimuliert
LOC214403	0,000003075	-9,33507	LPS/IFNγ down vs unstimuliert

Gene Symbol	p-value LPS/IFNγ vs. Unstimulated	Fold change	direction of regulation
H2-Ab1	0,000003137	22,9245	LPS/IFNγ up vs unstimuliert
Cyp27a1	0,000003347	-5,08546	LPS/IFNγ down vs unstimuliert
Trem2	0,000003396	-12,2676	LPS/IFNγ down vs unstimuliert
Serpina3f	0,000003506	23,1733	LPS/IFNγ up vs unstimuliert
Kif3c	0,000003508	5,26101	LPS/IFNγ up vs unstimuliert
Cdc42ep2	0,000003544	7,32605	LPS/IFNγ up vs unstimuliert
Il1rn	0,000003972	27,456	LPS/IFNγ up vs unstimuliert
Tmem86a	0,000004136	-8,03672	LPS/IFNγ down vs unstimuliert
St8sia4	0,000004390	-6,63451	LPS/IFNγ down vs unstimuliert
Dusp2	0,000004569	9,88949	LPS/IFNγ up vs unstimuliert
Tnf	0,000005255	34,0518	LPS/IFNγ up vs unstimuliert
Cd40	0,000005526	15,1349	LPS/IFNγ up vs unstimuliert
Ugt1a10	0,000005615	-6,84131	LPS/IFNγ down vs unstimuliert
Gadd45b	0,000005665	6,65211	LPS/IFNγ up vs unstimuliert
Hpgd	0,000006045	-33,3754	LPS/IFNγ down vs unstimuliert
Klhl6	0,000006067	-6,86331	LPS/IFNγ down vs unstimuliert
Irg1	0,000006132	32,462	LPS/IFNγ up vs unstimuliert
9030625A04Rik	0,000006337	9,15259	LPS/IFNγ up vs unstimuliert
Tgtp	0,000006803	5,5026	LPS/IFNγ up vs unstimuliert
Slc7a2	0,000006850	13,257	LPS/IFNγ up vs unstimuliert
Vcam1	0,000007180	10,0603	LPS/IFNγ up vs unstimuliert
Cyp27a1	0,000007923	-7,39103	LPS/IFNγ down vs unstimuliert
6430527G18Rik	0,000009294	-5,4621	LPS/IFNγ down vs unstimuliert
Slamf8	0,000010283	18,3966	LPS/IFNγ up vs unstimuliert
H2-Ab1	0,000011461	13,2007	LPS/IFNγ up vs unstimuliert
Abca9	0,000011531	-7,46284	LPS/IFNγ down vs unstimuliert
Ccnd2	0,000011962	5,9939	LPS/IFNγ up vs unstimuliert
Il27	0,000012057	7,96124	LPS/IFNγ up vs unstimuliert
Idh1	0,000012082	-9,33374	LPS/IFNγ down vs unstimuliert
2810025M15Rik	0,000012240	-7,91927	LPS/IFNγ down vs unstimuliert
Cd274	0,000012390	19,0593	LPS/IFNγ up vs unstimuliert
Slamf7	0,000012606	16,2731	LPS/IFNγ up vs unstimuliert
St3gal5	0,000013628	7,78582	LPS/IFNγ up vs unstimuliert
Cxcl10	0,000013684	19,3291	LPS/IFNγ up vs unstimuliert
Cd84	0,000014519	-5,21425	LPS/IFNγ down vs unstimuliert
Ugt1a10	0,000014961	-7,67064	LPS/IFNγ down vs unstimuliert
Stx11	0,000015283	8,56581	LPS/IFNγ up vs unstimuliert
Fcrls	0,000015573	-10,015	LPS/IFNγ down vs unstimuliert
Man2b1	0,000015785	-6,32384	LPS/IFNγ down vs unstimuliert

Gene Symbol	p-value LPS/IFNγ vs. Unstimulated	Fold change	direction of regulation
Slco2b1	0,000016481	-25,119	LPS/IFNγ down vs unstimuliert
Psat1	0,000016574	9,85566	LPS/IFNγ up vs unstimuliert
Nrp1	0,000017508	-11,9706	LPS/IFNγ down vs unstimuliert
Arl4c	0,000017842	-8,53712	LPS/IFNγ down vs unstimuliert
Gpr18	0,000019949	16,2252	LPS/IFNγ up vs unstimuliert
Snx24	0,000020195	-5,17935	LPS/IFNγ down vs unstimuliert
Gngt2	0,000020378	-5,32871	LPS/IFNγ down vs unstimuliert
Camk1	0,000021252	-7,04374	LPS/IFNγ down vs unstimuliert
Ccdc50	0,000022866	5,46496	LPS/IFNγ up vs unstimuliert
Cd40	0,000023589	60,2488	LPS/IFNγ up vs unstimuliert
Tnf	0,000024078	28,6234	LPS/IFNγ up vs unstimuliert
Fads1	0,000025228	-14,5594	LPS/IFNγ down vs unstimuliert
Marco	0,000025747	7,49812	LPS/IFNγ up vs unstimuliert
Slc31a2	0,000025809	5,02978	LPS/IFNγ up vs unstimuliert
Ccnd2	0,000025854	7,76334	LPS/IFNγ up vs unstimuliert
Msr2	0,000026663	-14,3005	LPS/IFNγ down vs unstimuliert
Centd3	0,000028415	-10,1757	LPS/IFNγ down vs unstimuliert
Rgs10	0,000028787	-6,24468	LPS/IFNγ down vs unstimuliert
Csf1r	0,000029133	-6,33355	LPS/IFNγ down vs unstimuliert
Nfkbiz	0,000030750	9,29682	LPS/IFNγ up vs unstimuliert
9930022F21Rik	0,000031726	9,52981	LPS/IFNγ up vs unstimuliert
Acot7	0,000036488	5,87794	LPS/IFNγ up vs unstimuliert
St6gal1	0,000036803	-24,8128	LPS/IFNγ down vs unstimuliert
Igf1	0,000037953	-10,1735	LPS/IFNγ down vs unstimuliert
Man2b1	0,000038690	-5,3006	LPS/IFNγ down vs unstimuliert
Rab11fip5	0,000041518	-5,86683	LPS/IFNγ down vs unstimuliert
Nuak1	0,000043724	-9,17977	LPS/IFNγ down vs unstimuliert
Nrp1	0,000048318	-9,10131	LPS/IFNγ down vs unstimuliert
Mmp25	0,000048384	6,43068	LPS/IFNγ up vs unstimuliert
Ugt1a10	0,000048669	-7,56389	LPS/IFNγ down vs unstimuliert
Sesn1	0,000051103	-7,13237	LPS/IFNγ down vs unstimuliert
C330023M02Rik	0,000051221	5,49544	LPS/IFNγ up vs unstimuliert
Rbl1	0,000051522	5,98474	LPS/IFNγ up vs unstimuliert
Dab2	0,000052668	-7,12165	LPS/IFNγ down vs unstimuliert
Hfe	0,000052831	-7,68533	LPS/IFNγ down vs unstimuliert
Msr2	0,000055256	-11,5294	LPS/IFNγ down vs unstimuliert
Nod1	0,000055568	6,39281	LPS/IFNγ up vs unstimuliert
Clec4e	0,000059036	6,91178	LPS/IFNγ up vs unstimuliert
Mlkl	0,000062138	10,6563	LPS/IFNγ up vs unstimuliert

Gene Symbol	p-value LPS/IFNγ vs. Unstimulated	Fold change	direction of regulation
Upp1	0,000063113	7,97708	LPS/IFNγ up vs unstimuliert
Klhl6	0,000063595	-5,34471	LPS/IFNγ down vs unstimuliert
Nav1	0,000065351	-5,39574	LPS/IFNγ down vs unstimuliert
BC006779	0,000065381	8,81328	LPS/IFNγ up vs unstimuliert
AI504432	0,000066631	5,62655	LPS/IFNγ up vs unstimuliert
H2-Aa	0,000067775	8,41795	LPS/IFNγ up vs unstimuliert
1700052O22Rik	0,000072859	-8,78234	LPS/IFNγ down vs unstimuliert
Cx3cr1	0,000077531	-36,1871	LPS/IFNγ down vs unstimuliert
Upp1	0,000077948	8,21734	LPS/IFNγ up vs unstimuliert
Syngr1	0,000078051	-6,98651	LPS/IFNγ down vs unstimuliert
Fgl2	0,000082120	8,53862	LPS/IFNγ up vs unstimuliert
Cenpa	0,000082309	-6,80898	LPS/IFNγ down vs unstimuliert
Aldh2	0,000085367	-5,15761	LPS/IFNγ down vs unstimuliert
Slc46a3	0,000086441	-10,5032	LPS/IFNγ down vs unstimuliert
Mmp13	0,000088175	25,3931	LPS/IFNγ up vs unstimuliert
Trf	0,000090128	-14,4254	LPS/IFNγ down vs unstimuliert
Mef2c	0,000092486	-13,0977	LPS/IFNγ down vs unstimuliert
Irf1	0,000092778	7,58188	LPS/IFNγ up vs unstimuliert
LOC675594	0,000094292	8,17083	LPS/IFNγ up vs unstimuliert
Cd40	0,000095450	34,8661	LPS/IFNγ up vs unstimuliert
Oasl1	0,000097129	18,4831	LPS/IFNγ up vs unstimuliert
Acot7	0,000099622	5,21199	LPS/IFNγ up vs unstimuliert
2810410A03Rik	0,000116024	-6,26004	LPS/IFNγ down vs unstimuliert
Ppap2a	0,000117140	7,95095	LPS/IFNγ up vs unstimuliert
Oasl1	0,000117587	19,1701	LPS/IFNγ up vs unstimuliert
Igsf9	0,000121269	6,28876	LPS/IFNγ up vs unstimuliert
Gbp2	0,000123416	59,2781	LPS/IFNγ up vs unstimuliert
Car13	0,000123590	9,49493	LPS/IFNγ up vs unstimuliert
AW212394	0,000127753	-5,22722	LPS/IFNγ down vs unstimuliert
Tnfaip3	0,000135044	6,40143	LPS/IFNγ up vs unstimuliert
Olfml3	0,000135511	-17,5991	LPS/IFNγ down vs unstimuliert
Fas	0,000140068	7,44264	LPS/IFNγ up vs unstimuliert
Gcnt1	0,000143864	-5,48294	LPS/IFNγ down vs unstimuliert
Gng10	0,000156662	-6,08036	LPS/IFNγ down vs unstimuliert
Itgb5	0,000157710	-10,0411	LPS/IFNγ down vs unstimuliert
Ybx3	0,000157788	6,23065	LPS/IFNγ up vs unstimuliert
Irg1	0,000159551	36,5363	LPS/IFNγ up vs unstimuliert
Slc9a9	0,000161855	-7,33609	LPS/IFNγ down vs unstimuliert
Cd86	0,000162934	6,69893	LPS/IFNγ up vs unstimuliert

Gene Symbol	p-value LPS/IFNγ vs. Unstimulated	Fold change	direction of regulation
Cxcl10	0,000168920	59,7482	LPS/IFNγ up vs unstimuliert
Rapgef2	0,000183816	7,98721	LPS/IFNγ up vs unstimuliert
Gbp3	0,000186402	21,4569	LPS/IFNγ up vs unstimuliert
Il6	0,000193580	9,16687	LPS/IFNγ up vs unstimuliert
Hmha1	0,000206294	-6,08257	LPS/IFNγ down vs unstimuliert
Phf11	0,000207076	12,501	LPS/IFNγ up vs unstimuliert
Spp1	0,000219133	-6,96018	LPS/IFNγ down vs unstimuliert
Gp38	0,000221276	8,9914	LPS/IFNγ up vs unstimuliert
E330036I19Rik	0,000227758	-12,5766	LPS/IFNγ down vs unstimuliert
Phf11	0,000228136	12,1965	LPS/IFNγ up vs unstimuliert
Paox	0,000228269	-5,75759	LPS/IFNγ down vs unstimuliert
H2-Ab1	0,000231619	9,8647	LPS/IFNγ up vs unstimuliert
Tsc22d3	0,000261189	-5,67165	LPS/IFNγ down vs unstimuliert
Mef2c	0,000262738	-9,05806	LPS/IFNγ down vs unstimuliert
Alox5ap	0,000263493	-7,08299	LPS/IFNγ down vs unstimuliert
Igtp	0,000273490	9,30745	LPS/IFNγ up vs unstimuliert
Samhd1	0,000277792	6,07672	LPS/IFNγ up vs unstimuliert
Alox5ap	0,000296825	-7,97218	LPS/IFNγ down vs unstimuliert
Tmem176b	0,000313854	-6,52854	LPS/IFNγ down vs unstimuliert
Samhd1	0,000330440	6,68572	LPS/IFNγ up vs unstimuliert
BC006779	0,000340599	7,449	LPS/IFNγ up vs unstimuliert
Tmem176a	0,000358802	-8,53238	LPS/IFNγ down vs unstimuliert
Lhfpl2	0,000377096	-8,58915	LPS/IFNγ down vs unstimuliert
Cd74	0,000397637	5,85477	LPS/IFNγ up vs unstimuliert
Kynu	0,000443516	5,64514	LPS/IFNγ up vs unstimuliert
Rsad2	0,000466516	24,6573	LPS/IFNγ up vs unstimuliert
Gbp2	0,000467275	10,3301	LPS/IFNγ up vs unstimuliert
Casp4	0,000478330	5,86426	LPS/IFNγ up vs unstimuliert
Dab2	0,000494236	-6,82223	LPS/IFNγ down vs unstimuliert
Adssl1	0,000495266	-20,3041	LPS/IFNγ down vs unstimuliert
AI451557	0,000499132	7,16751	LPS/IFNγ up vs unstimuliert
Gbp3	0,000541200	18,5106	LPS/IFNγ up vs unstimuliert
Igf1	0,000545759	-6,5758	LPS/IFNγ down vs unstimuliert
Ank	0,000617500	-5,02468	LPS/IFNγ down vs unstimuliert
X99384	0,000622396	-7,07142	LPS/IFNγ down vs unstimuliert
Irf1	0,000655921	7,72625	LPS/IFNγ up vs unstimuliert
Acot1	0,000701224	-5,11192	LPS/IFNγ down vs unstimuliert
Ifi47	0,000708196	12,9409	LPS/IFNγ up vs unstimuliert
Mrc1	0,000709051	-24,6651	LPS/IFNγ down vs unstimuliert

Gene Symbol	p-value LPS/IFNγ vs. Unstimulated	Fold change	direction of regulation
Rnase4	0,000754738	-13,7787	LPS/IFNγ down vs unstimuliert
Sema4a	0,000775485	8,95869	LPS/IFNγ up vs unstimuliert
Cst7	0,000800342	8,02575	LPS/IFNγ up vs unstimuliert
Abi3	0,000868728	-5,28494	LPS/IFNγ down vs unstimuliert
Wwp1	0,000944831	-5,21404	LPS/IFNγ down vs unstimuliert
Scamp5	0,000950599	-5,22048	LPS/IFNγ down vs unstimuliert
3830612M24	0,000958864	-6,73607	LPS/IFNγ down vs unstimuliert
Slfn1	0,000962630	11,9817	LPS/IFNγ up vs unstimuliert
Serpina3g	0,001004780	28,4094	LPS/IFNγ up vs unstimuliert
D14Ertd668e	0,001028560	7,63763	LPS/IFNγ up vs unstimuliert
Il1rn	0,001059460	10,7319	LPS/IFNγ up vs unstimuliert
Ifi205	0,001061630	6,21575	LPS/IFNγ up vs unstimuliert
Il2rg	0,001061810	5,17188	LPS/IFNγ up vs unstimuliert
Tap1	0,001165770	7,40811	LPS/IFNγ up vs unstimuliert
Lip1	0,001196680	-6,98058	LPS/IFNγ down vs unstimuliert
Sort1	0,001200800	-16,2828	LPS/IFNγ down vs unstimuliert
Fcgrt	0,001236310	-5,29271	LPS/IFNγ down vs unstimuliert
Fosl2	0,001298850	-5,21188	LPS/IFNγ down vs unstimuliert
Phlda1	0,001300390	5,06369	LPS/IFNγ up vs unstimuliert
Ccl2	0,001339500	6,43043	LPS/IFNγ up vs unstimuliert
Mx1	0,001409770	5,49427	LPS/IFNγ up vs unstimuliert
Dnase1l3	0,001464030	17,8663	LPS/IFNγ up vs unstimuliert
Ccl4	0,001523600	9,89419	LPS/IFNγ up vs unstimuliert
LOC100044430	0,001759420	8,62834	LPS/IFNγ up vs unstimuliert
Tyki	0,001826600	13,3824	LPS/IFNγ up vs unstimuliert
Slc2a6	0,001837330	8,23077	LPS/IFNγ up vs unstimuliert
Slco4a1	0,001853560	-8,65505	LPS/IFNγ down vs unstimuliert
Cd9	0,001868300	-6,68483	LPS/IFNγ down vs unstimuliert
LOC100045005	0,001940340	-5,27024	LPS/IFNγ down vs unstimuliert
C3	0,001963890	6,28793	LPS/IFNγ up vs unstimuliert
Ly6a	0,002090480	11,0664	LPS/IFNγ up vs unstimuliert
Ch25h	0,002273480	13,9967	LPS/IFNγ up vs unstimuliert
Csf1r	0,002297740	-6,35677	LPS/IFNγ down vs unstimuliert
9030216K14Rik	0,002315440	5,63413	LPS/IFNγ up vs unstimuliert
Igf2bp2	0,002374080	6,30582	LPS/IFNγ up vs unstimuliert
Sort1	0,002419700	-11,9219	LPS/IFNγ down vs unstimuliert
Dab2	0,002465630	-5,32544	LPS/IFNγ down vs unstimuliert
Il1a	0,002476510	6,59061	LPS/IFNγ up vs unstimuliert
Gpr109a	0,002541590	10,2752	LPS/IFNγ up vs unstimuliert

Gene Symbol	p-value LPS/IFNγ vs. Unstimulated	Fold change	direction of regulation
2310079N02Rik	0,002936530	-5,52973	LPS/IFNγ down vs unstimuliert
Slamf9	0,003059820	8,344	LPS/IFNγ up vs unstimuliert
Irgm1	0,003170460	5,54606	LPS/IFNγ up vs unstimuliert
Cxcl14	0,003185680	-5,45262	LPS/IFNγ down vs unstimuliert
Ccl4	0,003268000	6,10476	LPS/IFNγ up vs unstimuliert
Ifi205	0,003295310	12,4911	LPS/IFNγ up vs unstimuliert
Lip1	0,003330020	-5,24692	LPS/IFNγ down vs unstimuliert
Tlr2	0,003376530	-8,69729	LPS/IFNγ down vs unstimuliert
Gab1	0,003387520	-5,28188	LPS/IFNγ down vs unstimuliert
Ccl3	0,003502270	7,15818	LPS/IFNγ up vs unstimuliert
LOC100044190	0,003639270	5,40243	LPS/IFNγ up vs unstimuliert
Gpr34	0,003768190	-5,18212	LPS/IFNγ down vs unstimuliert
Adssl1	0,003951930	-9,75132	LPS/IFNγ down vs unstimuliert
Ccl5	0,004103090	29,1417	LPS/IFNγ up vs unstimuliert
Usp18	0,004346220	9,8215	LPS/IFNγ up vs unstimuliert
Fpr2	0,005001000	8,39895	LPS/IFNγ up vs unstimuliert
Dlm1-pending	0,005120310	6,95296	LPS/IFNγ up vs unstimuliert
Creg1	0,005250270	-6,22827	LPS/IFNγ down vs unstimuliert
Arsb	0,005388890	-5,2503	LPS/IFNγ down vs unstimuliert
Itgal	0,005642510	5,15274	LPS/IFNγ up vs unstimuliert
Tgfbi	0,005668630	-12,8429	LPS/IFNγ down vs unstimuliert
Irgb10	0,006014780	6,18701	LPS/IFNγ up vs unstimuliert
Fcgrt	0,006321330	-5,72821	LPS/IFNγ down vs unstimuliert
LOC100044190	0,006681300	5,55782	LPS/IFNγ up vs unstimuliert
LOC100038882	0,006855700	11,0229	LPS/IFNγ up vs unstimuliert
Icam1	0,006865090	5,04934	LPS/IFNγ up vs unstimuliert
EG240327	0,007268270	6,78614	LPS/IFNγ up vs unstimuliert
Usp18	0,008533240	5,0712	LPS/IFNγ up vs unstimuliert
Cd74	0,009407120	5,89866	LPS/IFNγ up vs unstimuliert
Ccl7	0,009626600	13,9294	LPS/IFNγ up vs unstimuliert
Socs3	0,011147800	7,94277	LPS/IFNγ up vs unstimuliert
LOC638301	0,011294500	5,8313	LPS/IFNγ up vs unstimuliert
LOC100048346	0,012048800	8,29704	LPS/IFNγ up vs unstimuliert
Cd74	0,014077500	5,97373	LPS/IFNγ up vs unstimuliert
Ifit2	0,014555500	6,14837	LPS/IFNγ up vs unstimuliert
LOC623121	0,015154300	7,14181	LPS/IFNγ up vs unstimuliert
Ccl7	0,015974600	12,5006	LPS/IFNγ up vs unstimuliert
Ifit2	0,021739300	7,70743	LPS/IFNγ up vs unstimuliert
Cxcl4	0,021824100	-7,84284	LPS/IFNγ down vs unstimuliert

Gene Symbol	p-value LPS/IFNγ vs. Unstimulated	Fold change	direction of regulation
Spint1	0,024560500	-9,09821	LPS/IFNγ down vs unstimuliert
LOC100048556	0,026343600	12,696	LPS/IFNγ up vs unstimuliert
Irf7	0,040257100	7,58237	LPS/IFNγ up vs unstimuliert

Genes regulated in response to IL-4 stimulation:

Gene Symbol	p-value IL-4 vs. unstimulated	Fold change	Direction of regulation
BC057079	0,000000726	2,07301	IL-4 up vs unstimulated
Klhl6	0,001121520	-2,32809	IL-4 down vs unstimulated
Retnla	0,000002534	28,3509	IL-4 up vs unstimulated
Dusp4	0,000007449	5,4617	IL-4 up vs unstimulated
Smap2	0,000126231	2,21006	IL-4 up vs unstimulated
Nfkbiz	0,017851000	-2,06553	IL-4 down vs unstimulated
Klhl6	0,003381010	-2,36409	IL-4 down vs unstimulated
Slc7a2	0,001816510	2,88742	IL-4 up vs unstimulated
Smap2	0,000148200	2,24484	IL-4 up vs unstimulated
Arg1	0,000028153	45,7117	IL-4 up vs unstimulated
Lpxn	0,000208513	2,11405	IL-4 up vs unstimulated
Fyn	0,000012973	2,38615	IL-4 up vs unstimulated
Clic4	0,000083300	2,53831	IL-4 up vs unstimulated
Atp6v0a1	0,001108230	2,17431	IL-4 up vs unstimulated
Centd3	0,012222600	-2,25215	IL-4 down vs unstimulated
Cd274	0,003145870	3,30363	IL-4 up vs unstimulated
Nuak1	0,006471190	-2,57707	IL-4 down vs unstimulated
Gcnt1	0,009049360	-2,26346	IL-4 down vs unstimulated
Olfml3	0,025572800	-2,93922	IL-4 down vs unstimulated
Abca9	0,003795000	-2,17726	IL-4 down vs unstimulated
Fam134b	0,000179136	-3,22584	IL-4 down vs unstimulated
Arg1	0,000061961	29,643	IL-4 up vs unstimulated
Gcnt1	0,006623650	-2,49123	IL-4 down vs unstimulated
Il4i1	0,000092960	2,69605	IL-4 up vs unstimulated
Cx3cr1	0,003727240	-6,45659	IL-4 down vs unstimulated
Fpr2	0,011211800	-6,07205	IL-4 down vs unstimulated
Ap2m1	0,000188750	3,27293	IL-4 up vs unstimulated
Mgl2	0,000115087	5,20617	IL-4 up vs unstimulated
4732429D16Rik	0,003193290	2,18297	IL-4 up vs unstimulated
Tfrc	0,000267486	2,87737	IL-4 up vs unstimulated
Dusp4	0,000189400	3,03022	IL-4 up vs unstimulated

Gene Symbol	p-value IL-4 vs. unstimulated	Fold change	Direction of regulation
Golm1	0,021672200	-2,05839	IL-4 down vs unstimulated
Lmna	0,001477800	2,41922	IL-4 up vs unstimulated
Lmna	0,002474070	2,53372	IL-4 up vs unstimulated
Map3k12	0,001157340	2,30151	IL-4 up vs unstimulated
Egr2	0,000070806	4,47798	IL-4 up vs unstimulated
Spp1	0,004321460	-3,17539	IL-4 down vs unstimulated
Capg	0,000179893	2,16147	IL-4 up vs unstimulated
Phlda1	0,029175100	-2,35932	IL-4 down vs unstimulated
Lmna	0,004007970	2,5034	IL-4 up vs unstimulated
Cd74	0,001040720	4,49307	IL-4 up vs unstimulated
5033414K04Rik	0,001363300	-2,80969	IL-4 down vs unstimulated
St7	0,000363583	2,86483	IL-4 up vs unstimulated
Apoc1	0,009343100	-3,03558	IL-4 down vs unstimulated
Satb1	0,002117910	-2,13845	IL-4 down vs unstimulated
AW212394	0,003737050	-2,53246	IL-4 down vs unstimulated
Alox5ap	0,017286500	-2,64214	IL-4 down vs unstimulated
Alox5ap	0,010155600	-2,74749	IL-4 down vs unstimulated
Mgl2	0,000433857	2,77022	IL-4 up vs unstimulated
Cxcl14	0,027998300	-2,42589	IL-4 down vs unstimulated
Ibrdc3	0,009460580	2,65899	IL-4 up vs unstimulated
C920004C08Rik	0,028313600	-2,01316	IL-4 down vs unstimulated
Lmna	0,012311600	2,41474	IL-4 up vs unstimulated
Sdc4	0,015296100	2,39704	IL-4 up vs unstimulated
Ak2	0,001215730	2,00205	IL-4 up vs unstimulated
Tmem176b	0,011888700	-2,62055	IL-4 down vs unstimulated
LOC100046781	0,011278700	-2,29273	IL-4 down vs unstimulated
Lmna	0,013281300	2,66136	IL-4 up vs unstimulated
Cd74	0,014015400	5,0944	IL-4 up vs unstimulated
Ear11	0,001017710	11,0219	IL-4 up vs unstimulated
Cxcl14	0,010492400	-3,80958	IL-4 down vs unstimulated
Adrb2	0,001974430	-2,16129	IL-4 down vs unstimulated
Pik3cg	0,001940190	-2,08469	IL-4 down vs unstimulated
Tmem176a	0,003106760	-4,36087	IL-4 down vs unstimulated
2310033F14Rik	0,023992500	-2,00585	IL-4 down vs unstimulated
Fchsd2	0,004794450	2,50471	IL-4 up vs unstimulated
Jak2	0,026654100	2,19526	IL-4 up vs unstimulated
Flt1	0,004103060	4,62264	IL-4 up vs unstimulated
Anxa4	0,002087490	2,00236	IL-4 up vs unstimulated
Epb4.1l3	0,005800840	-2,7144	IL-4 down vs unstimulated

Gene Symbol	p-value IL-4 vs. unstimulated	Fold change	Direction of regulation
Pik3cg	0,001851120	-2,07545	IL-4 down vs unstimulated
LOC331595	0,001171890	-4,05587	IL-4 down vs unstimulated
Apoc1	0,043224000	-2,61455	IL-4 down vs unstimulated
Tbc1d2b	0,007016940	2,00594	IL-4 up vs unstimulated
Cd74	0,020100300	5,19313	IL-4 up vs unstimulated
Pilra	0,034508700	-3,72099	IL-4 down vs unstimulated
Tfrc	0,004382240	3,01893	IL-4 up vs unstimulated
Mid1ip1	0,033076600	-2,13188	IL-4 down vs unstimulated
Gpr84	0,018721600	-4,89429	IL-4 down vs unstimulated
Cd14	0,001458650	-4,35231	IL-4 down vs unstimulated
LOC100046232	0,006042600	2,89108	IL-4 up vs unstimulated
Gpr84	0,021139500	-4,59542	IL-4 down vs unstimulated
Tlr2	0,012094200	-5,32531	IL-4 down vs unstimulated
Anpep	0,005291170	2,74333	IL-4 up vs unstimulated
1110032E23Rik	0,010942600	2,57634	IL-4 up vs unstimulated
Znrf2	0,001982870	2,02902	IL-4 up vs unstimulated
Stk17b	0,001148580	-2,19845	IL-4 down vs unstimulated
Prps1	0,010691200	4,0893	IL-4 up vs unstimulated
Clic4	0,020420200	2,08114	IL-4 up vs unstimulated
Itga6	0,027767100	-2,27052	IL-4 down vs unstimulated
Cst7	0,033696900	2,65519	IL-4 up vs unstimulated
Cd93	0,002141220	-2,08298	IL-4 down vs unstimulated
Cysltr1	0,039330300	-2,0075	IL-4 down vs unstimulated
P2ry13	0,009672530	-4,32052	IL-4 down vs unstimulated
Chchd10	0,003330800	2,3423	IL-4 up vs unstimulated
9130211I03Rik	0,003547830	2,35959	IL-4 up vs unstimulated
Ccl24	0,005466740	5,03002	IL-4 up vs unstimulated
Atp8a1	0,011525400	-2,23696	IL-4 down vs unstimulated
Slc39a4	0,010450500	-3,01377	IL-4 down vs unstimulated
Il13ra1	0,006174320	-3,10854	IL-4 down vs unstimulated
9530018I07Rik	0,026837300	-2,03846	IL-4 down vs unstimulated
LOC100046781	0,010688800	-2,54244	IL-4 down vs unstimulated
Pcyox1l	0,010683500	2,30682	IL-4 up vs unstimulated
Spata13	0,033172200	-2,83523	IL-4 down vs unstimulated
P2ry5	0,014771900	-2,86202	IL-4 down vs unstimulated
B430201A12Rik	0,027747000	-2,33159	IL-4 down vs unstimulated
Flrt2	0,012271700	2,14911	IL-4 up vs unstimulated
Ear2	0,007955580	2,97144	IL-4 up vs unstimulated
Cox6a2	0,010376600	2,09569	IL-4 up vs unstimulated

Gene Symbol	p-value IL-4 vs. unstimulated	Fold change	Direction of regulation
Dusp6	0,017220900	-2,99331	IL-4 down vs unstimulated
Anxa4	0,030115300	2,11356	IL-4 up vs unstimulated
Cd93	0,009217890	-2,91525	IL-4 down vs unstimulated
Smad3	0,004513700	-2,18059	IL-4 down vs unstimulated
Pecam1	0,017716700	2,53949	IL-4 up vs unstimulated
Clec4d	0,003084720	-2,3308	IL-4 down vs unstimulated
Ear2	0,011084100	2,13783	IL-4 up vs unstimulated
Tarbp2	0,009718220	2,56161	IL-4 up vs unstimulated
Igfbp4	0,010014000	-3,71017	IL-4 down vs unstimulated
Clec4n	0,005038790	-6,91907	IL-4 down vs unstimulated
Gpx3	0,038447400	-2,03069	IL-4 down vs unstimulated
Apoc2	0,041276800	-2,15022	IL-4 down vs unstimulated
9330175B01Rik	0,023238500	-2,34821	IL-4 down vs unstimulated
Cd33	0,046299500	-2,53521	IL-4 down vs unstimulated
Idb2	0,025377900	-2,28696	IL-4 down vs unstimulated
Igfbp4	0,041497800	-3,65096	IL-4 down vs unstimulated

Genes regulated in response to TGFβ stimulation:

Gene Symbol	p-value TGFβ vs. unstimulated	Fold change	Direction of regulation
Mmp13	0,009277810	-2,28508	TGFβ down vs unstimulated
Smpdl3b	0,002163690	-2,13613	TGFβ down vs unstimulated
Klhl6	0,000923407	2,39627	TGFβ up vs unstimulated
Ctse	0,000027607	2,26607	TGFβ up vs unstimulated
Irg1	0,017247400	-2,44748	TGFβ down vs unstimulated
Gas6	0,012480500	-2,00337	TGFβ down vs unstimulated
Gtf2h2	0,000051053	2,441	TGFβ up vs unstimulated
Zdhhc14	0,005426880	-2,04652	TGFβ down vs unstimulated
Klhl6	0,004119410	2,29027	TGFβ up vs unstimulated
Cyp27a1	0,000483675	-2,1245	TGFβ down vs unstimulated
Ebi3	0,001076100	-2,4581	TGFβ down vs unstimulated
Psat1	0,000495021	3,82297	TGFβ up vs unstimulated
Syngr1	0,011567900	2,23559	TGFβ up vs unstimulated
Cyp27a1	0,003031170	-2,14619	TGFβ down vs unstimulated
Rgl1	0,003230980	-2,38248	TGFβ down vs unstimulated
Irf1	0,023645100	-2,07788	TGFβ down vs unstimulated
Olfml3	0,033557200	2,73555	TGFβ up vs unstimulated
Golm1	0,000773998	3,67067	TGFβ up vs unstimulated

Gene Symbol	p-value TGFβ vs. unstimulated	Fold change	Direction of regulation
AI504432	0,001203290	2,9356	TGFβ up vs unstimulated
TGFβr1	0,007604910	2,30536	TGFβ up vs unstimulated
Clec4a3	0,000298035	-5,70756	TGFβ down vs unstimulated
Fpr2	0,003590270	-9,66298	TGFβ down vs unstimulated
Dab2	0,009631950	-2,21404	TGFβ down vs unstimulated
Rassf4	0,000437045	-2,86951	TGFβ down vs unstimulated
Casp4	0,032497500	-2,15501	TGFβ down vs unstimulated
Sgk1	0,004092890	3,20063	TGFβ up vs unstimulated
Rai14	0,002059210	2,69569	TGFβ up vs unstimulated
4732429D16Rik	0,002605140	-2,24972	TGFβ down vs unstimulated
Dok2	0,002535830	-2,73902	TGFβ down vs unstimulated
Golm1	0,002349990	3,12859	TGFβ up vs unstimulated
Dusp1	0,012595900	-2,12312	TGFβ down vs unstimulated
Clec4a1	0,000836753	-10,9493	TGFβ down vs unstimulated
EG433229	0,018801900	2,28269	TGFβ up vs unstimulated
Havcr2	0,001764450	2,91606	TGFβ up vs unstimulated
AU020206	0,003199260	3,89601	TGFβ up vs unstimulated
Mrc1	0,005860140	-8,86864	TGFβ down vs unstimulated
Ccl9	0,000161458	-10,5041	TGFβ down vs unstimulated
Mfge8	0,021632100	2,01972	TGFβ up vs unstimulated
Lrrc33	0,001526280	-2,18501	TGFβ down vs unstimulated
Havcr2	0,003107000	2,61035	TGFβ up vs unstimulated
5033414K04Rik	0,000352485	-3,66626	TGFβ down vs unstimulated
Pkp2	0,005984290	2,20017	TGFβ up vs unstimulated
Pmepa1	0,002654270	2,73551	TGFβ up vs unstimulated
Rassf4	0,001827910	-2,80403	TGFβ down vs unstimulated
Syngr1	0,026306300	2,34844	TGFβ up vs unstimulated
Slc9a9	0,004338990	-3,09464	TGFβ down vs unstimulated
Pcp4l1	0,000927065	-2,03206	TGFβ down vs unstimulated
Gas7	0,004945250	-2,65162	TGFβ down vs unstimulated
F11r	0,008434870	2,43854	TGFβ up vs unstimulated
Rassf4	0,005185170	-2,45871	TGFβ down vs unstimulated
Fmnl3	0,011420700	2,13279	TGFβ up vs unstimulated
Ednra	0,000692460	3,55779	TGFβ up vs unstimulated
Ap1b1	0,010099800	-2,12041	TGFβ down vs unstimulated
Cxcl14	0,036833300	2,28304	TGFβ up vs unstimulated
Dpep2	0,003563810	-2,12244	TGFβ down vs unstimulated
Spsb1	0,001737290	2,58577	TGFβ up vs unstimulated
Chst1	0,010855100	4,62155	TGFβ up vs unstimulated

Gene Symbol	p-value TGFβ vs. unstimulated	Fold change	Direction of regulation
Lbr	0,000446801	-2,66025	TGFβ down vs unstimulated
Fcgr4	0,021504300	-2,9013	TGFβ down vs unstimulated
Notch4	0,004229920	2,18395	TGFβ up vs unstimulated
Igfbp5	0,001602520	8,00116	TGFβ up vs unstimulated
Gas7	0,005071780	-3,31471	TGFβ down vs unstimulated
Dab2	0,035686400	-2,26533	TGFβ down vs unstimulated
Igfbp5	0,002156210	6,99022	TGFβ up vs unstimulated
Egln3	0,026895300	2,05939	TGFβ up vs unstimulated
Tmem8	0,009208470	-2,07435	TGFβ down vs unstimulated
D10Wsu52e	0,013172200	2,17323	TGFβ up vs unstimulated
Tmem176a	0,028174800	-2,51018	TGFβ down vs unstimulated
Extl3	0,025781000	2,02014	TGFβ up vs unstimulated
Ifitm1	0,000820070	-4,59605	TGFβ down vs unstimulated
Flt1	0,028049300	2,74475	TGFβ up vs unstimulated
Cyp4f18	0,005479500	2,38286	TGFβ up vs unstimulated
Htr2b	0,001647520	3,47653	TGFβ up vs unstimulated
Serpine2	0,025038400	2,50064	TGFβ up vs unstimulated
Serpine2	0,040053600	3,87378	TGFβ up vs unstimulated
Il1b	0,022784700	-5,42021	TGFβ down vs unstimulated
Marcksl1	0,040450000	-3,64256	TGFβ down vs unstimulated
A430107D22Rik	0,020171000	2,1771	TGFβ up vs unstimulated
Pkp2	0,013007400	2,40492	TGFβ up vs unstimulated
4930431B09Rik	0,008774780	2,93568	TGFβ up vs unstimulated
2810402K13Rik	0,020232400	2,40762	TGFβ up vs unstimulated
Stk17b	0,001582060	-2,10565	TGFβ down vs unstimulated
Cst7	0,012673400	3,43014	TGFβ up vs unstimulated
Egr1	0,013977100	2,59941	TGFβ up vs unstimulated
Cd93	0,001380020	-2,21166	TGFβ down vs unstimulated
Cysltr1	0,029640900	-2,11812	TGFβ down vs unstimulated
Ccl6	0,005785520	-2,41955	TGFβ down vs unstimulated
Atp8a1	0,008430930	-2,36368	TGFβ down vs unstimulated
Dab2	0,042947100	-2,45018	TGFβ down vs unstimulated
Lst1	0,016877700	-3,62515	TGFβ down vs unstimulated
Igfbp5	0,006567010	8,17602	TGFβ up vs unstimulated
B230343A10Rik	0,005617830	-2,83601	TGFβ down vs unstimulated
Sepp1	0,013463100	-2,50355	TGFβ down vs unstimulated
D0H4S114	0,019935800	3,27075	TGFβ up vs unstimulated
Tmem8	0,029480700	-2,01014	TGFβ down vs unstimulated
LOC100044439	0,020031400	3,79893	TGFβ up vs unstimulated

Gene Symbol	p-value TGFβ vs. unstimulated	Fold change	Direction of regulation
Ifitm2	0,005198770	-6,99499	TGFβ down vs unstimulated
Ifitm1	0,025250400	-6,51132	TGFβ down vs unstimulated
Fos	0,009111140	-2,45243	TGFβ down vs unstimulated
Cd44	0,019651100	-2,21167	TGFβ down vs unstimulated
Cfp	0,008709720	-11,1303	TGFβ down vs unstimulated
Cd93	0,002942780	-3,8184	TGFβ down vs unstimulated
Sparc	0,043754400	2,79803	TGFβ up vs unstimulated
H2-DMa	0,019340400	2,7111	TGFβ up vs unstimulated
Cd47	0,012665800	-2,38806	TGFβ down vs unstimulated
Igfbp4	0,010554300	-3,65645	TGFβ down vs unstimulated
Adap1	0,044440900	3,09134	TGFβ up vs unstimulated
Clec4n	0,013689300	-4,81509	TGFβ down vs unstimulated
Cytip	0,021294900	-4,73811	TGFβ down vs unstimulated
Clec4b1	0,009816860	-3,56765	TGFβ down vs unstimulated
Plk3	0,021868300	2,22947	TGFβ up vs unstimulated
scl0002975.1_346	0,027512100	-2,37011	TGFβ down vs unstimulated
H2-DMa	0,025139900	2,91269	TGFβ up vs unstimulated
LOC100047419	0,028049300	-4,84116	TGFβ down vs unstimulated
Clec4b1	0,012850500	-2,13911	TGFβ down vs unstimulated
Txnip	0,010937900	-2,5653	TGFβ down vs unstimulated
Txnip	0,011000300	-2,45255	TGFβ down vs unstimulated
E230029F23Rik	0,045864500	-2,55436	TGFβ down vs unstimulated
Qpct	0,033804900	2,00121	TGFβ up vs unstimulated
Fabp3	0,034044400	2,27564	TGFβ up vs unstimulated
Igfbp4	0,034369500	-3,90448	TGFβ down vs unstimulated

A.11 Declaration

I hereby solely declare that I prepared this thesis entitled “Investigation of the endocannabinoid system using *in vivo* and *in vitro* models” entirely by myself except otherwise stated. All text passages that are literally or correspondingly taken from published or unpublished papers/writings are indicated as such. All materials or services provided by other persons are equally indicated.

Bonn, April 2013

(Svenja Ternes)

Acknowledgement

Besonders bedanken möchte ich mich bei Herrn Prof. Dr. Andreas Zimmer für die Überlassung des Themas, für seinen fachlichen Rat und seine konstante Unterstützung während meiner gesamten Zeit als Doktorandin.

Herrn Prof. Dr. Albert Haas danke ich recht herzlich für die bereitwillige Übernahme der Funktion als Zweitgutachter meiner Arbeit.

Bei Dr. Judith Alferink bedanke ich mich sehr für die außerordentliche Betreuung des Microglia Projektes, für immunologische Experise, Rat und Unterstützung zu jeder Zeit.

Bei Dr. David-M. Otte bedanke ich mich herzlich für unzählige Ratsschläge und ein offenes Ohr für alle Fragen und Probleme, die mich rund um meine Mäuse immer wieder beschäftigt haben.

Ein großes Dankeschön richtet sich an unsere Verhaltensexperten Dr. Ildikò Racz und Dr. Andras Bilkei-Gorzo, die mich tatkräftig bei der Durchführung der Verhaltensexperimente unterstützt haben.

Ebenfalls bedanken möchte ich mich bei allen Kooperationspartnern für eine sehr gute Zusammenarbeit und die Bereitstellung von Zeit, Material und Expertise. Im Besonderen danke ich Dr. Ermelinda Lomazzo und Dr. Laura Bindila sowie Prof. Dr. Joachim Schultze und den Mitgliedern seiner Arbeitsgruppe Dr. Marc Beyer, Maren Mai und Dr. Thomas Ulas.

Bei all meinen Kollegen im Institut für Molekulare Psychiatrie möchte ich mich für die angenehme Arbeitsatmosphäre und die allseitige Hilfsbereitschaft bedanken. Besonders erwähnen möchte ich Anna-Lena, Alex, Eva, Ben, Irene, Britta, Kim, Ramona und Anne, die neben der Arbeit auch gute Freunde für mich geworden und geblieben sind…was hätte ich nur ohne euch gemacht?

Meine Familie läuft außer Konkurrenz: Da reichen alle Worte nicht- DANKE für ALLES!

Patric, du hast die Tapferkeitsmedaille verdient! Danke, dass du da bist! I. L. U.

An die Mädels:…ich lass‘ das jetzt so! Es ist so schön, dass es euch gibt!